DISCLAIMER:

This document does not meet the
current format guidelines of
the Graduate School at
The University of Texas at Austin.

It has been published for
informational use only.

THE DISSERTATION COMMITTEE FOR JONATHAN THOMAS PETERS CERTIFIES THAT THIS IS THE APPROVED VERSION OF THE FOLLOWING DISSERTATION:

COMPOSITE NANOGELS FOR THE TRIGGERABLE RELEASE OF CHEMOTHERAPEUTICS

Committee:

Nikolaos A. Peppas, Supervisor

Benny Freeman

Keith Johnston

Isaac Sanchez

Janeta Zoldan

COMPOSITE NANOGELS FOR THE TRIGGERABLE RELEASE OF CHEMOTHERAPEUTICS

BY

JONATHAN THOMAS PETERS, B.S.

DISSERTATION

Presented to the Faculty of the Graduate School of

The University of Texas at Austin

in Partial Fulfillment

of the Requirements

for the Degree of

DOCTOR OF PHILOSOPHY

THE UNIVERSITY OF TEXAS AT AUSTIN

DECEMBER, 2015

DEDICATION

This document is dedicated to my family and friends for their support and ability to make light of any situation.

COMPOSITE NANOGELS FOR THE TRIGGERABLE RELEASE OF CHEMOTHERAPEUTICS

Jonathan Thomas Peters, PhD

The University of Texas at Austin, 2015

Supervisor: Nikolaos Peppas

The development of external stimuli responsive nanoparticles has progressed greatly since its inception in the seventies. However, apart from some clinical success for slow release delivery via liposomes, the technology has stalled for the delivery of chemotherapeutics due to a myriad of problems with cytocompatibility and premature diffusion of drug payload.

The solution to cytocompatibility has been the coating of the system with polyethylene glycol. New methods have been developed to attach polyethylene glycol (PEG) tethers to the surface of otherwise unreactive particles. Surface hydrolysis of acrylamide containing polymers can be used to produce carboxylic acid functional groups near the surface of the polymeric nanoparticles. These nanoparticles can then be functionalized with PEG via EDC/NHS chemistry. The use of surface hydrolysis not only allows for reaction with these neutral polymers, but also provides greater control of PEG localization and leads to an unintrusive method to add the much needed stealth coating.

In order to address the issue with premature release, new polymer systems have been developed. These systems are based around theory of hydrophobic interaction in

order to improve the polymer/drug interaction in order to limit the unwanted diffusional release of drug payload. This interaction was addressed in a number of ways, focusing on both compartmentalization and copolymerization in order to develop nanogels that can entrap and withhold more drug from the surrounding area.

An in depth look into the interactions that encourage drug uptake in these systems was performed by altering the copolymer chosen for these systems. This work looks into effects on phase transition, functional groups, hydrophobicity, and any structural changes that occur as a result of the polymerization scheme.

After drawing conclusions on the interactions that encourage drug uptake, complex systems were devised to take advantage of these interactions. Core shell systems were designed to take advantage of the convective release of lower critical solution systems while still utilizing the mechanisms that improve drug retention. These systems were synthesized by two methods, emulsion polymerization and micelle crosslinking. These systems have been showed to improve the drug interaction and retention of doxorubicin as a model chemotherapeutic.

TABLE OF CONTENTS

LIST OF TABLES

LIST OF FIGURES

LIST OF ILLUSTRATIONS

Chapter 1

Introduction

Externally triggered theranostic delivery schemes are an attractive treatment method for localized diseases with devastating treatments. The beautiful marriage between therapeutic and diagnostic technologies allows for improved treatment, granting physicians added control and providing real time data about the progress of the disease and treatment[1]. The primary disease focus for these systems in the past has been tumorous cancers. Cancer is an ideal disease for these systems due to the natural accumulation of particles due to the fenestrated vasculature allowing for particle accumulation and the devastating effects of the treatment as well as the disease[2].

Current treatment for tumorous cancers involves surgery, radiotherapy, chemotherapy, or some combination of the three. For localized tumors surgery is often the best form of treatment, excising the tumor before the cancer can spread to the surrounding tissue. However, cancer is rarely caught when surgery is capable of completely curing the disease, and surgery can be debilitating calling for one of the other two major treatments[3].

Radiotherapy uses focused radiation to damage and kill cancer cells, often times damaging the healthy cells surrounding the neoplasm. Radiotherapy can be effectively targeted with some of the newer radiation technology, such as proton beam therapy, though the overall success is still limited. Until the fabled “magic bullet” is developed, cancer will continue to be a disease that requires multiple modes of treatment. In this vein, more work must be done to provide doctors every possible improvement to help them better treat cancers while limiting the often devastating side effects.

These side effects can be limited by localizing the drugs to cancerous areas. Localization of chemotherapeutics can aid treatment by limiting off site effects, increasing the level of drugs delivered, and ensuring their unabated delivery to the target area. This technology can increase doctors' ability to maintain chemotherapeutic drugs within the therapeutic range. Development and optimization of this technology will be an important step in improving the chemotherapeutic aspect of cancer treatment.

Externally triggered theranostic devices are comprised of four major components: a visualizable and external stimuli responsive core, a stimuli sensitive coating, biocompatible stabilization coating, and a targeting moiety. This thesis will focus on the synthesis and interaction of the first three components with a brief discussion on the inclusion of the targeting moiety. For the purpose of this work this technology will be based around temperature sensitive hydrogels encasing magnetic nanoparticles.

These systems can provide an important tool for doctors as they battle the wide variety of cancers that exist. However, there are a number of questions to answer about these systems, not limited to the investigation of the interaction of all of the components necessary to develop a fully functioning composite system.

Chapter 2: Background

Externally triggerable theranostic drug delivery vehicles offer a solution to the problem with non-specific drugs. Externally triggered drugs allow for the localization of drugs and eliminating the issues that can arise from systemic delivery; such as toxicity and unnecessary off site effects. However, due to the complex nature of these treatments these nano-devices are not recommended for chronic diseases. With these considerations there are a few diseases that would lend themselves well to theranostic delivery. They are HIV; a disease that, in the early stages, can be treated with anti-retrovirals[4], and Cancer; for which chemotherapeutic treatment provides a long list of devastating side effects[3].

The majority of this work has focused on the use of these composite nanoparticles for the treatment of cancer. Due to the fenestrated vasculature, the deleterious off site effects, and the already complex nature of the treatment, Cancer is an ideal target for the development of this technology.

2.1 Cancer and its Treatment

Cancer is a difficult disease to identify; each presentation of the disease has different physiological and chemical characteristics, even when the disease is structurally similar. This has led to treatments that have a broad spectrum of effect, killing or removing all of the cells in their radius of impact. Until recently, the only three methods for treatment have been surgery, chemotherapy, and radiation therapy. Recent advances in targeted protein based treatments have shown some slight success, however they are specialized in the types of cancer they treat and can still require the other forms of treatment for noticeable success[3]. Until further progress is made the original three treatment methods are necessary.

Surgery has so far proven the most effective of completely removing cancers, when this is an option. Often, the tumors grow in sensitive areas or are noticed too late for surgery to be a viable option for the eradication of the cancer. This leaves patients dependent on radiotherapy and chemotherapy, both of which have devastating side effects. Much research has been developed to limit these undesirable effects for radiotherapy, with recent advances in proton beam therapy. This technology allows for improved accuracy of the beam limiting the damage to the cancerous region[5]. Similar work has been looked to for chemotherapy, however much work is still needed to perfect it.

In order to do this, researchers looked for a commonality among cancer types to exploit. Although different types of cancer have a wide range of physical and chemical markers, research has identified a few common characteristics that are present in most tumors. The most attractive of which is the leaky vasculature caused by the increased angiogenesis[2]. The astounding rate at which tumors grow requires rapid and, subsequently, faulty development of vasculature in order to supply blood to the foreign tissue. This fact results in the phenomenon known as the enhanced permeability and retention (EPR) effect. Essentially, this states that the leaky vasculature common to most tumors allows for the increased uptake of large molecular weight drugs[2]. This form of passive targeting has been pursued for years as a mechanism to treat cancer.

Nanoparticles have been looked to as a means to prevent the side effects caused by the systemic application of chemotherapeutics by passively targeting to the site of the tumor via the EPR effect[6]. One of the common issues encountered with these nanoparticles is the accumulation in the liver and other tissues with vasculature similar to tumors[7]. There are a few methods to limit this off target accumulation. The simplest of these methods is difference in particle size. Some studies have proven that, with some cancer types, by increasing the size of gold and liposomal

nanoparticles over the normally affirmed 100 nm particle size; in the range of 150-300 nm[8, 9].

The issue with this is that it is not universal among all cancer lines. Much as the differences in cancer genetics can lead to large differences in genetic markers, it also can lead to differences in the endothelial lining, with no real pattern to describe the differences in the fenestrations leading to particle uptake[6]. Another mechanism is altering the hydrophobicity/hydrophilicity of the particles. Research has shown that hydrophobic particles are more likely to accumulate in the liver and removed by other parts of the reticuloendothelial system (RES)[6, 10]. The common method to accomplish this is to graft polyethylene glycol (PEG) to the surface. This unique molecule allows for the stealthing of particles, though this is not a perfect solution for the undesired accumulation in the liver, though it can limit this problem[5].

The method that shows the highest level of improvement is to affix some form of active targeting to the nanoparticles. Among all cancer types, the inclusion of an appropriate targeting moiety can increase the accumulation in the tumor, thus limiting its presence in other tissues[6]. However each cancer type must be targeted by a different moiety, leading to specialized particle drugs being needed. To this extent many targeting moieties have been attempted to be identified for their use with nanoparticles, with the most promising being anti-enhanced growth factor receptor (EGFR)[11]. However, the issue with these antibodies is that they tend to activate the growth of the cancer, leading to a growth increase before triggering. Before particle based systems are widely and freely applied a better option for active targeting needs to be identified.

Current Methods for Particle Based Chemotherapeutic Delivery

The predominant methods for particle based drug delivery fall into four major categories:

Liposomes

Polymeric Micelles

Dendrimers

Hydrogel Nanoparticles

2.1.1 Liposomal Drug Delivery

The only clinically-approved particle based drug delivery of chemotherapeutics for many years has been Doxil©, a PEGylated liposome for the delivery of Doxarubacin (DOX)[5]. Doxil© is a liposomal drug carrier that contains tightly packed DOX inside a single bilayer of a combination of lipids and cholesterol like molecules. This is the simplest design of such particle based delivery vehicles, as it serves as only a carrier for the hydrophobic drug molecules, using only the EPR effect to localize the drug to the cancerous region.

Liposomal drug delivery has turned to the use of stimuli responsive lipids in order to increase control of drug release while also providing diagnostic tools. Temperature sensitive liposomes composed of cholesterols and the temperature sensitive lipid, hydrogenated-L-α-phosphatidylcholine, have been combined with nanoparticles and large molecules that can be triggered via external stimuli and monitored. The *in vitro* release of these drugs were examined and proven that the release rate is dependent on temperature, and maximum release is achieved in a relatively harmless range of 38-40 ºC[12, 13]. However, these advances are limited, as significant drug release is still seen at physiological temperatures. However, their ability to be triggered by ultrasound triggered small molecules, such as Gd(HPDO3A)(H_2O), is a unique technique for liposomes[12].

Liposomes that respond to changes in pH have also been examined as delivery vehicles for chemotherapeutics. Two methods have been used in order to take advantage of these liposomes.

The first is using the intracellular pH change that occurs between cancerous regions and regions of healthy tissue, a drop from 7.4 to about 6.5. However, this drop is not consistent and is often used in addition to another response, such as thermosensitive or perhaps a second pH responsiveness[14]. This has been achieved by combining pH sensitivity with a pH sensitive hydrolyzeable linker between the liposome and PEG.

The other mechanism utilizes endosomal uptake and release in order to trigger a pH shift. In order to enhance uptake of neutral liposomes a ligand specific to cancer cells, anti-CD-19, has been affixed to pH sensitive liposomes in order to trigger internalization of the particles. Once in the endosome, the pH response was triggered, and the drug payload was successfully released. However, these particles still struggled with premature payload release[15]. This mechanism utilizes Dioleoylphosphatidylethanolamine (DOPE) or a thiol-PEG modified istearoylphosphatidylethanolamine (DSPE). DOPE is naturally pH responsive, breaking apart lipid bilayers as the pH drops to about 5.5. PEG modified DSPE requires the presence of reducing agents that are readily available inside cells.

2.1.2 Polymeric Micelles

Polymeric micelles are normally amphiphillic block copolymers that form stable micelles due to hydrophobic domains. With the advancements of block copolymerization, tri-block copolymers have even been formed to provide multiple stimuli responsive sections to attempt to provide extra barriers to drug release. Multi-responsive micelles have been developed with a variety of sensitivities; including temperature, pH, electromagnetic, and oxidative stress[16].

Micelles are only held together by the hydrophobic effect, partitioning the water insoluble and water soluble sections in order to limit the enthalpic effects. A common micelle involves block copolymers composed of polystyrene and a stimuli responsive block, eg. acrylic acid. The issue

encountered with micelles, is their sensitivity to changes in solution characteristics, such as ionic strength and pH. These sensitivities lead to unstable micelles that can begin to disassociate in the blood stream before reaching the target[17].

In order to improve the stability of the micelles, electrostatic interactions have been used. The ionic molecules are water soluble, but by combining oppositely charged polymers of similar length the block copolymers can form micelles due to association[18]. However, studies have shown that ionic block copolymers mixed with large molecules; eg amino acids or calcium ions, complexation is not dependent on the similar length postulate[19, 20]. Systems that are stabilized by the presence of Calcium ions can even be cross-linked by the addition of ethylene diamine tetraaetic acid[20].

Micelles sensitive to ultrasound have also been developed in order to provide external control over the delivery of the drug payload. In these studies a drastically hydrophobic core polymer was used, allowing for phase differentiation between the drug containing core and the surrounding aqueous environment[21]. The ultrasound release mechanism depends only on the sensitive nature of the micelles existence. To this point, the accumulation of the micelles has been entirely dependent on the EPR effect and the accuracy of the ultrasound waves. The pharmacokinetics have proven this an effective means for turmor treatment[22].

Dendrimers

Dendrimers are branched polymers that can be formed by three main mechanisms; convergent, divergent, and convergent/divergent, describing the method by which the sections of the dendrimer grow together (CITE). Dendrimers have shown some ability to naturally retain model chemotherapeutics, however covalently attaching the chemotherapeutics has proven more effective for the delivery of DOX via dendrimer[23, 24]. By attaching the drug with a

chemically liable linker, the drug can be contained until it reaches the destination with the necessary conditions to detach the drug.

Dendrimers are classified by their generation and their functional side group. The majority of dendrimers used for the delivery of chemotherapeutics are poly(amido amines), that produce amine terminated sequences[25]. Generation describes the number of consecutive reactions completed, essentially counting the rings from the origin. Each successive generation produces more functional groups and an increased size depending on the function of synthesis. For poly(amido amines) each successive generation doubles the number of free amines and increases the diameter of the particle[25].

Dendrimers have proven capable of dual payload delivery when two half dendrimers are joined to form a Janus dendrimer[26]. More impressively, these systems have proven capable of controlling the ratios of drugs delivered based upon the respective generation of the two halves. This capability could prove an effective mechanism for delivering drug pairs with

2.1.2 Hydrogel Nanoparticles

Hydrogel nanoparticles are composed of water soluble cross-linked polymers that swell in the presence of water. Poly(lactic-co-glycolic acid) is the common system that is both biocompatible and biodegradeable[27]. Hydrogels are often stimuli responsive, being composed of a polymer that undergoes a critical transition in response to a change of solution characteristics or a stimuli response, eg electromagnetic [28]. For the purpose of the delivery of chemotherapeutics, the majority of the research has been on temperature sensitive polymers in conjunction with another stimuli responsive inorganic particle[29, 30]. Like dendrimers, hydrogels can be produced with functional groups to which drugs can be conjugated to with a liable bond. Again, the issue with

these systems for the delivery of chemotherapeutics is identifying a bond that is unique for cancerous tissue.

2.2 Thermoresponsive Hydrogels for Externally Triggered Drug Delivery

Externally triggered drug delivery depends on the development of composite nanoparticle systems responsive to some form of external stimuli. These systems are often composed of a temperature sensitive polymeric shell and a core that heats in response to an external stimulus, as seen in Illustration 2.1. Further surface modification is necessary in order to allow these things to flow through the bloodstream without to be attacked by the body's immune response [27]. Finally a targeting moiety is necessary in order to improve targeting to the tumorous area.

Research into these responsive systems has largely focused on systems of polymers that display lower critical solution temperatures (LCSTs) in water, largely due to the early development of N-Isopropyl acrylamide (NIPAAm). However, there have been a few upper critical solution temperature (UCST) responsive polymers developed that have been reproduced in nanoscale systems. The issue encountered with these UCST systems, particularly those with physiologically relevant responses, is the presence of ionic functional groups that render these systems overly sensitive to ionic conditions[31]. For example, one of the more prevalent UCST systems developed by Okano is a interpenetrating polymer network (IPN) of acrylic acid (AA) and acrylamide (AAm)[32]. This system displays a UCST of 39ºC, but only under very specific ionic and pH conditions. Shifting away from these temperatures results in loss of swelling response altogether.

As far as LCST responsive systems, there are a variety of them that demonstrate temperature responses at or around the physiological temperature of 37ºC. These are mostly N-Alkyl

substituted acrylamides and their copolymers. NIPAAm is the original system to demonstrate the unusual response in water near physiological temperatures. For many years, research has attempted to shift the LCST response of NIPAAm polymers from its response of 32ºC by a number of copolymers and IPN networks[33]. One such successful system involves the copolymerization with 2-acrylamido-2-methyl-1-propanesufonic acid (AMPS). The sulfonic acid groups provide the necessary temperature response, however, it also provides a group sensitive to the ionic and pH shifts that can occur between patients[34].

Several neutral copolymers have been examined, and proven to shift the transition temperature above 37ºC, most promising of which is acrylamide. However, when this system is copolymerized into a gel, the higher levels of acrylamide lead to decreases in overall changes in swelling volume[35]. The addition of acrylamide is an attractive prospective, as it entails the addition of a completely neutral monomer, that has a swells independent of most solution conditions.

Other polymers have been developed based off of the success of NIPAAm, focusing mostly on finding ways to alter the N substituted acrylamides. By altering the alkyl group that extends from the nitrogen the transition temperature can be shifted, again, potentially limiting the overall swelling response. One system that shows promise is another isopropyl modified acrylamide. The simple addition of a methyl group to the vinyl carbon, creating N-Isopropylmethacrylamide (NIPMAM), significantly alters the transition temperature to above, to 45ºC [36]. This transition temperature has left a response well above physiological temperature which could lead to unwanted hypothermia[30]. In order to avoid this, the LCST of pNIPMAM must be depressed. This has been accomplished with NIPAAm polymers by the addition of a hydrophobic comonomer, such as butyl methacrylate[37].

These polymer systems can be tuned to show different properties, however the issue encountered is the foreign body response to these nanoparticles. In order to overcome this response a stealth coating is necessary. This leads to the necessity of a PEG coating in order to limit the RES from removing the particles before their arrival at the tumor and the subsequent release [27]. The issue with these neutral polymers is the only way to provide a PEG coating is to graft the PEG into the backbone. This method is problematic, as the grafting of PEG limits the swelling response of the polymer system[38]. However, these systems lead to many of the same problems, the statistical implementation of PEG chains into the thermoresponsive pNIPAAm chains results in loss of temperature sensitivity, particularly at concentrations necessary to limit the protein adhesion that leads to opsonization[27].

Core-shell systems were the next step in order to improve loading and release control. A number of systems have been developed along these lines, coupling thermosensitive polymers with a range of other stimuli sensitive polymers[39]. The predominant combination for delivery of chemotherapeutics is the combination of temperature and pH responsive systems, trying to take advantage of the acidic nature of tumorous areas in the body. Both cationic and anionic pH responsive systems have been successfully incorporated into what are known as “schizophrenic” micelles. These systems are identified as schizophrenic due to the ability to reverse the aqueous/non-aqueous phases by manipulation of pH and temperature. Anionic systems focus primarily around AA like polymers. These systems collapse as the pH drops below the critical point[40]. This leads to a double pumping mechanism for the release of a drug payload. However, it can also lead to limiting the release at lower pHs, which is not advantageous for chemotherapeutic delivery.

Cationic pH sensitive polymers could prove to be more promising, as the drop and pH will lead to a positive swelling response that will result in improved diffusion only in the cancerous area.

For this purpose, N'N' Dimethyl aminoethyl methacrylate (DAMEMA) This is a promising prospect, yet drug loading and delivery has not yet been performed on these complex systems, let alone with the inorganic nanoparticles necessary for the external temperature triggering[40].

2.3 Precipitation Polymerization

Nanogels composed of NIPAAm and other LCST free radical polymers are often synthesized via a technique known as precipitation polymerization. This technique is a two phase system, a continuous phase, water, and as surfactant stabilized spherical micelle phase. All of the reactive species are present in water at a temperature well above the transition point. As the polymerization proceeds, the temperature sensitive polymer precipitates out of the continuous phase into the micelle phase. Chains in both phases continue to grow and terminate leading to the production of spherical nanogels[41].

2.4 Stimuli Responsive Nanoparticles for Hyperthermia

2.4.1 Magnetic Nanopartices

Magnetic nanoparticles (MNPs) can be divided into four categories, diamagnetic, paramagnetic, ferromagnetic, and superparamagnetic. Each of these types of particles responds to magnetic fields in different ways due to the way their electrons occupy and move about different orbital spins. Similarly, their response to heating via alternating magnetic fields (AMFs) can yield drastically different results. However, superparamagnetic nanoparticles are often chosen, superparamagnetism is dependent on a combination of ferromagnetic domains and temperature high enough to overcome the energy required to do so. This switching can be utilized by an AMF to induce massive heating for the size of the particles [42]. Magnetic nanoparticles can be synthesized from a number of base materials, including iron, cobalt, nickel, and alloys thereof. For biological applications iron oxide nanoparticles are preferred since the body is naturally capable of breaking them down into nontoxic materials[43].

Magnetic nanoparticles provide an imaging moiety, as they have proven to be useful as MRI contrast agents. As magnetic nanopartilces accumulate in a specific area, the reflexive response time of magnetically aligned protons in that area decreases. By visualizing this data with a heat map the nanopartilces can be localized. This, combined with the EPR effect and a targeting mechanism, leads to an effective mechanism for visualizing and identifying cancerous tissue[44]. This can be combined with the hyperthermic abilities can lead to theranostic particle systems.

2.4.2 Gold Nanorods

Gold nanoparticles have been developed and pursued due to the phenomena known as surface plasmon resonance, caused by the surface oscillations of electrons. This phenomena allows for the visualization of gold particles, and even allows for heating in response to pulsed lasers. However, these lasers are often in the UV-visible spectrum, which is effectively filtered out by human skin. To overcome this, gold nanorods were developed, which respond to wavelengths in the near infrared spectrum. These wavelengths are more effective at penetrating human skin, and thus a more effective system for intravenous drug delivery[45].

The one advantage that gold nanorods have over their magnetic counterparts is the precision with which they can be heated. The lasers used for gold nanorods can be targeted heating specific tissues, unlike the coils necessary for heating magnetic nanoparticles. This adds another level of targeting to further control the delivery of chemotherapeutics. However, this comes at a cost of cytocompatibility. At low levels gold particles are harmless, but as they accumulate in the body due to lack of a clearance mechanism the concentration builds to dangerous levels. Some coatings have done a great deal to improve this, but there is still a toxic level achievable by repeated treatments[46].

2.5 The Thermodynamics of N-Alkyl Substituted Acrylamides

The LCST of N-alkyl substituted acrylamides arises from a balance of enthalpic and entropic forces. Hydrogen bonds between the water and carbonyl groups of the polymer provide enthalpic benefits while the increase in organization they require results in increased entropy. As the temperature increases the balance between the enthalpic and entropic effect results in the LCST phase transition as the water/polymer system phase separates to decrease the entropy of the system.

2.6 Effects of Ionic Species

The development of NIPAAm like polymeric drug vehicles has required the use of ionic surfactants that interact in peculiar ways with the responsive polymers. There have been many investigations into the impact of surfactants on the LCST response of these hydrogels. As the collapse is initiated the surfactant begins to stabilize the transition, leading to a peak in the absorption of the surfactant into the hydrogel. This surfactant stabilization on its own is relatively harmless, with no change in swelling response when the same studies were performed with non-ionic surfactant. However, the ionic species included with SDS leads to changes in swelling response and LCST[47].

This reaction is easily explained when examining the effect of free ions in the solution. The inclusion of ions depresses the LCST and increases swelling response. This is a function of the interference of the water cages that are necessary to balance the hydrophilic and hydrophobic in an aqueous environment. The presence of these ions interferes with these water cages resulting in a decrease in the enthalpic contribution. This leads to a depression of the LCST and an increase in the ΔT. However, when the ions are kosmotropic the interaction is more complex resulting in two LCST responses, though the impact on the LCST still follows the same trend[48].

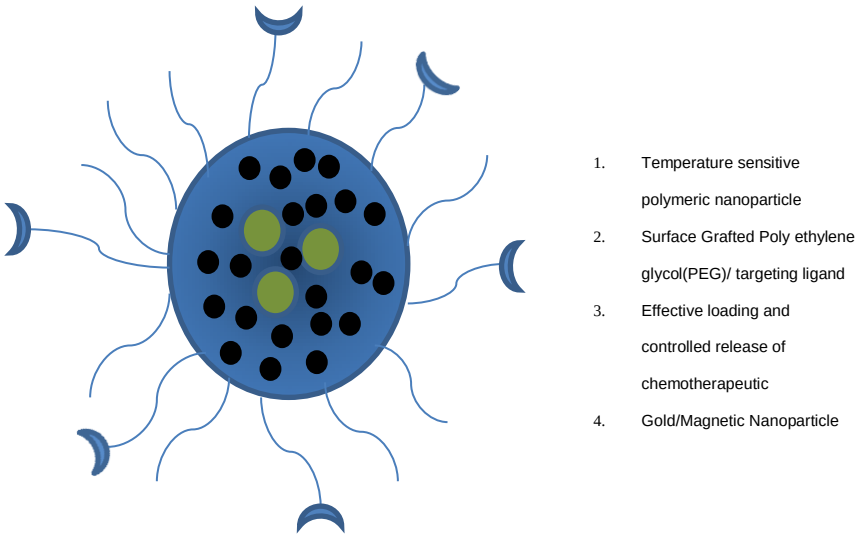

Illustration 2.1: Drawing of thermoresponsive nanocomposite loaded with model drug.

CHAPTER 3

Objectives

The overall objective of this work is to develop a full composite system for the externally controllable release of model chemotherapeutics. In order to achieve this objective this work is divided into categories in order to overcome many of the problems that are encountered with these systems. In that ilk the two major problems have been identified as biocompatibility and the polymer/drug interaction. This work will attempt to identify solutions to both of these issues and then bring them together with the other pieces of these nanocomposites to examine their impact on the system as a whole.

For the biocompatibility issue the solution that is necessary is addressing the complexities involved in the inclusion of long polymer chains of PEG to these stimuli responsive particles. This work will attempt to provide a solution to this problem that is both simple and effective. This work will depend heavily on the success of comonomer incorporation, and identifying a critical surface PEG concentration necessary to stealth these particles.

The bigger issue with these systems is the premature release of drug payload due to the poor drug/polymer interaction. Since the loading and retention of drugs in these systems is mostly dependent on diffusion, improving the partitioning of drugs into these hydrogels would be a big step in improving the loading and release. However, due to the aqueous nature of hydrogels. In order to address this issue the drug/polymer interaction aspect of this work will be broken down into two sections. First the inclusion of comonomers will be examined in order to see if a simple mechanism exists to improve drug uptake and retention, this will be covered in Chapter 5. Second, a complex core/shell system will be developed in attempt to provide a temperature sensitive pumping mechanism inside a drug compatible core.

The core shell system will further be divided into to methodologies to achieve this solution. First will be a traditional sequential free radical polymerization in order to grow the shell on the core, and will be discussed in chapter 6. The second method will be the development of amphiphilic hydrophobic/hydrophobic/hydrophilic block copolymers that will be cross-linked after self-assembly into micelles, the topic of chapter 7.

CHAPTER 4

Surface Hydrolysis Mediated PEGylation of P(NIPAAm-co-AAm) Nanogels

4.1 Background

The application of nanoparticles to intravenous drug delivery depends greatly on the circulation half-life. This is a necessity for particles of all types, as their increased size leads to their immediate attack via the RES. Systems based on functionalized amides, such as NIPAAm, are stable to the point of not being able to react with many of the functional PEG groups available, requiring the addition of a reactive comonomer. However, the inclusion of these functional groups results in significant modification of the temperature response, and potentially introduces undesirable pH sensitivity[6].

In order to overcome the problems inherent with the copolymerization of many of these PEG comonomers and other charged functional groups we turn to a copolymer that has proven to both have little to no pH responsiveness as well as a positive impact on the swelling response of NIPAAm based nanogels. P(NIPAAm-co-AAm) nanogels prepared at a molar feed ratio with 15%-20% AAm were shown to increase in the overall swelling response; at the same time the LCST was shifted up to 37- 39ºC [35].

AAm is susceptible to is hydrolysis, under extreme pH and temperatures AAm can be converted to AA in the presence of water. Under normal conditions this is not beneficial, as it leads to the distribution of AA throughout the nanoparticle. The syneresis of PNIPAAm can be used to protect the amide groups in the core of the particles. This protection is attained by the expulsion of water, preventing hydrolysis. By triggering the response and then exposing the hydrogels to an

extreme pH, the AAm near the surface of the nanogel can be localized due to the increased concentration of water at the surface[49].

Hoare and Pelton have proven this result with P(NIPAAm-co-AAm) with AAm at a 10% molar feed concentration of the total monomer feed. In their studies, they demonstrate the relative hydrolysis of P(NIPAAm-co-AAm) gels performed at 30ºC and 60ºC and a range of pH conditions. Increasing temperature increases the rate and extent of hydrolysis; however they proved that the increased temperature resulted in lower hydrolytic conversion. The effect of titration speed was further proof that there was a localization of the hydrolyzed groups near the surface of the nanogels. As the speed of the titration of the 30ºC hydrolyzed system increased the concentration of carboxylic acid groups determined decreased. Comparatively, the 60ºC hydrolysis sample showed no dependence on the rate of titration. This result speaks to the dependence of ion diffusion into the nanogels. Meaning the time scale of diffusion to the core of the particles is a significant burden. The critical titration step time is equivalent to the average depth of the functional group[49].

This conversion of surface localized acrylic acid provides a simple mechanism for PEGylation with an amine terminated PEG and EDC/NHS chemistry. This technique also lends itself to the concentration of PEG chains to the surface, limiting its impact on the overall swelling response of the nanoparticle.

4.2 Materials and Methods

4.2.1 Nanogel Synthesis

NIPAAm from Scientific Polymer, Ammonium Persulfate (APS), AA, AAm N'N'-Methylenebisacrylamide (MBAM), from Sigma Aldrich (St Louis, MO), and Sodium Dodecyl Sulfate (SDS) from Fisher Scientific (Pittsburgh, PA) were all used as received. In a standard

reaction NIPAAm, the comonomer (AA or AAm), MBAM, and SDS were mixed together in 18.2 MΩcm water in the amounts specified in the table below for the 20% comonomer nanogels. This solution was purged for 30 minutes at 70ºC with Nitrogen under 200 rpm stirring with a football shaped stir bar in a round bottom flask. Then APS dissolved in 18.2 MΩcm water was injected and the reaction was allowed to progress for 2 hours under constant stirring. The reaction was then terminated by exposure to air. Nanogels not destined for surface hydrolysis were then purified against 18.2 MΩcm water for two weeks with twice daily water changes then freeze dried.

Component	mol % of total solution	% Monomer mol feed
NIPAAm	0.020%	71%
AAm or AA	0.0072%	20%
MBAM	9.0×10^{-5}%	9%
SDS	1.9×10^{-5}%	NA
Water	99.8%	NA

Table 4.1: Molar composition of nanogel synthesis.

4.2.2 Surface Hydrolysis

Sodium hydroxide and hydrochloric acid from Fisher Scientific (Pittsburgh, PA) were used as received. Unpurified nanogel solution is heated to 60ºC and then mixed in equal volumes with 1N sodium hydroxide. This system was allowed to set for 3 days under constant stirring. The solution was sonicated at 60ºC twice daily to break up aggregates. At the end of 3 days an equivalent volume of 1N hydrochloric acid is added to bring down the temperature and pH simultaneously. The pH is then adjusted with 0.1 N hydrochloric acid to a pH of 7. The nanogel

product was then dialyzed against 18.2 MΩcm water for two weeks with twice daily water changes then freeze dried.

4.2.3 EDC/NHS PEG Attachment

N-Hydroxysuccimide (NHS) and 1-Ethyl-3-(3-dimethylamiopropyl)carbodiimide (EDC) from Thermo Scientific (Waltham, MA), and NH_2-PEG from Lysan Bio. (Arab, AL) were all used as received. In a standard reaction carboxylic acid containing particles were suspended in Borate buffer at a pH of 8.4 at a concentration of 4.7 mg/mL. EDC and NHS were suspended in Borate buffer at a concentration of 25 mM and amine-PEG was suspended at a concentration of 20 mM. Then 3 parts particle solution, 3 parts PEG solution, and 2 parts NHS solution are mixed. Two parts EDC solution is added and the solution is allowed to react overnight. It was then dialyzed against 18.2 MΩcm water for 1 week with twice daily water changes to remove unreacted PEG and excess buffer then freeze dried.

4.2.4 Zeta Potential and Swelling Measurements

Zeta potential and particle size were measured using a Malvern Zetasizer ZS (Malvern, UK). The effect of temperature on swelling size was collected by dissolving freeze dried particles in 1 mL f DI water and adjusting the temperature by 3ºC increments and then allowed to equilibrate for 60 seconds. Temperature was ramped 20ºC-59ºC-20ºC to examine the effect of hysteresis on the samples particle size.

4.2.5 Titrations

Titrations are completed using an autotitrator (Hanna instruments HI902c, Carrolton, TX). A known mass of nanoparticles were suspended in 5 mM KCl. The samples were then auto-titrated with a 0.01N NaOH solution. The exact normality of the titrant was determined by titration of a known mass of potassium hydrogen phthalate.

4.2.6Protein Adsorption Studies

To determine the effectiveness of the PEGylation reaction, these systems were incubated with model proteins, primarily Bovine Serum Albumin (BSA). Unmodified, AA, and PEGylated particles were incubated at 1 mg/mL in a 10 mg/mL BSA/ 1X PBS solution at 37ºC and 45ºC to compare the protein adsorption of swollen and collapsed particles. The particles and bound proteins were separated out via filtration through a 0.2 micron syringe filter, and their concentration left was determined by a micro BCA assay.

4.2.7 TEM Microscopy

Images were obtained on a Transmission Electron Microscope (FEI Tecnai, Hillsboro, OR) operating at 80 kV. Carbon coated copper grids (400 mesh) were plasma treated using an Emitech Glow Discharge instrument to render them hydrophilic prior to adding 5 µL of the nanoparticle suspension. After 30 seconds, the nanoparticle suspension was wicked off using Whatman 1 filter paper. The particles were negatively stained by placing a 5 µL drop of 2% uranyl acetate on the particle-coated grid for 30 seconds before being wicked off with Whatman 1 filter paper.

4.2.8 QCM Studies Protein Adsorption Studies

A dynamic Quartz Crystal Microbalance (dQCM) (Q4, Biolin Scientific, Stockholm, SW) was used. In order to attach nanogels to the gold surface, first cysteine HCl was dissolved in a pH 8.4 borate buffer and passed over the surface to form a gold-sulfur bond. Then unattached cysteine was washed off. Carboxylic acid containing monomers were then mixed with 25 mg of EDC and 25 mg of NHS in pH 8.4 borate buffer then immediately flowed over the cysteine coated gold surface. Particles modified with PEG were synthesized as in the EDC/NHS PEG Attachent section above, only including a 1:10 ratio of sulfur-PEG-NH_2 (Laysan Biotech, Arab, AL) to the PEG-NH_2, both MW 2000. These particles were bound by suspension in a Borate buffer, pH 8.4

then flowed over the gold surface. Unattached particles were washed off with 1X PBS. Particle modified surfaces then had a 10 mg/mL BSA solution in 1X PBS until saturation was obtained, signified by a constant Δf. Then 1X PBS was flowed to wash off BSA not adsorbed to the particles.

4.3 Results and Discussion

4.3.1 Nanogel Copolymerization Synthesis and Swelling Response

NIPAAm was copolymerized with 15%, and 20% of total monomer feed percentages of both AAm and AA. The cross linker concentration (MBAM), was kept constant at 9% of the total monomer feed. Scanning electron microscope (SEM) images, seen in Figure 4.1, show the particles to be spherical. The swelling responses for these systems can be seen in Figure 4.2 and Figure 4.3 for AAm and AA respectively. Equilibrium swelling ratio (ESR) is defined as:

$$ESR = \left(\frac{d}{d_{50^{o}C}}\right)^{3}$$

The overall swelling response observed with 15 % AA is greater than that observed with AAm, however 20% AA significantly diminishes the swelling response while 20% AAm has no effect on the overall swelling response or the LCST. These results demonstrate the need for utilizing AAm as the comonomer for PEGylation, as comonomer levels as high as 20% are likely necessary and with AAm no effects are seen on the swelling response up to this point.

When 20% AAm is suspended in 1x phosphate buffered saline (PBS) an interesting phenomenon is observed as the temperature increases, as seen in Figure 4.4. The left graph shows aggregation of particles as the temperature increases above 40ºC. This effect is a function of an increase in the Van der Waals interactions being by the presence of ionic species. The temperature sensitive nature of this effect is due to the discharge of water from the polymer system resulting in a

change in the average chemical makeup of the system. This phenomenon is defined by the van der Waals net attraction parameter as seen in the equations below[50].

$$V_A = -\frac{A_{eff} d_s}{24h}$$

$$A_{eff} = \left(A_M^{1/2} + A_W^{1/2}\right)^2$$

$$A_M = \left[A_P^{1/2}\phi + (1-\phi)A_W^{1/2}\right]^2$$

Where d_s is the diameter of the swollen gel, h is the separation of two particles, and A_{eff} is the Hamaker constant. The Hamaker constant for a hydrogel sphere is a function of the Hamaker constants of the polymer, water, and the volume fraction of the hydrogel. As water is expelled the Hamaker coefficient increases closer to the value of PNIPAAm. This leads to an increase in the magnitude of the van der Waals attraction, signifying the aggregation of particles.

This phenomenon is entirely reversible, as raising and lowering the temperature returns the diameter of the particles to the same size in the DLS. These results are promising for *in vivo* applications, as the particles will remain suspended swollen up to 40ºC, which is the desired response for these systems as the temperature response needs to be above physiological temperature. The physiological aggregation will likely also not be a problem due to lower concentrations and the pulsatile flow of the blood stream.

4.3.2 Surface Hydrolysis and PEGylation

The surface hydrolysis of P(NIPAAm-co-AAm) was confirmed by measurement of Zeta potential after each step of the process. The results in Figure 4.5 show the Zeta potential results for 15% and 20% AAm formulations. The low initial magnitude of Zeta potential demonstrates the neutrality of the AAm polymer, with the only charge a symptom of surfactant that is necessary to stabilize the nanogels in solution. The Zeta potential greatly increases after the conversion of AAm to the anionic AA. After PEGylation, the Zeta potential drops to a mild level, showing that the PEG tethers are shielding the charge of the nanoparticle. Even though the

surface density of PEG tethers does not completely neutralize the Zeta Potential, it is still possible that the PEG tethers are able to efficiently stealth the particle. The negative charge measured could be due to the fact that the Zeta potential, in this instance, is measured by way of electrophoretic mobility. This means that even though the surface might be neutralized, the presence of deeper ionic species still result in a response to the current applied by the Zetasizer.

Figure 4.6 examines the temperature response of surface hydrolyzed 15% AAm and surface hydrolyzed 20% AAm. Both nanogel compositions exhibited a swelling response similar to their unmodified counterparts in Figure 4.2 in the range of 37ºC to 60ºC, which is the temperature range that will likely be utilized in application. The large error and unusual swelling response visualized up to 37ºC is potentially due to contaminates, though unlikely since the TEM micrographs show no signs of contaniments as seen in Figure 4.7. It could also be an experimental artifact due to large swelling ratios and inconsistencies in refractive index due to the core/shell nature of these particles. These inconsistencies are neutralized at higher temperatures as the particles begin their collapse.

This could also simply be the function of the large error observed, as it has been shown by others in the lab that ionic species tend to have larger errors in their swollen state, although this is a larger extent of this error than previously observed. These large error bars are troubling, however the swelling response from 37ºC to 45ºC remain intact, which is what is important for physiological application.

After PEGylation, the AA functional groups get capped resulting in a decrease in overall swelling as a shell of non-temperature responsive PEG containing PNIPAAm groups gets functionalized. However, the LCST remains unchanged and the swelling response is still sufficient for drug delivery purposes.

4.3.3 Carboxylic Acid Concentration

The titration results, listed in Table 4.2, match the expected results based on the work by Hoare and Pelton [50]. The 20% AAm and AA systems obey the predicted values rather closely, though there is the slight chance that the AA experienced the mass transfer limited titration phenomenon observed by the Hoare and Pelton. The result for 20% AAm could be a sign of hydrolysis beyond the surface, but the groups are probably still concentrated at the surface. This is confirmed by the minimal impact this observed on the swelling response seen in Figure 4.8.

Surface hydrolyzed 15% AAm studies followed the surface hydrolysis results closely, displaying a limited hydrolysis of only about 30% of the included AAm. 15% AA also demonstrates a limited inclusion of carboxylic monomers, as the titration indicates only 24% of the feed ratio is present in the final hydrogel. Again, this discrepancy could be due to mass transfer limitations during the titration; however it is a fairly large discrepancy considering the 20% AA system contained 72% of the feed ratio.

The titration of surface hydrolyzed P(NIPAAm-co-AAm) with 20% AAm surface modified with PEG shows that the PEG reaction capped about 37% of the available carboxylic groups, which falls in line with the fact that EDC/NHS reaction was performed in a alkaline solution which favors activation of the PEG-amines. This result matches the zeta potential measurements which show a drop of 45 ± 9% of the surface charge.

4.3.4 Cytotoxicity

These nanogels were measured for toxic impact against RAW 264.7 macrophages. The results are shown in Figure 4.14. These results show that none of the PNIPAAm based nanogels show any appreciable toxic effects, where all particles are statistically similar to the positive control up to a concentration of 1 mg/mL.

4.3.5 Protein Adsorption Studies

The protein binding studies showed no significant effect of PEGylation between PEGylated and unmodified AAm containing copolymers. However, there is significant reduction compared to its highly anionic counterpart, 20% AA. These results also indicate a negligible protein adsorption at physiological temperature, as the results show statistically insignificant binding. At higher temperatures the protein adsorption increases. This is counter-intuitive, as there is decreased surface area for adsorption and increased PEG density on the PEGylated nanogels. This can be explained by protein stability; however the more likely cause is the aggregation of the nanogels in ionic fluids. The aggregation, as observed in Figure 4.4 leads to potential entrapment of BSA. The surface hydrolysis mediated PEGylation did prevent a significant level of protein from adsorbing onto the particles, as the protein binding levels are statistically insignificant from no protein adsorption.

The dQCM studies are depicted in Figure 4.16. These studies show that there is a significant amount of protein adsorption on the p(NIPAAm-co-AA) particles, and though some of it does wash off, a large portion of it remains on the surface of these particles. In contrast, particles modified with PEG experiences a much smaller frequency shift, signifying less protein adsorption. Furthermore, the frequency shift returns to zero after a short period of time, showing no significant protein binding. The studies at 45ºC in Figure 4.17 show a similar result, with no significant binding to the P(NIPAAm-co-AAm) 20% AAm surface hydrolyzed and PEGylated sample, while the P(NIPAAm-co-AA) 20% AA sample has significant protein adsorption.

The dQCM studies do differ from the suspension studies, in that the increase in temperature led to a smaller adsorption of BSA compared to its 37ºC, at least for the non-surface modified sample. This confirms that the increase in protein adhesion seen in the suspension protein

binding studies is due to the aggregation, and not any increase in protein activity or other phemnoena.

4.4 Conclusions

The use of AA and AAm has been tested as potential routes for incorporation of carboxylic acid functional groups. AAm was proven to have less of an impact on the temperature response at relatively high comonomer concentrations than AA, as seen in the temperature response swelling curves. The particles synthesized are spherical and stable in pure DI water. The subsequent aggregation in aqueous solutions with physiologically relevant ionic strength is worrying but overall a non-problem, as the blood stream will keep the particles well mixed. However, this does prevent an understanding of the full swelling response in high ionic strength conditions.

The surface hydrolysis process was proven to have little to no effect on the structure of the nanogels, beyond what was intended. The particles remain structurally intact and retain the LCST and overall response to variations of temperature. The 15% AAm sample demonstrates a better response to the overall localization of the hydrolysis process, however the increased hydrolysis observed with the 20% AAm sample has no limiting impact on the temperature response as seen by other PEG grafting mechanisms.

The EDC/NHS surface modification mechanism was proven efficient enough to passivate the nanogels, even though the EDC/NHS scheme is a relatively inefficient means for PEG attachment, yielding only about a 45% attachment. That being said, the studies to characterize protein binding do show that PEG attachment effectively prevents protein adsorption. This shows that these systems should prove effective in an *in vivo* study to determine bioavailability and circulation half-life of this PEGylation scheme. This mechanism could also be adapted to

other neutral yet hydrolysable based systems to provide a noninvasive route for surface modification.

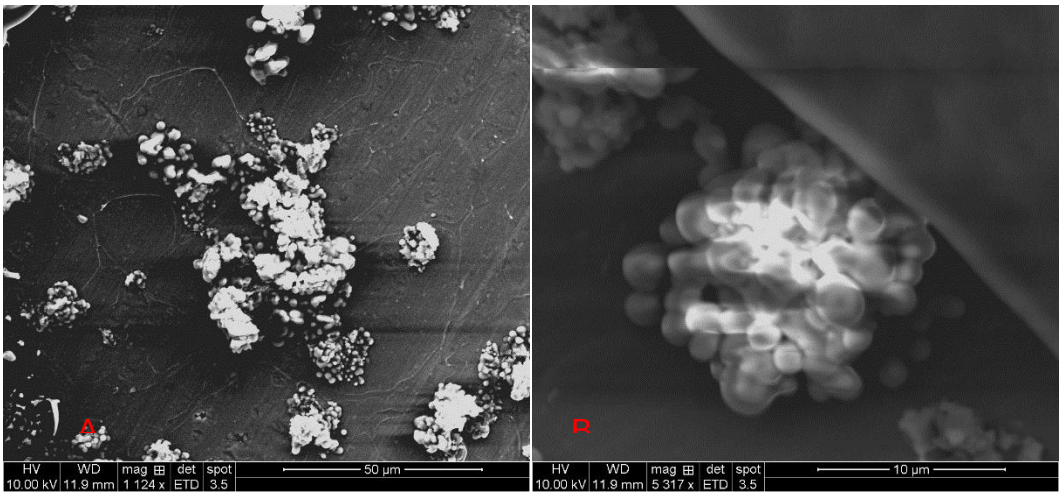

Figure 4.1: SEM micrographs P(NIPAAm-co-AAm) nanogels. A. 10% AAm. B. 20% AAm. Percentages are molar percentages of total monomer concentration in the feed.

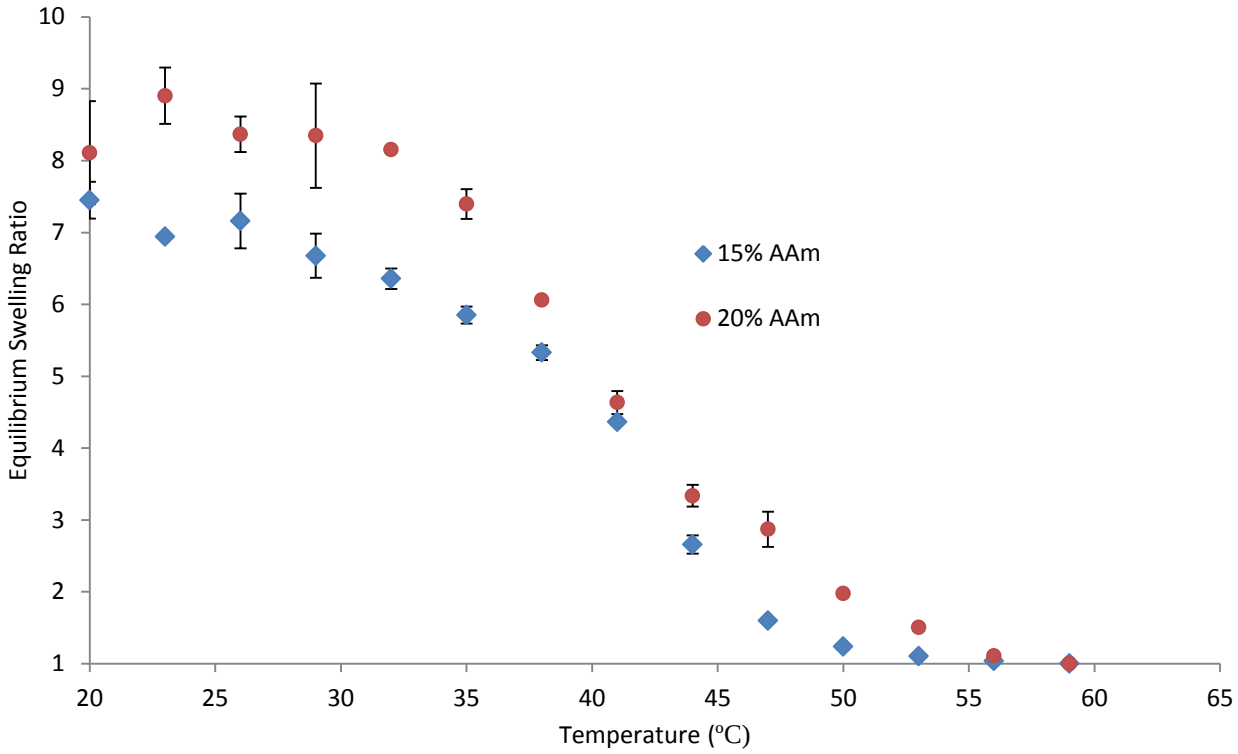

Figure 4.2: Equilibrium swelling ratio vs temperature of P(NIPAAm-co-AAm) nanogels prepared at different total monomer molar feed percentages. Percentages are molar percentages of total monomer concentration in the feed. (N=3)

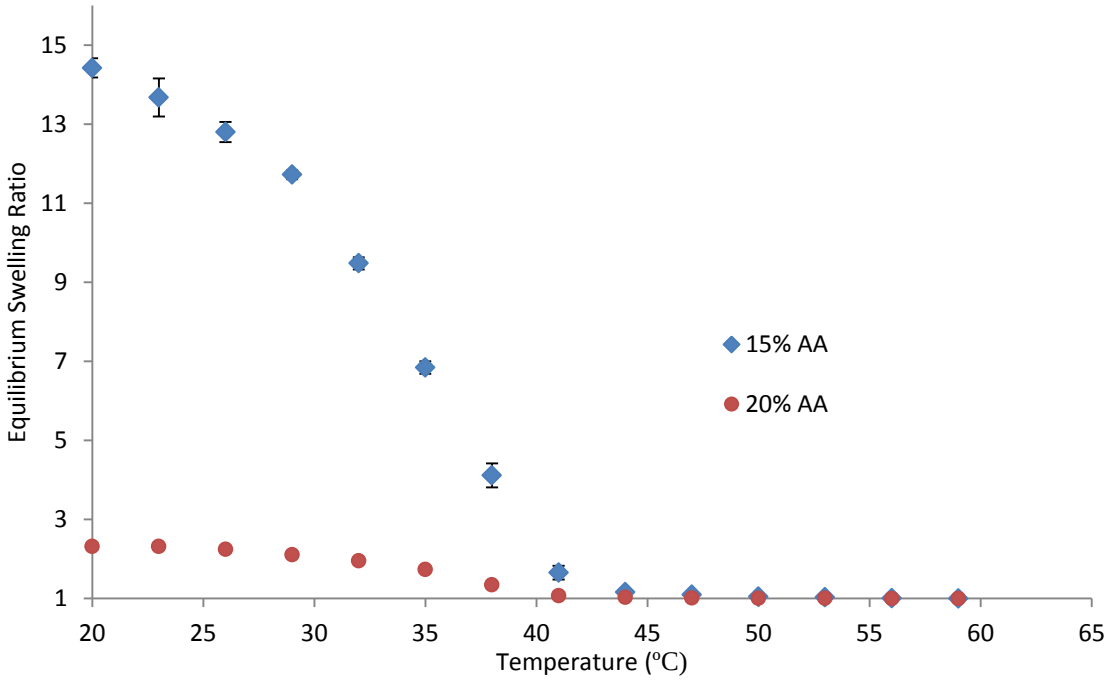

Figure 4.3: Equilibrium swelling ratio vs temperature of P(NIPAAm-co-AA) nanogels prepared at different total monomer feed percentages. Percentages are molar percentages of total monomer concentration in the feed. (N=3)

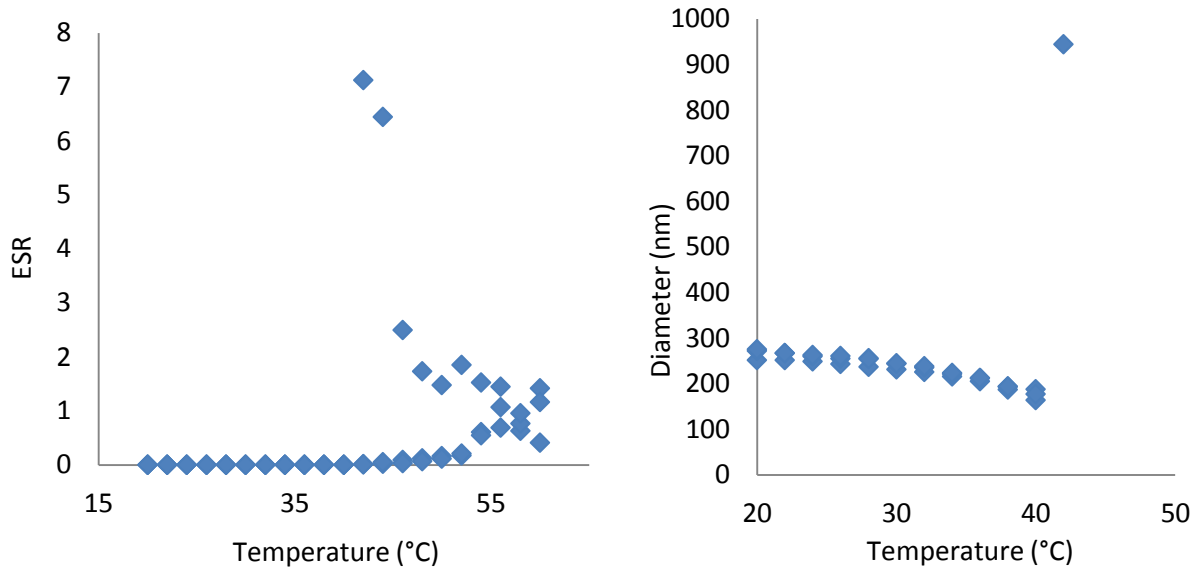

Figure 4.4: Equilibrium swelling ratio vs temperature of 15% AAm in P(NIPAAm-co-AAm) in 1x PBS. Percentages are molar percentages of total monomer concentration in the feed.

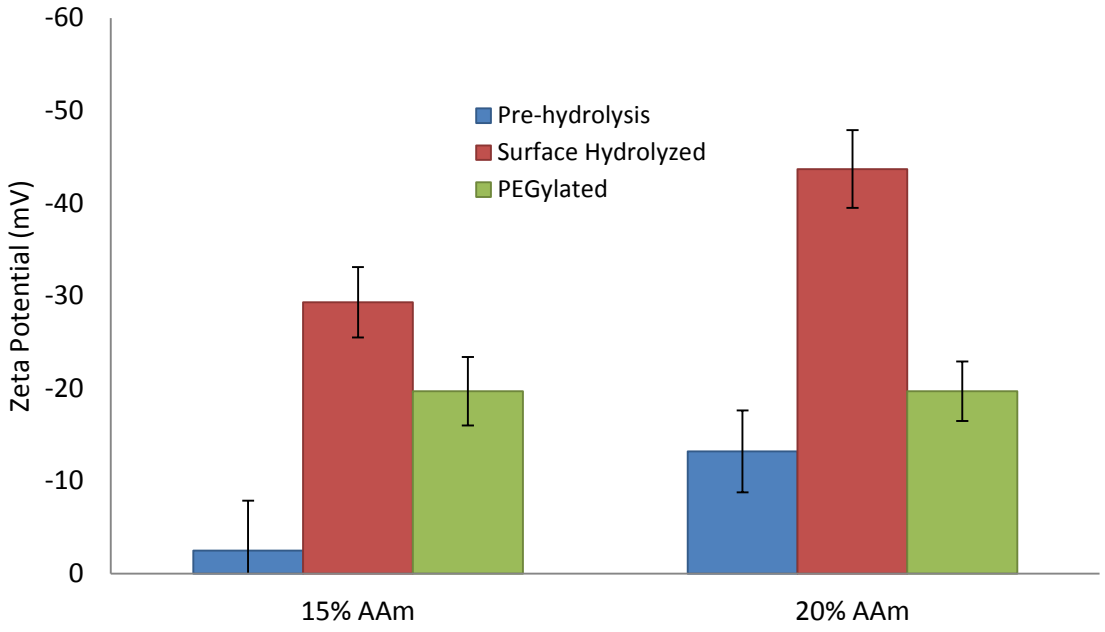

Figure 4.5: Zeta potential of P(NIPAAm-co-AAm) nanogels. Comparing surface charge of unmodified, surface hydrolyzed, and PEGylated nanogels. Percentages are molar percentages of the total monomer feed. (N=3)

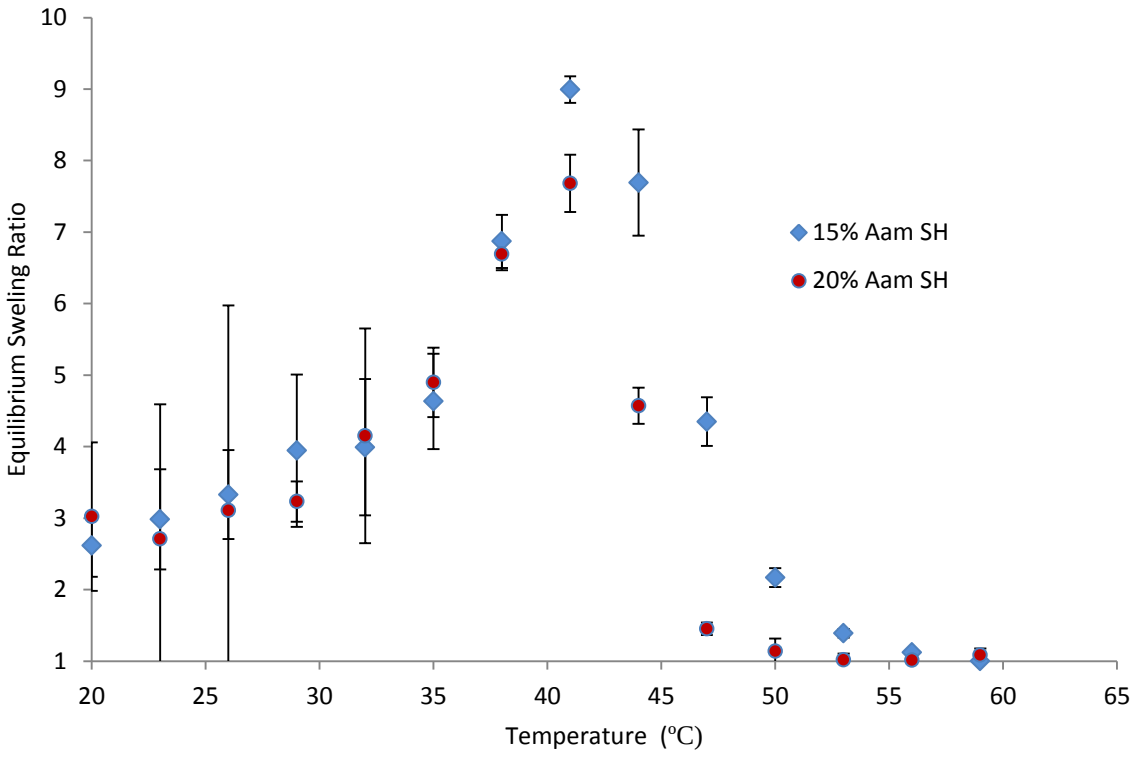

Figure 4.6: Equilibrium swelling ratio vs temperature of surface hydrolyzed P(NIPAAm-co-AAm) prepared with 15% and 20% AAm. Percentages are molar percentages of total monomer concentration in the feed. (N=3)

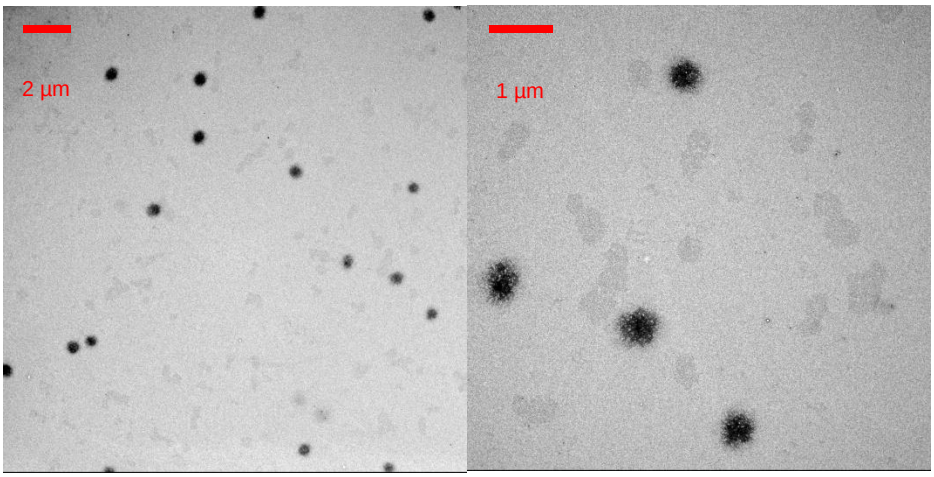

Figure 4.7: TEM micrgraphs of surface hydrolyzed 20% AAm, P(NIPAAm-co-AAm) nanogels. Percentages are molar percentages of total monomer concentration in the feed.

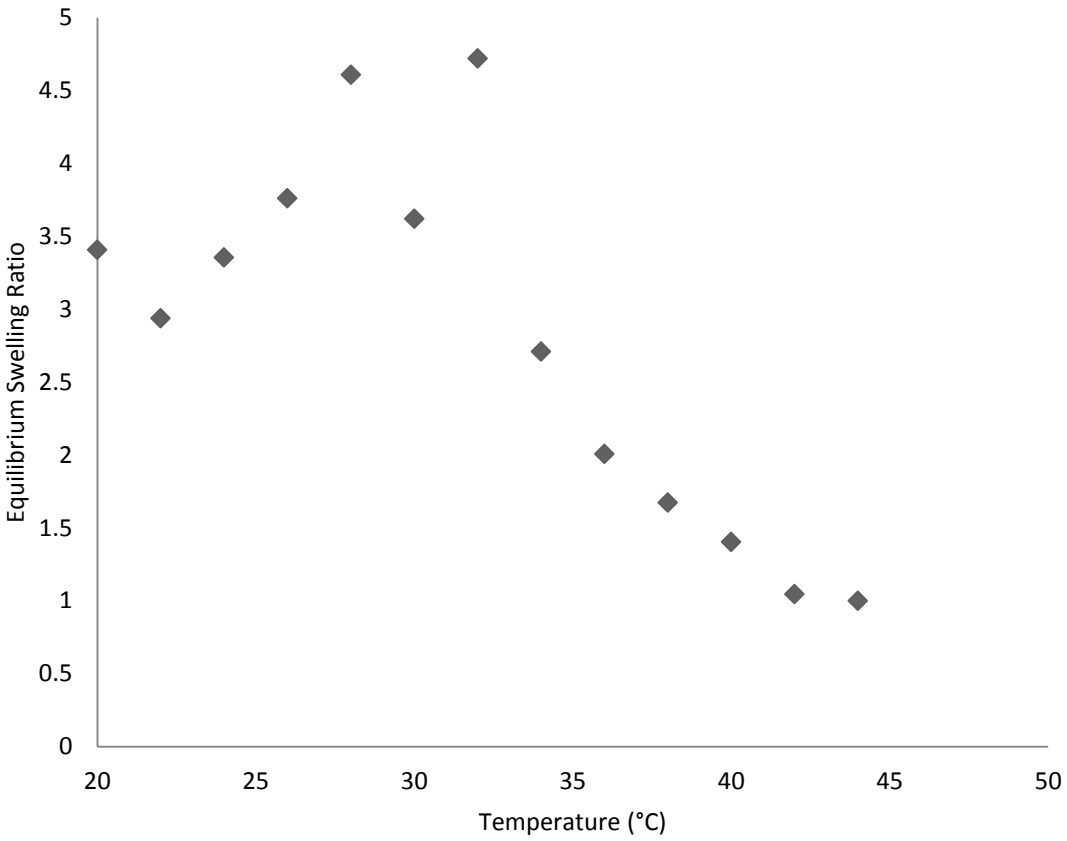

Figure 4.8: Equilibrium swelling ratio vs temperature of Surface Hydrolyzed 20% AAm P(NIPAAm-co-AAm) nanogels surface modified with 2000 MW PEG DLS. (N=3)

Polymer Type	Titration Result (mol acid/g nanogels)	Expected Result (mol acid/g nanogels)	% of Expected
P(NIPAAm-co-AAm) 20% AAm SH	1.1×10^{-3}	1.1×10^{-3}	100 %
P(NIPAAm-co-AA) 20% AA	1.3×10^{-3}	1.8×10^{-3}	72 %
P(NIPAAm-co-AAm) 20% AAm SH	4×10^{-4}	4×10^{-4}	100 %
P(NIPAAm-co-AA) 15% AA	3×10^{-4}	1.3×10^{-3}	24 %
P(NIPAAm-co-AAm) 20% AAm SH	7×10^{-4}	$<1.1 \times 10^{-3}$	NA

Table 4.2: Concentration of carboxylic acid functional groups in AA and surface hydrolyzed AAm PNIPAAm comonomers. Expected values from feed ratios and assuming a 70% hydrolysis from surface hydrolysis.

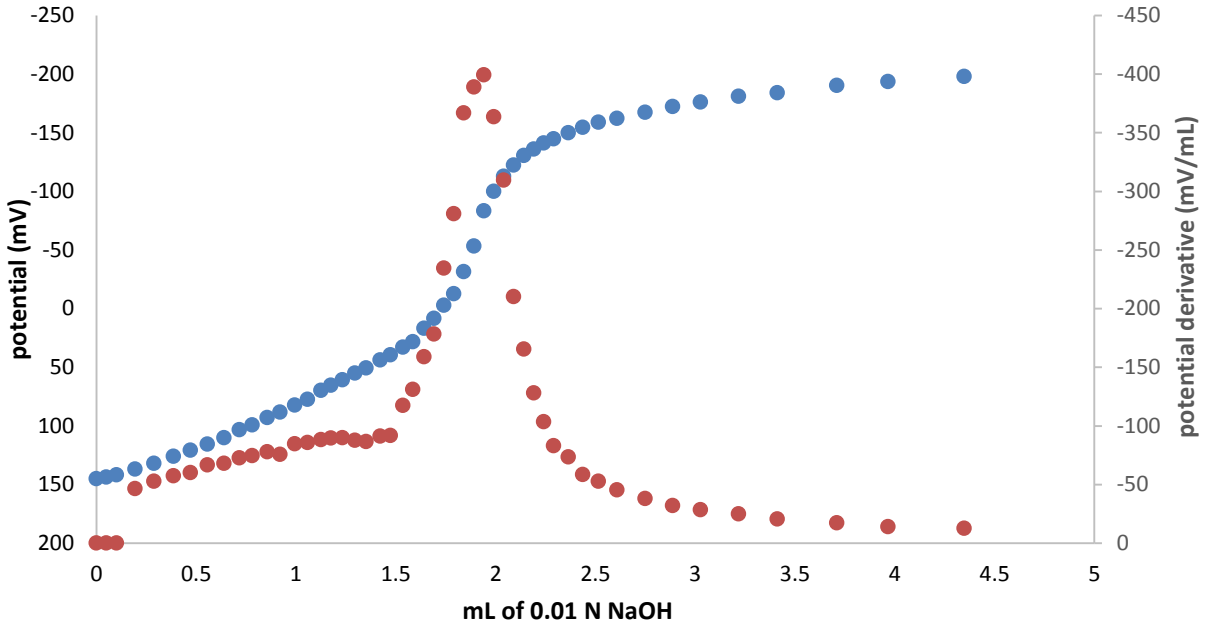

Figure 4.9: Titration of P(NIPAAm-co-AAm) 20% AAm surface hydrolyzed.

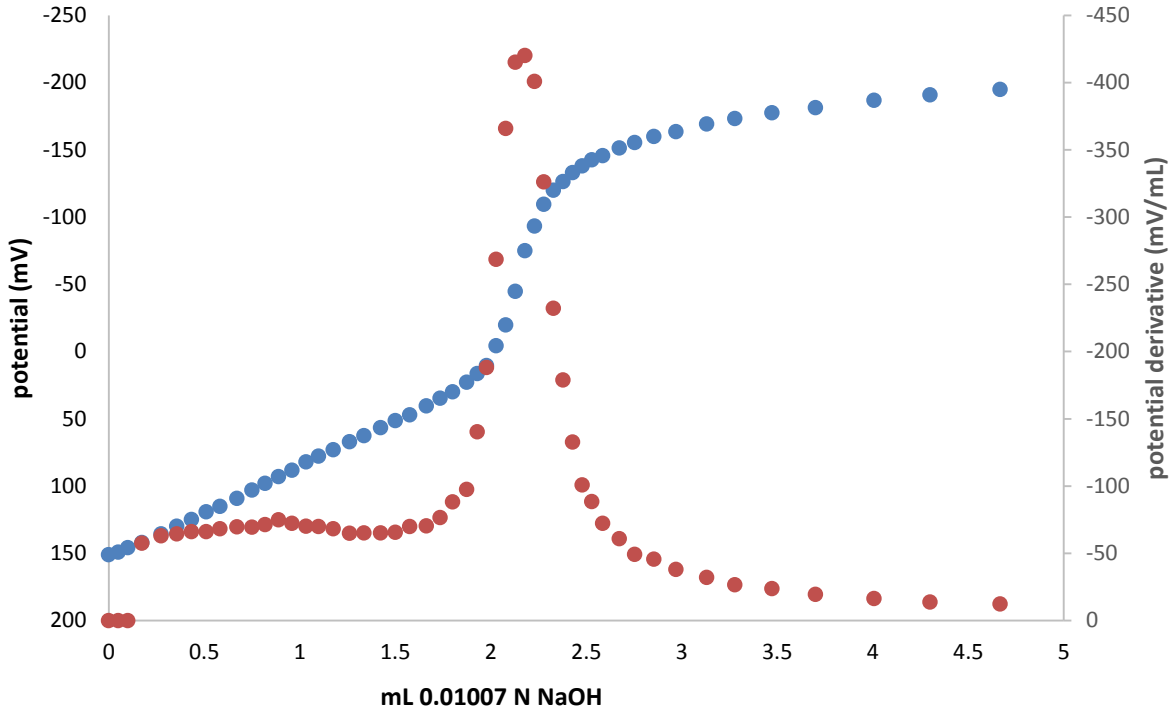

Figure 4.10: Titration of 20%AA P(NIPAAm-co-AA).

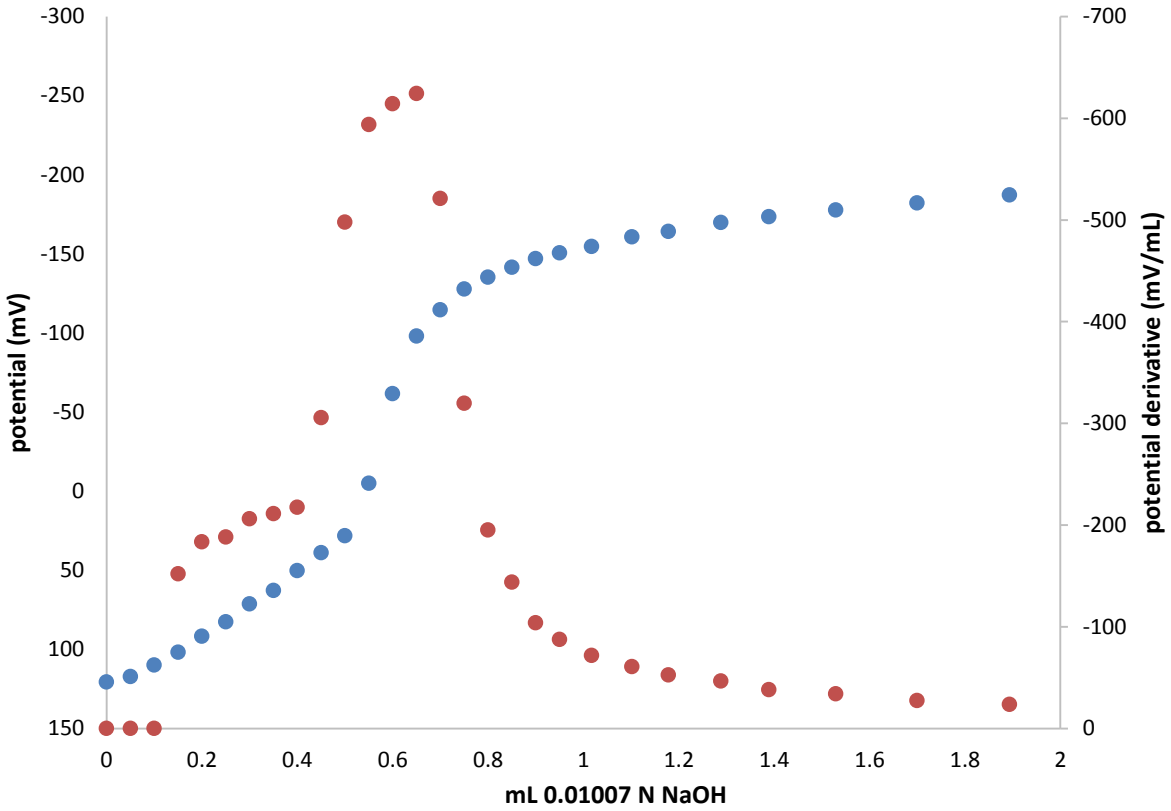

Figure 4.11: Titration of surface hydrolyzed 15% AAm P(NIPAAm-co-AAm).

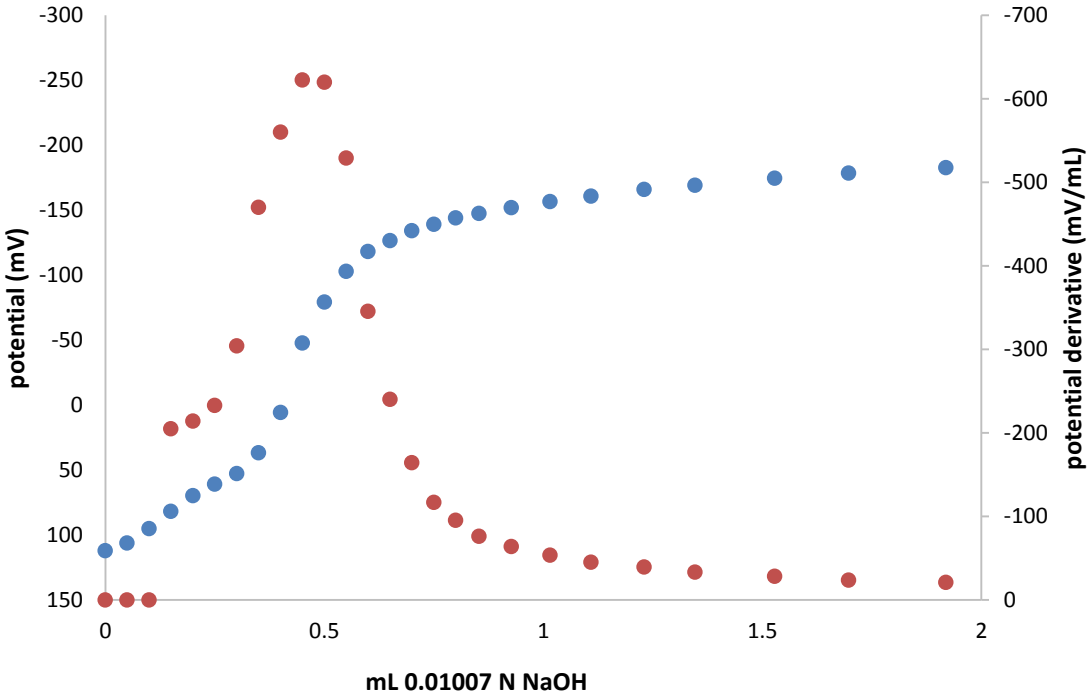

Figure 4.12: Titration of 15% AA P(NIPAAm-co-AA).

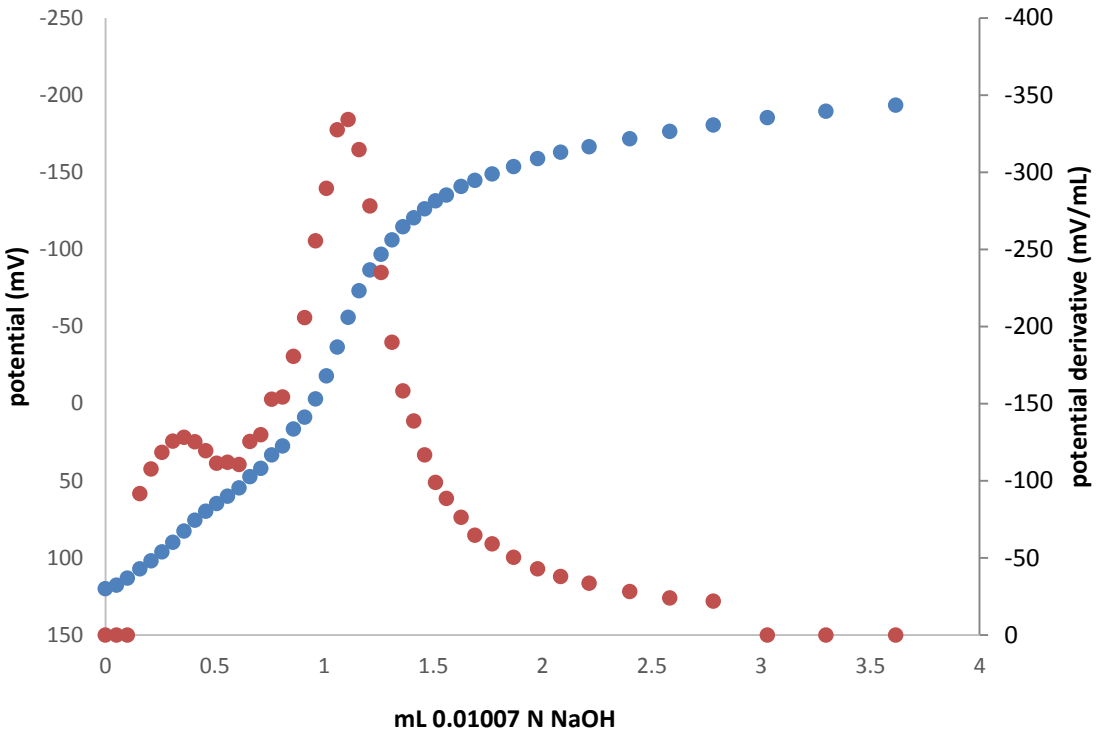

Figure 4.13: Titration of Surface Hydrolyzed 20% AAm P(NIPMAAm-co-AAm) surface modified with 2000 MW PEG.

A

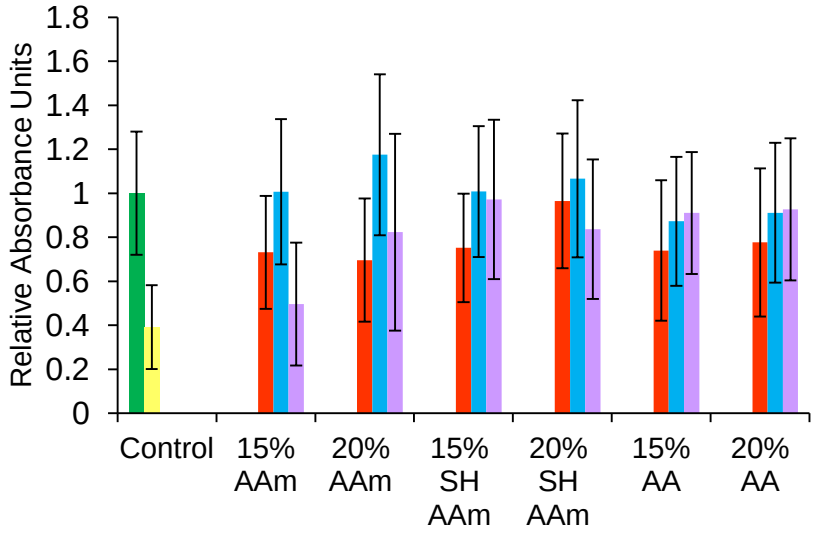

B

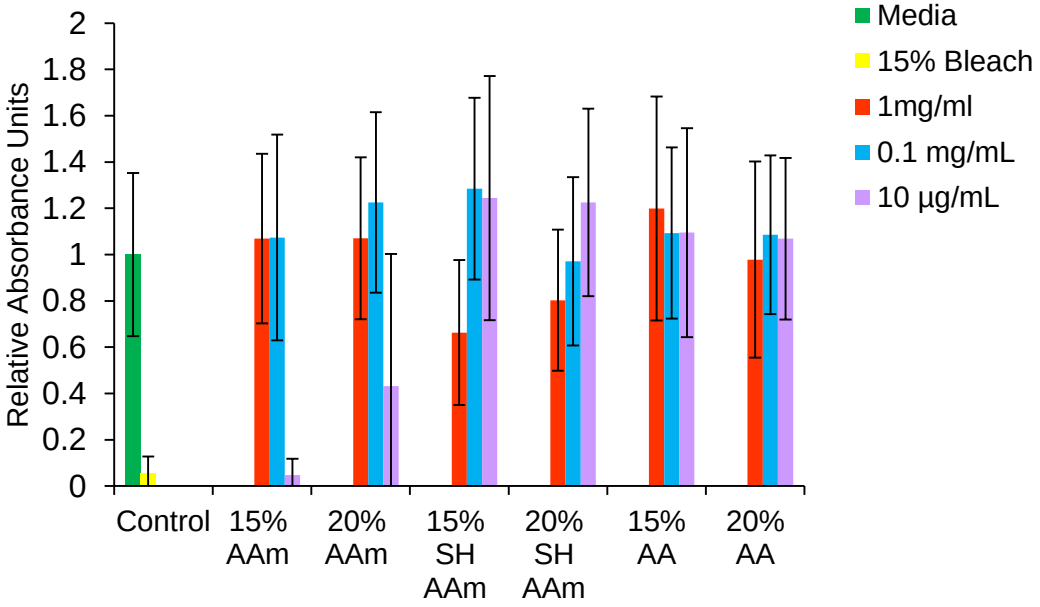

Figure 4.14: MTS proliferation assay of P(NIPAAm-co-AAm) and P(NIPAAm-co-AA) nanogels with RAW 264.7 macrophages. N=4. A. 2 hours. B. 24 hours. Percentages are molar percentages of total monomer concentration in the feed. (N=4)

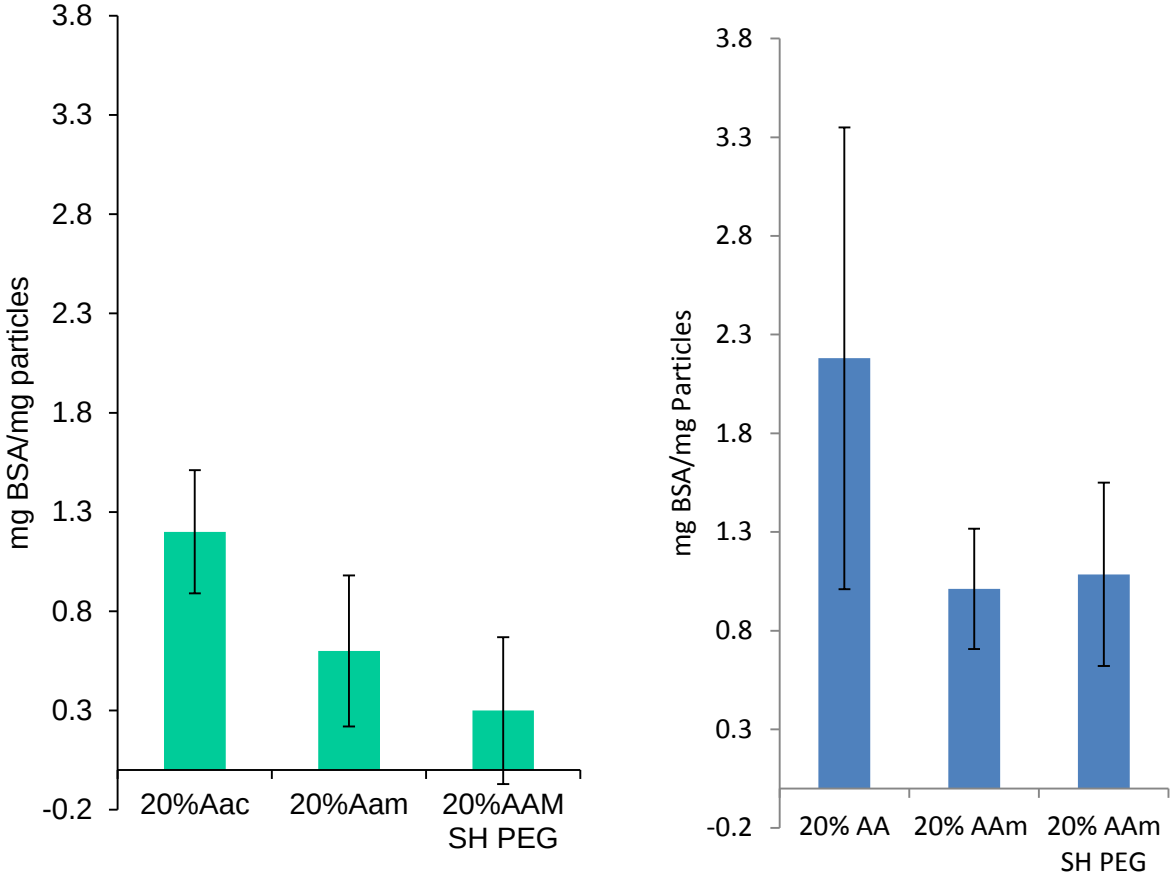

Figure 4.15: Mass of protein adsorbed to P(NIPAAm-co-AAm) and P(NIPAAm-co-AA) nanogels before and after PEGylation. Percentages are molar percentages of total monomer concentration in the feed. (N=3)

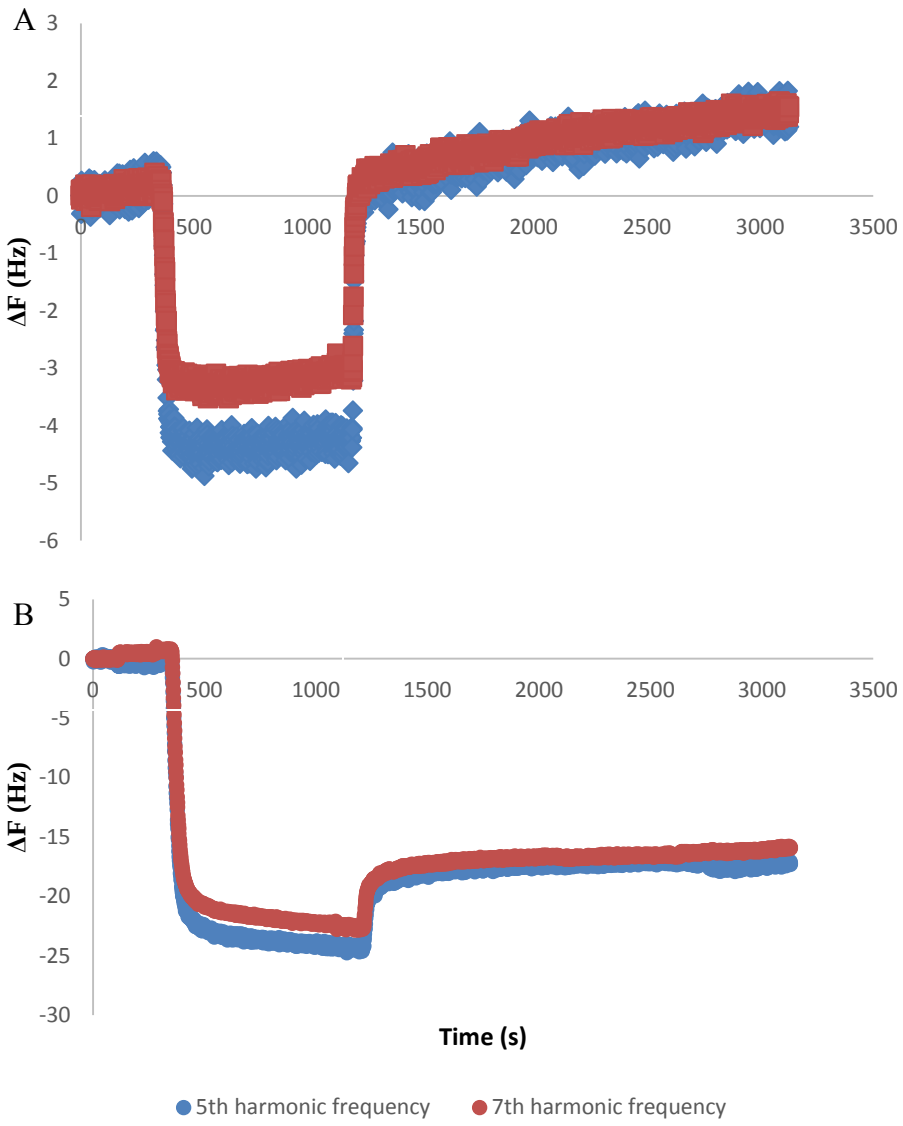

Figure 4.16: QCM Protein binding study of A.P(NIPAAm-co-AAm) 20% AAm surface hydrolyzed and PEGylated and B. P(NIPAAm-co-AA) 20% AA at 45ºC. A solution of 10 mg/mL BSA was introduced at the 400 second mark then washed off at the 1200 second mark.

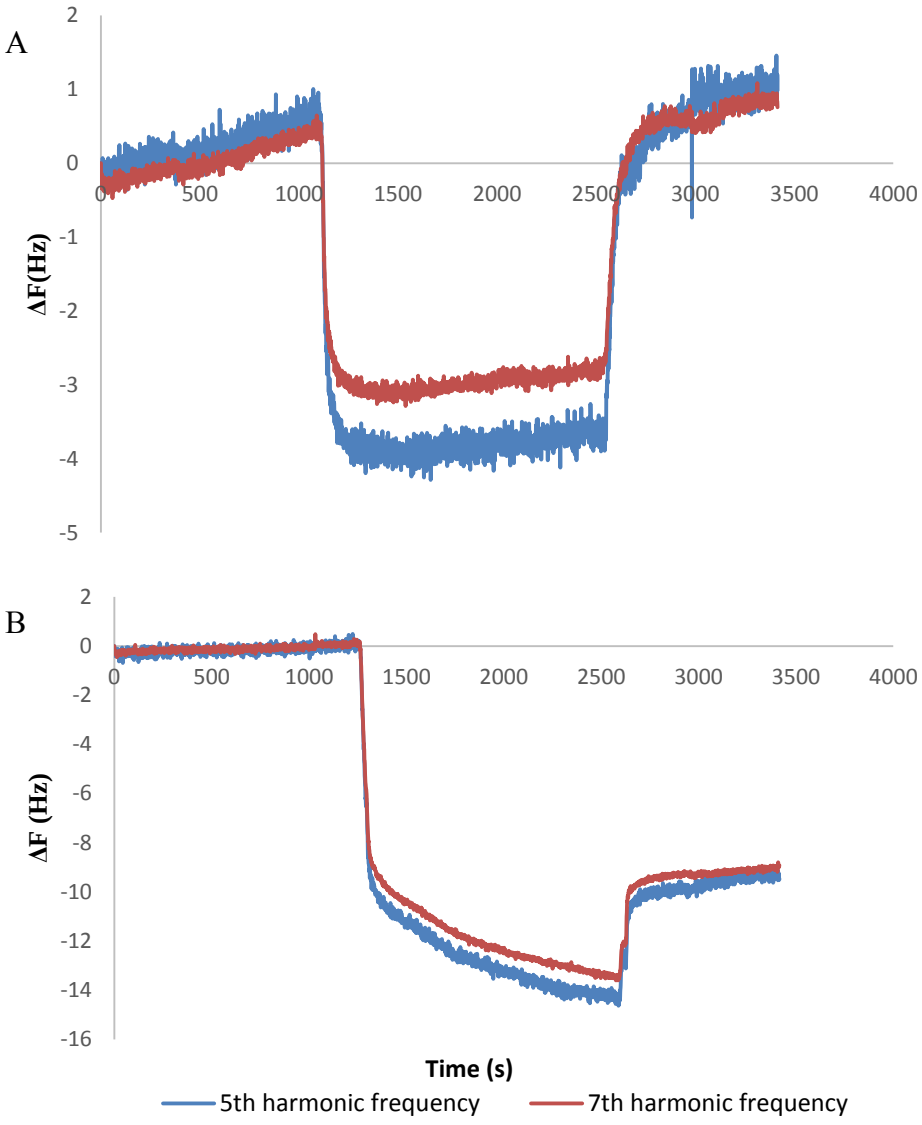

Figure 4P: QCM Protein binding study of A.P(NIPAAm-co-AAm) 20% AAm surface hydrolyzed and PEGylated and B. P(NIPAAm-co-AA) 20% AA at 37ºC. A solution of 10 mg/mL BSA was introduced at the 400 second mark then washed off at the 1200 second mark.

CHAPTER 5

Drug Delivery From PNIPMAAm Homo and Copolymers

5.1 Background

The use of NIPMAM as a monomer to prepare physiologically relevant temperature sensitive polymers is an attractive premise for two reasons. First, the critical response of PNIPMAAm does not begin until the temperature is well above physiological temperature (37ºC). Secondly, the only criticism is the necessity of attaining temperatures that could induce hyperthermia in order to actuate drug release[51]. This calls for copolymerization to depress the LCST response of NIPMAM based nanogels.

NIPAAm has been copolymerized with a variety of monomers with different traits, including hydrophobic, hydrophilic, and ionic traits. Figure 5.1 shows the general trends for how incorporation of different commoners impacts the LCST of PNIPAAm based copolymers. In general the more hydrophobic the copolymer the lower the LCST drops. Conversely, the addition of hydrophilic comonomers tends to increase the LCST of PNIPAAm based systems[52].

For example copolymerization with AAc increases the LCST as mol% is increased while the addition of butyl methacrylate (BMA) lowers the LCST. The decline/increase of the LCST response with respect to the incorporation of the polymer is a linear trend, with the slope dependent primarily on the relative increase of hydrophilicity that the comonomer imparts. For example the inclusion of ionically charged AA imparts a far greater increase in the LCST response as compared to AAm. Theoretically, the same should be true for NIPMAAm copolymer nanogels.

This would be advantageous for the delivery of hydrophobic drugs, as used in chemotherapy, as the inclusion of more hydrophobic pockets could improve the inclusion of hydrophobic drugs.

5.2 Materials and Methods

5.2.1 Nanogel Synthesis

NIPMAAm, APS, tert-butyl methacrylate (TBMA), Phenyl Methacrylate (PhMA), ethylene glycol phenyl ether acrylate (EGPhA), N-Vinyl Pyrrolidone (NVP), and MBAM, from Sigma Aldrich (St Louis, MO); and SDS from Fisher Scientific (Pittsburgh, PA) were all used as received. In a standard reaction NIPMAAm, the comonomer, MBAM, and SDS were mixed together in 18.2 MΩcm water in the amounts specified in table 5.1 for the 20% comonomer nanogels. This solution was then purged for 30 minutes at 70ºC with Nitrogen under 200 rpm stirring with a stir bar in a round bottom flask. Then APS dissolved in 18.2 MΩcm water was injected and the reaction was allowed to progress for 2 hours under constant stirring. The reaction was then terminated by exposure to air. The resultant suspensions were then dialyzed against 18.2MΩcm water for 2 weeks with twice daily water changes. All comonomer percentages reported in this section are molar feed ratios to total monomer, including crosslinker.

Component	mol % of total solution	% monomer mol feed
NIPMAM	0.020%	71%
TBMA or NVP	0.0072%	20%
MBAM	9.0×10^{-5}%	9%
SDS	1.9×10^{-5}%	NA
Water	99.8%	NA

Table 5.1: Molar composition of nanogel synthesis.

5.2.2 PARTICLE SIZING

The effect of temperature on particle size was measured using a Malvern Zetasizer ZS (Malvern, UK). The data was collected by dissolving freeze dried particles in 1 mL of DI water and adjusting the temperature by 3ºC increments and then allowed to equilibrate for 60 seconds. Temperature was ramped 20ºC-59ºC-20ºC to examine the effect of hysteresis on the samples particle size.

5.2.3 LOADING

5-flurouracil (5-FU) and Fluorescein from Sigma Aldrich (St. Louis, MO) were used as received. The loading procedure involves incubating purified and freeze dried particles in 1xPBS with the model drug at known concentrations. Samples were diluted with DI water, centrifuged for 10 minutes at 14,000 rpm in a microcentrifuge to collapse particles out of solution. The supernatant was removed and measured by a BIO TEK Synergy HT plate reader at 350 nm and 290 nm for fluorescein and 5-FU respectively. The resultant concentration was subtracted from the initial concentration and the difference is determined to be the total amount loaded into the particles. At the end of the study a final loading is determined and particles are washed 3 times with 18.2 MΩcm water and then freeze dried.

5.2.4 Pyrene Fluorescence

Pyrene was initially dissolved in acetone at a concentration of 0.2 mg/mL. 10 µL of this solution was then dropped into a 96 well plate and the acetone was allowed to evaporate in a fume hood. 200 µL of particles at a concentration of 0.1 mg/mL was then added to the wells and allowed to mix overnight. These samples were then read in a Biotek Cytation 3 plate reader at an excitation wavelength of 336 nm and emission at 373 nm and 383 nm.

5.2.5 Partition Coefficient Studies

DOX in water at a concentration of 1 mg/mL was mixed with an equal volume of particles at a concentration of 1 mg/mL both at 37ºC. This suspension was then held at 37ºC for 2 hours, to allow equilibration. All particles and a control solution were then filtered through a 0.2 µm filter to remove particles. These samples were then measured at a wavelength of 450 nm to determine the concentration of drug left after filtration.

5.2.6 Cytotoxicity

Particle cytotoxicity was determined using L929 fibroblasts as model cells. Cells were initially grown in Dulbecco's Modified Eagle Medium (DMEM) with 10% fetal bovine serum (FBS) with phenol red. All cells were allowed to be passaged three times before studies were performed. Cells were grown for 24 hours at a seeding density of 2.0×10^4 cells per well. The media was then replaced with phenol red free media containing 2% FBS with particles at varying concentrations. Media containing no particles and a 15% bleach solution were used as controls. These solutions were allowed to incubate with particles for 2 and 24 hours and then cytotoxicity was measured using and MTS assay.

5.3 Results and Discussion

5.3.1 Effect of SDS Concentration

Figure 5.2 demonstrates the effect of SDS concentration on particle size and batch-to-batch variability The increase of the surfactant concentration leads to a linear decrease in the size of the particles and a decrease in variability between batches. Below 3E-4 mol % SDS the size levels off and is highly reproducible. This is likely due to a limited effect of variations in the SDS:Monomer ratio. Figure 5.3 examines the impact of the particle size on cytotoxicity; however there is no significant cytotoxicity of any PNIPMAAm nanogels.

5.3.2 Swelling Response of PNIPMAAm Copolymers

The temperature dependent swelling results from synthesis of nanogels with different comonomers are summarized in Table 5.3. The graphs of the swelling response of the different comonomers as well as their sigmoidal fit (as described by Equation 5.1) are graphed in figures 5.4-5.13. The fit of the sigmoidal fit provides a quantitative measurement of the sharpness of the temperature response in the form of the value of the exponent (p).

$$ESR = \frac{ESR_{max} - 1}{1 + (\frac{T}{T_{LCST}})^{P}} + 1 \qquad \text{Equation 5.1}$$

The addition of all comonomers has a negative impact on the overall swelling response. They also diminish the sharpness of the response as seen by the fit's sigmoidal exponent, with the exception of 10% TBMA. However, this is mildly uncertain as the fit is dubious due to the invalidation of the first 10 points of the curve for the model fit. In all instances increasing the comonomer decreases the sharpness of the response.

All comonomers decrease the particle size, though the hydrophilic comonomers (AAm and EGPhA) increase particle size as the concentration increases while the hydrophobic comonomers (TBMA and PhMA) have the inverse effect. Though there are many factors that could impact the particle size, including purity and polymer reaction kinetics, these trends do exist outside of the batch-to-batch error observed in Figure 5.2.

The shift of the LCST of PNIPMAAm's copolymers does not follow the same trend seen for PNIPAAm in Figure 5.1. Hydrophilic comonomers seem to decrease the LCST while the hydrophobic comonomer, TBMA, raises the LCST slightly, which is the inverse to the trends observed with PNIPAAm [53]. The shift in the LCST response due to the inclusion of the

hydrophilic comonomers is likely another symptom of the decrease of the sharpness of the temperature response. The elongation of the swelling curve results in the shift of the LCST. This is also seen for the other hydrophobic comonomer used, PhMA, which results in the greatest shift of the LCST. As seen in their swelling curves, all of the nanogel systems achieve total collapse at or around 50ºC, while their collapse onsets vary from 30ºC-40ºC. This wide range of onsets leads to different midpoints in the line, which causes the shifts observed in the LCSTs.

Copolymerizations with TBMA demonstrated flat repeatable swelling responses, as exhibited by their small error bars and linear ESR above the LCST. The 10% TBMA sample in Figure 5.4 exhibits a linear increase in ESR until its critical onset at 41ºC. 10% TBMA shows one of the more drastic collapses between physiological temperature and 47ºC, seeing a 70% change in volume in this range. Increasing the comonomer concentration to 20% TBMA eliminates the steady increase, as the swelling remains constant until 41ºC where collapse begins, and collapses to about 50% of its initial volume around 47ºC. The TBMA systems have the highest exponent values of the comonomer nanogels, signifying that the addition of these hydrophobic comonomers results in the sharpest response to variation of temperature.

Copolymerization with PhMA greatly reduces the onset temperature of the collapse to 30ºC, however full collapse still takes until 50ºC, as seen in Figure 5.5 and 5.6. This could be due to a number of factors, but is likely due to variations of the comonomer concentration as the particles were formed. Both PhMA formulations demonstrate a repeatable and reproducible uptick in swelling volume around 37ºC before attaining full collapse between 44ºC-50ºC. These systems could prove interesting as drug delivery vehicles, as there is still a significant change in the swelling volume between physiological temperature and 47ºC.

The copolymerization with NVP shows a similar uptick to that exhibited by the PhMA copolymers, however, the large error in the swollen state hides this phenomenon. The collapse starts well before physiological temperature, this combined with the hydrophilic nature of the system signifies that these NVP based systems are not suitable for drug delivery.

The EGPhA copolymer nanogels show a much more gradual response, beginning their collapse at 30ºC and attaining full collapse at 50ºC. Increasing the comonomer concentration from 10%-20% leads to a slight increase in the maximum ESR, but the overall trend remain. These modifications are likely due to the hydrophilic nature of EGPhA, as they increase the hydrophilicity of the nanogel and thus the overall swelling volume, but then also limit the ability of the system to collapse due to the increased presence of hydrophilic domains.

Similar trends are not seen with AAm as a comonomer, though this can be explained by the fact that AAm is less hydrophilic. The inclusion of AAm greatly reduced the maximum ESR with the 20% AAm nanogels exhibiting the smallest ESR of all the nanogels synthesized. These gels also exhibit a broad response of the collapse, as both nanogels begin their collapse around 33ºC and reach a steady ESR at 50ºC.

5.3.3 Loading Results

The loading of particles with model drugs showed an interesting, however predicted, phenomena. As seen in Figure 5.14 the hydrophobic comonomer increases the loading of the hydrophobic drugs. The NVP polymers show no signs of successfully loading the more hydrophilic 5-FU. This result might be indicative of less of a phase separation between the more hydrophobic polymer systems and the surrounding water. Since the loading and entrapment of

these drugs in these LCST systems is dependent on phase separation, and improved solubility in the polymer phase.

5.3.4 Pyrene Fluorescence

Pyrene fluorescence experiments in Figure 5.15 show that, largely, these nanogels do not have a hydrophobic makeup that varies significantly from that of water, which makes sense as hydrogels are known for being hydrated systems. The TBMA copolymer systems are the only systems to exhibit a change in pyrene fluorescence between 37ºC and 45ºC, while 20% TBMA is the only one to significantly vary from water at 37ºC, showing that TBMA is the most hydrophobic comonomer used in this study. These trends are observed, however no system demonstrates any large variation from fluorescence in water.

5.3.5 Partition Coefficient Studies

All of the systems demonstrate similar partition coefficients with the exception of 20% EGPhA, as seen in Figure 5.16. This is likely due to EGPhA being hydrophilic. The data also shows that increasing the temperature results in a large drop in the partition coefficient, especially TBMA. This could be explained by a number of factors, including an increase in DOX's solubility in water and a decrease in volume of the particles, as the partition coefficients are based on dry weight of particles.

These studies are slightly surprising, due in large part to the hydrophobic nature of Dox and the hydrophobic shift that is experienced across the LCST of these nanoparticles. However, the 45ºC is in the middle of the phase transition for most of these systems, and was chosen mainly as the highest temperature at which limited exposure demonstrates little hyperthermic ablation in tissue (cite). These results demonstrate a shift in solubility that could likely be used for drug delivery. The 10% TBMA sample, in particular, shows a significant partitioning effect at 37ºC

that drops to 0 at 45ºC. This could be beneficial for drug delivery, as it would encourage entire release of the drug payload.

5.3.6 Cytotoxicity Studies

Figure 5.17 shows the cytotoxic effect of the copolymer based nanogels. Again, there is no significant toxicity of the nanogels at 6 or 24 hours up to a concentration of 5 mg/mL. The particles do demonstrate an increase in the enzymatic activity of the cells. The MTS assay used t measure the toxicity of the nanoparticles depends on the presence of nicotinamide adenine dinucleotide (NADH). This molecule is produced from the activity of dehydrogenases necessary for cell proliferation. This increase could be due to either an experimental anomaly or it could be stress induced due to the presence of the nanoparticles.

5.4 Conclusions

PNIPMAAm copolymers can be synthesized with a range of different copolymer types. The analysis of the swelling response shows that the hydrophobicity of the comonomer does not have the same impact as that observed on PNIPAAm based copolymers. No copolymer system demonstrated a significant increase in LCST and the only decrease observed occurred largely due to in inhomogeneities in the swelling response.

Further, analysis of these systems for hydrophobicity showed that no systems are significally more hydrophobic than water, likely due to the hydrated nature of the polymers. This result is surprising as the partition coefficient studies demonstrated high partitioning of DOX into the hydrogels. These studies also revealed a preference for systems containing hydrophobic comonomers, such as TBMA and PhMA over their hydrophilic counterpart, EGPhA. These results were even the trend for more hydrophilic model drugs such as 5-FU. The hydrophilic comonomers demonstrated that even though the Pyrene studies revealed similar hydrophobicity, the drug had no preferential loading for these systems.

Studying the effect of temperature on these systems revealed that these systems exhibt a decrease in partitioning that cannot be explained by their swelling response. The trend reveals nothing about the amount of comonomer's effect on the partitioning. These studies do show that the release of the drug is due to a decrease of the partitioning, though could be mildly related to the collapse and drop in overall volume of the nanoparticles.

These studies even went on to prove that these particles have no cytotoxic effect even at relatively high concentrations of 5 mg/mL, regardless of comonomer. Overall these studies demonstrate that comonomer can affect the impact of these systems as drug delivery vehicles. The higher the hydrophobicity of the comonomer, as demonstrated by TBMA, the better the swelling response and drug compatibility of the system. However, increasing the comonomer concentration to higher levels can start to diminish the temperature sensitivity of these nanogels, as pure PNIPMAAm demonstrated a sharper temperature response than its copolymerized counterparts.

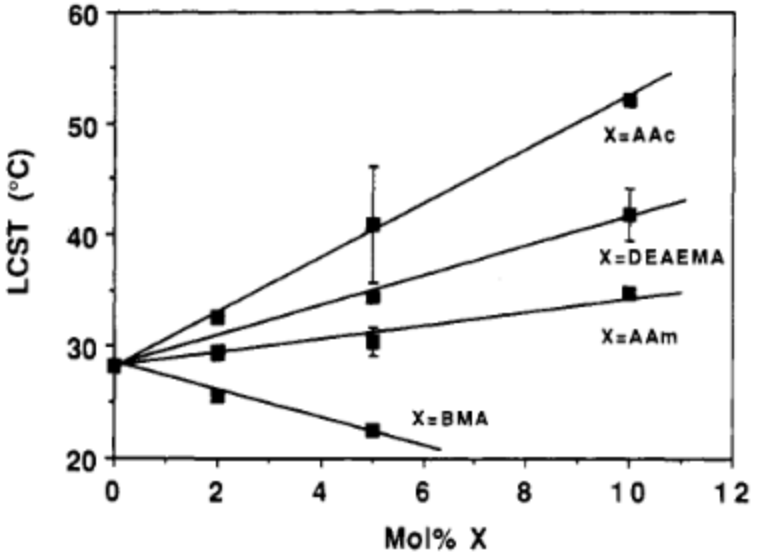

Figure 5.1: Effect of comonomer concentration and type on the LCST of PNIPAAm based hydrogels [53].

Name	5-Fluorocuracil	Fluorescein	Doxorubicin HCL
Structure	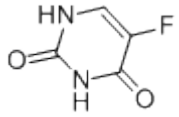	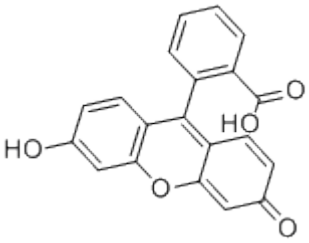	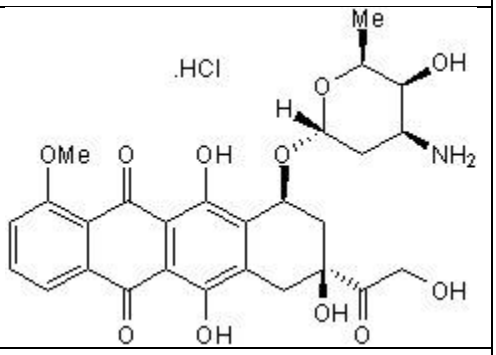
Molecular Weight	130.08 g/mol	332.31 g/mol	579.88 g/mol
λ of absorbance	290 nm	350 nm	450 nm
Water Solubility	12.2 mg/mL	insoluble	10 mg/mL

Table 5.2: Model drug information.[54, 55] Chemical BOOK

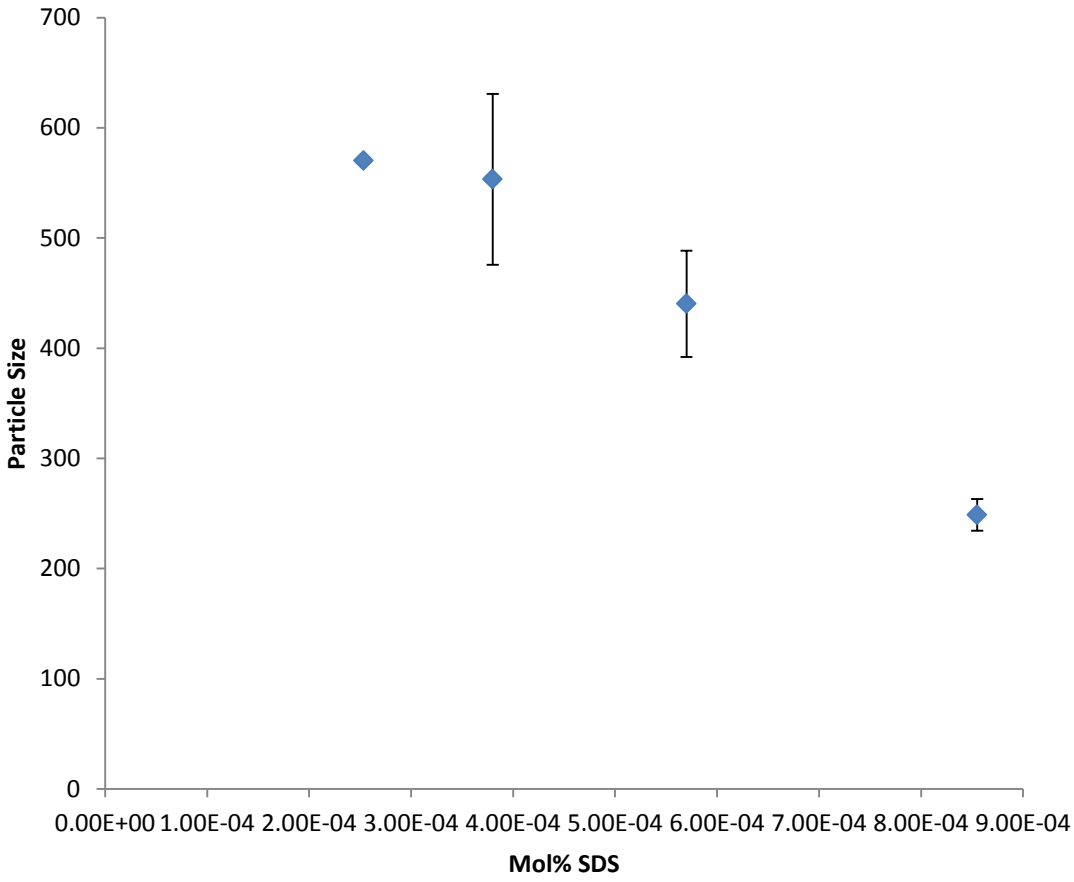

Figure 5.2: Effect of SDS concentration of total mols on the size and batch-to-batch variability of PNIPMAm nanogels at 25ºC. (N=3)

A

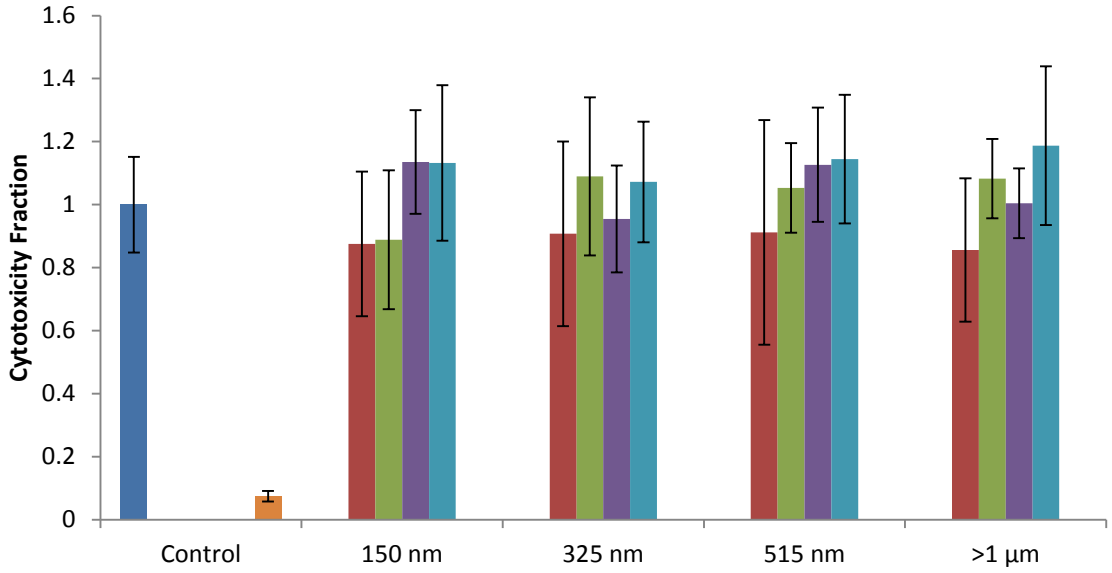

B

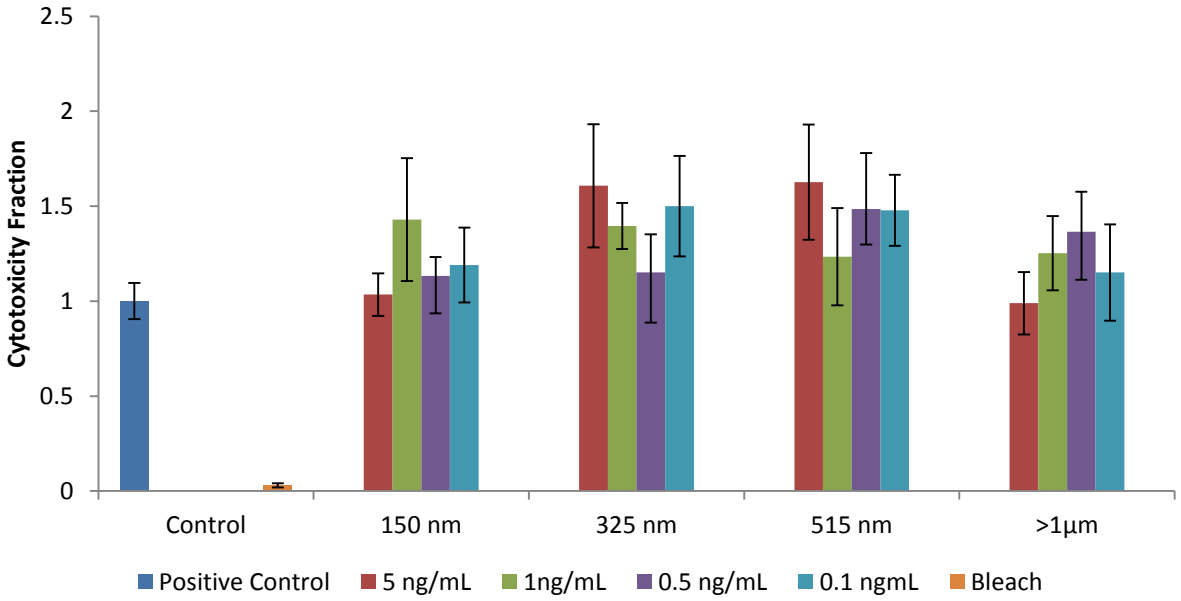

Figure 5.3: Cytotoxicity of PNIPMAAm nanogels of varying particle size. MTS Assay of L929 fibroblasts at A. 6 hours. B. 24 hours. n=4. Positive control 2% FBS in Dulbecco's Modified Eagle Medium.

Comonomer Concentration	Zavg diameter 25ºC (nm)	PDI	LCST(ºC)	Overall Volume Swelling Response	Power Exponent	R^2 Value of Fit
NIPMAAm	615.8	0.073	45	11.5	19.14	0.681
10% TBMA	366.45	0.172	46	5.68	61.4	0.998
20% TBMA	309.5	0.118	46	5.78	18.7	0.963
10% PhMA	427.8	0.299	33	8.93	11.6	0.962
20% PhMA	341.5	0.316	44	4.43	8.95	0.323
10% EGPhA	242.1	0.022	41	2.89	9.80	0.861
20% EGPhA	272.5	0.002	42	3.80	8.63	0.806
10% AAm	478.6	0.019	41	4.01	11.94	0.939
20% AAm	716.8	0.187	38	2.23	7.86	0.738
20% NVP	666.9	0.156	41	9.0	8.29	0.656

Table 5.3: Characteristics of swelling curves of PNIMAAm copolymer nanogels. Percentages are percentages of total monomer concentration in the feed.

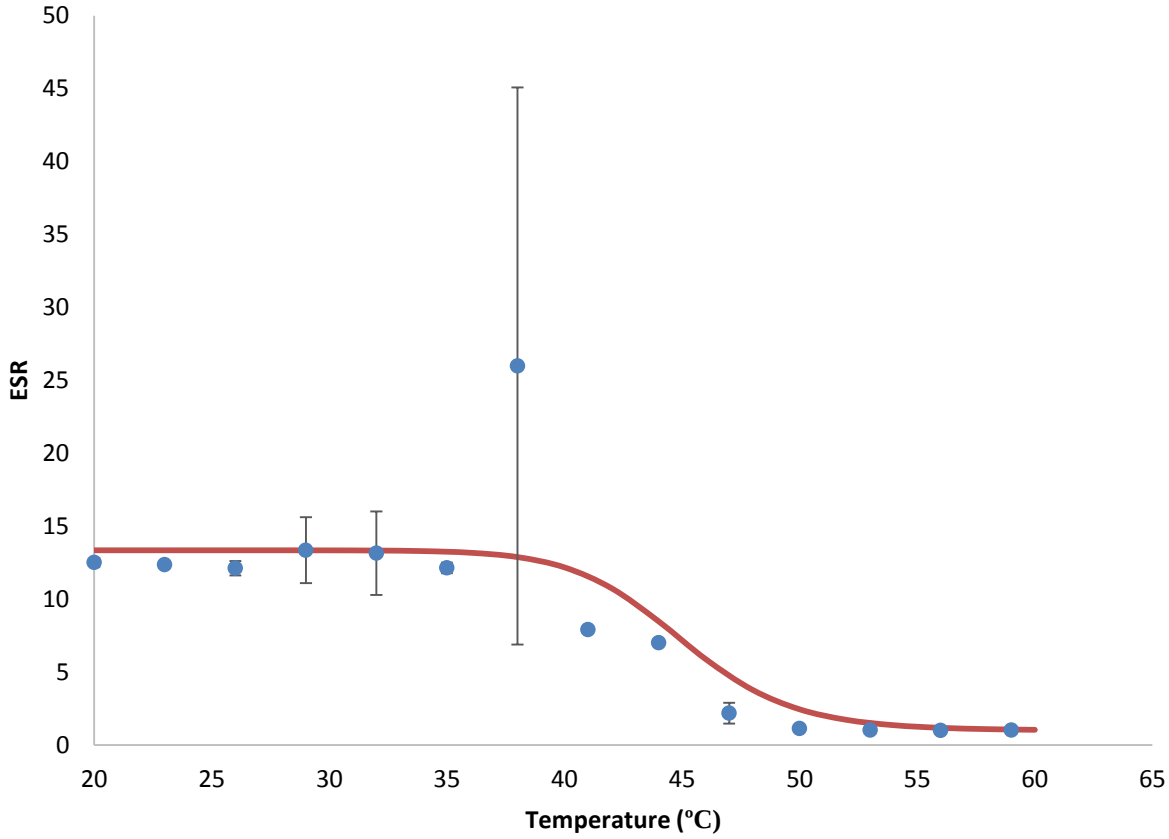

Figure 5.4: Equilibrium swelling ratio vs temperature of PNIPMAAm nanogels.

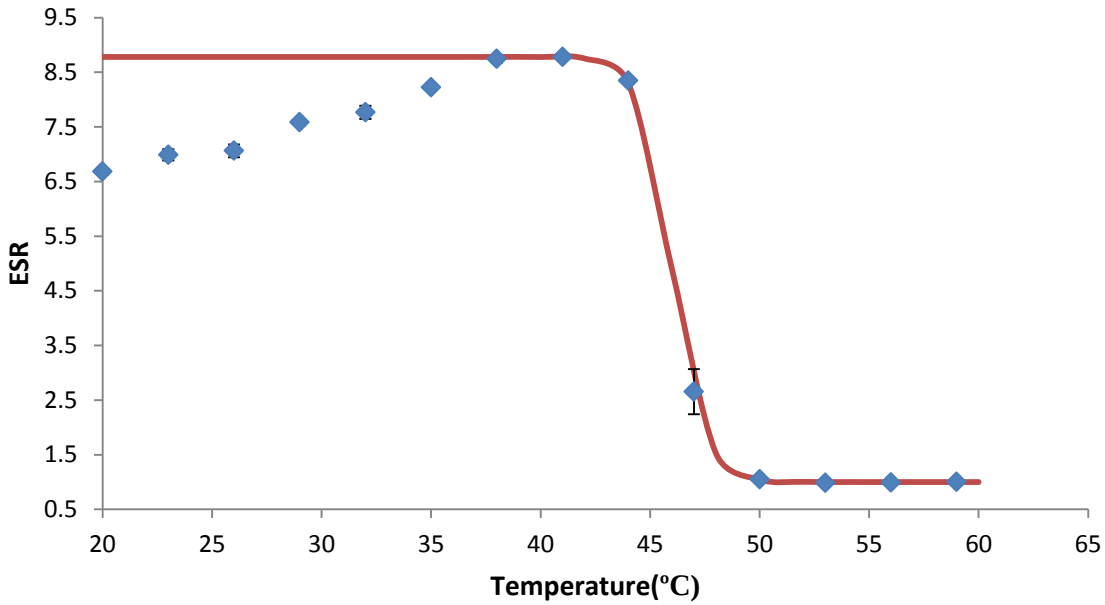

Figure 5.5: Equilibrium swelling response vs temperature of P(NIPMAAm-co-TBMA) 10% TBMA nanogels. (N=3)

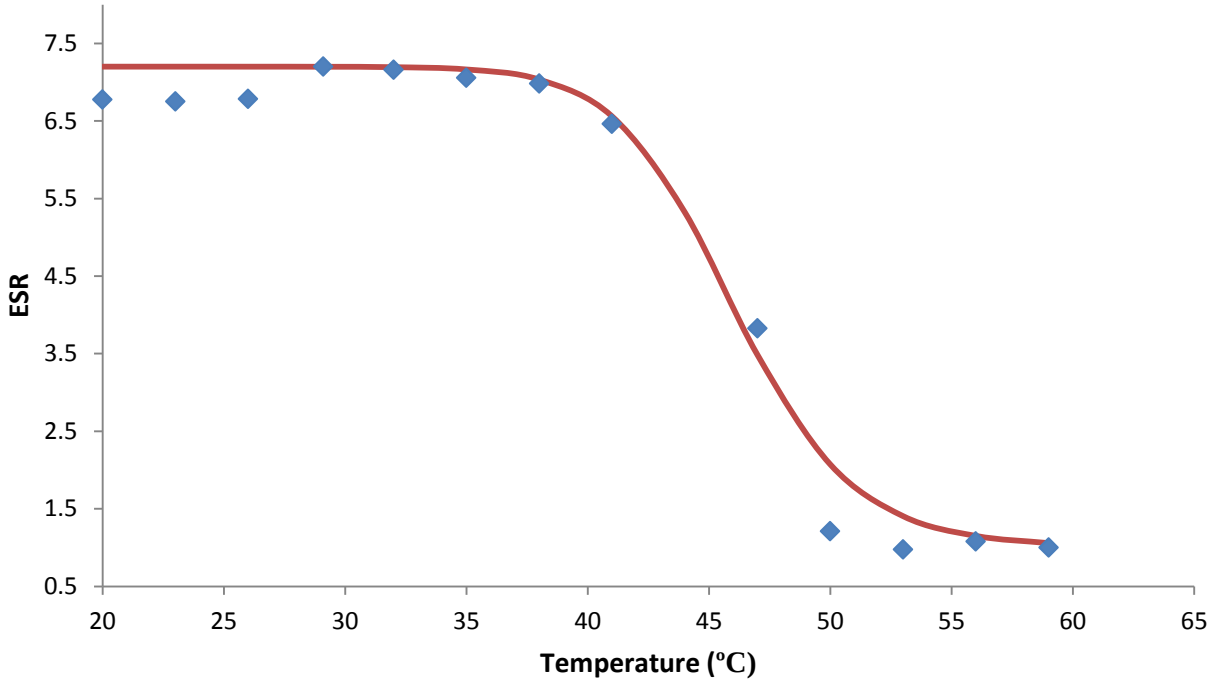

Figure 5.6: Equilibrium swelling ratio vs temperature of P(NIMAAm-co-TBMA) 20% TBMA nanogels. (N=3)

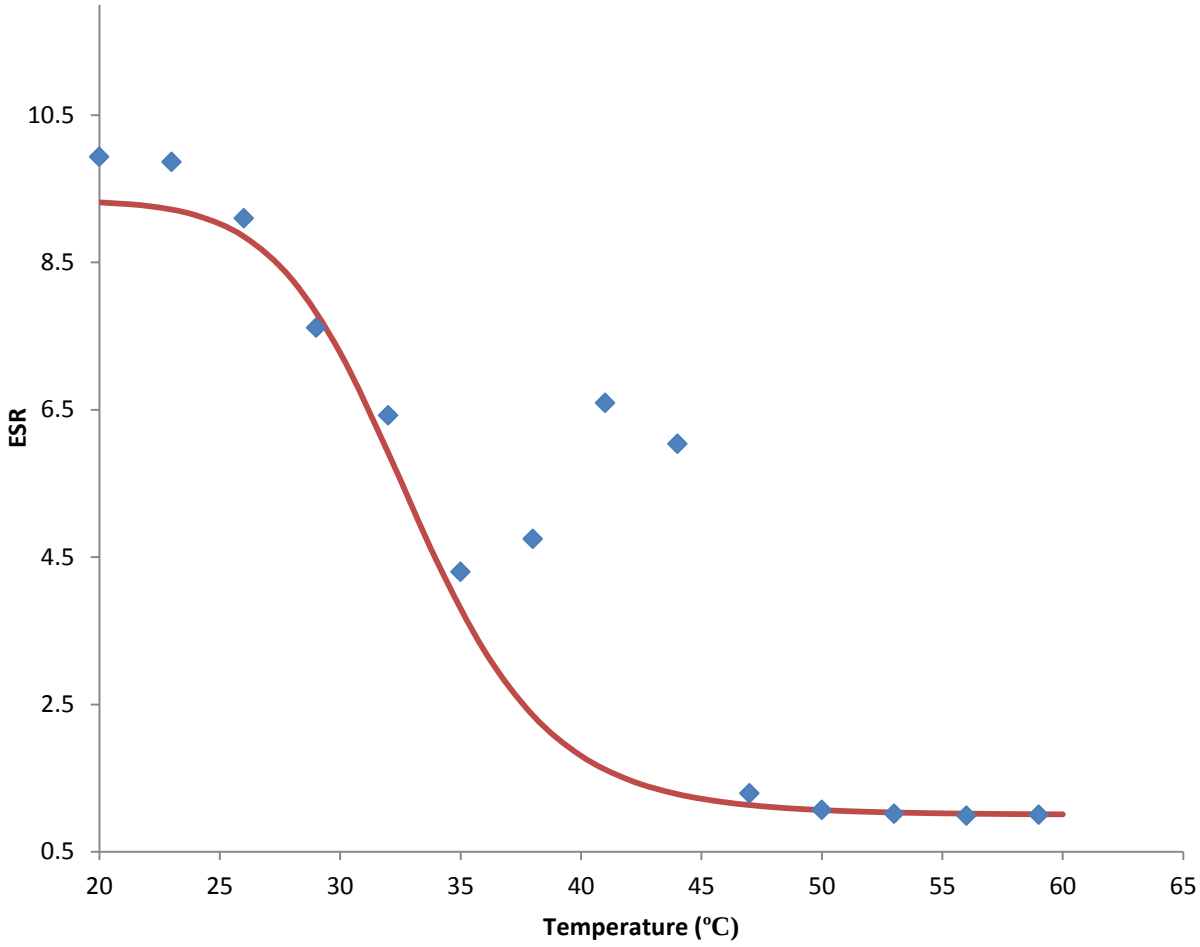

Figure 5.7: Equilibrium swelling ratio vs temperature of P(NIPMAAm-co-PhMA) 10% PhMA nanogels.

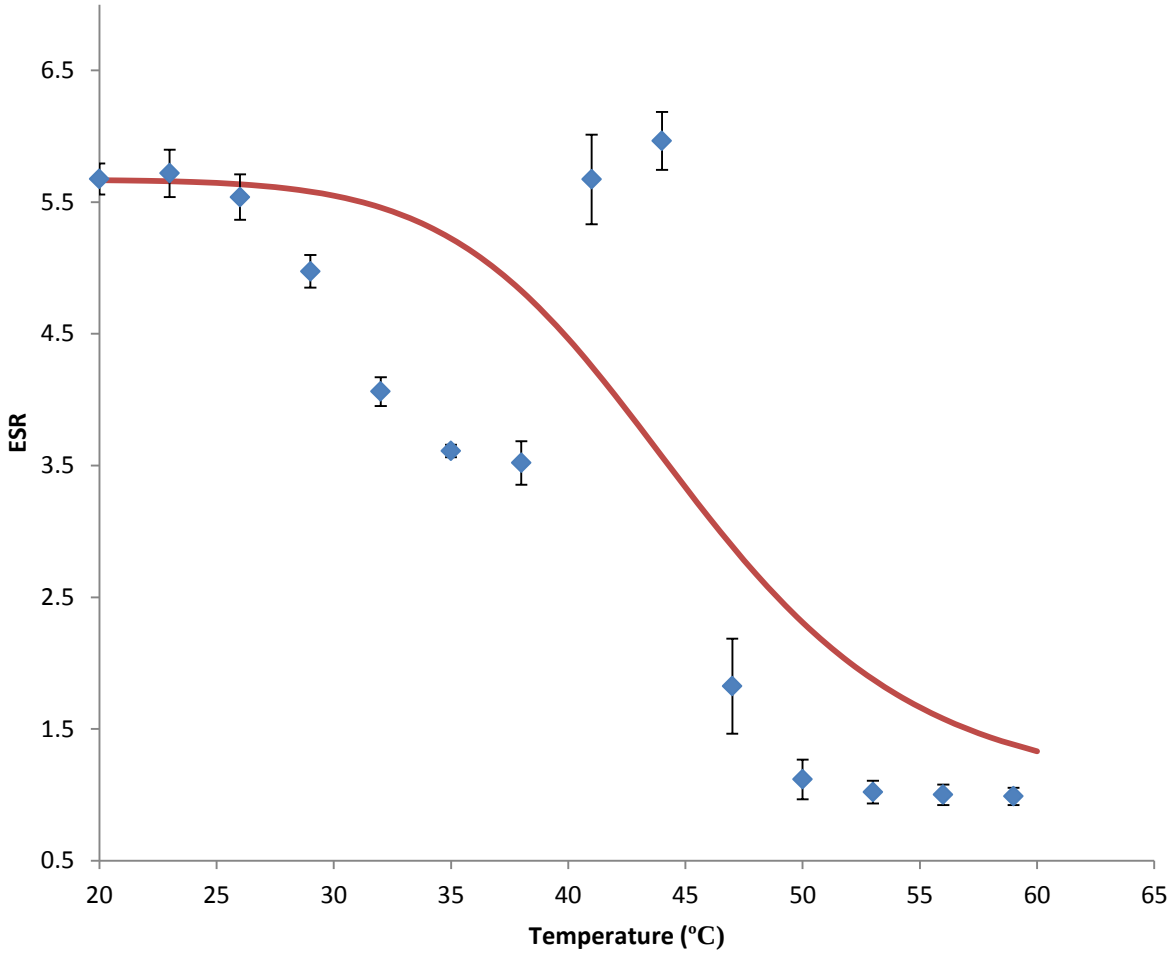

Figure 5.8: Equilibrium swelling ratio vs temperature of P(NIPMAAm-co-PhMA) 20% PhMA nanogels. (N=3)

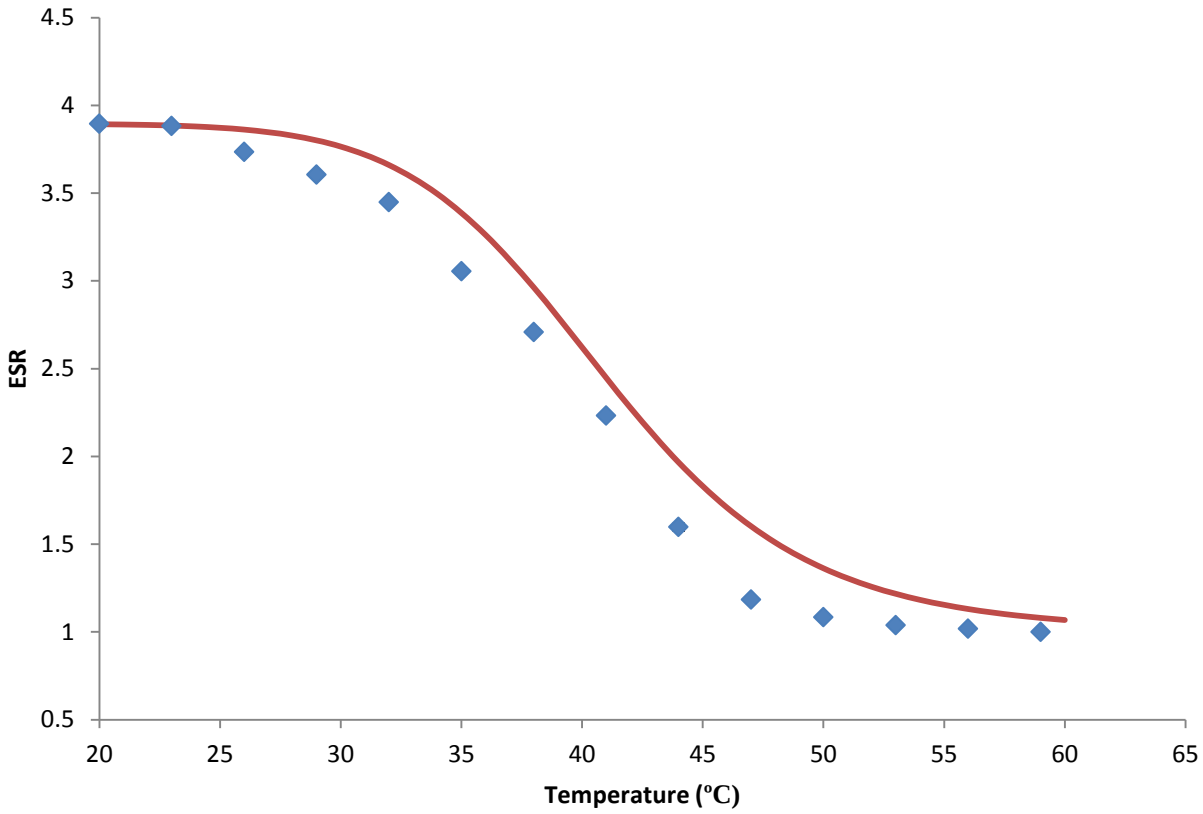

Figure 5.9: Equilibrium swelling ratio vs temperature of P(NIPMAAm-co-EGPhA) 10% EGPhA nanogels. (N=3)

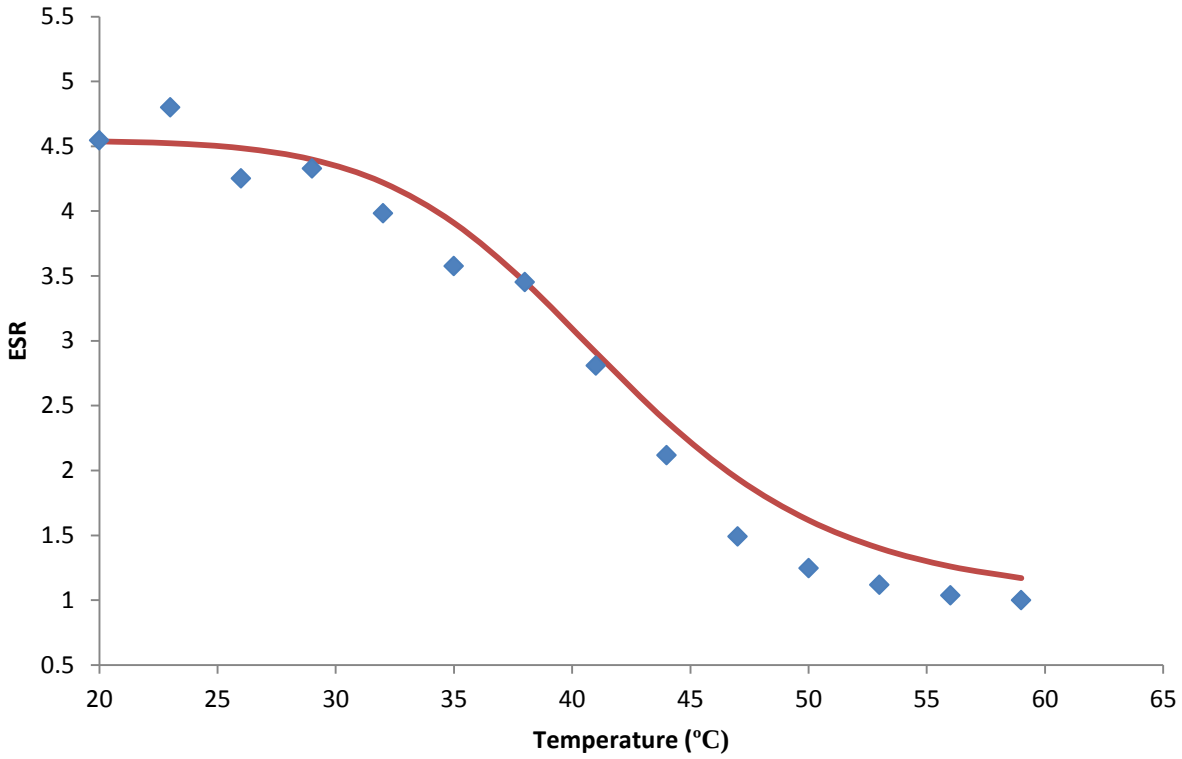

Figure 5.10: Equilibrium swelling ratio vs temperature of P(NIPMAAm-co-EGPhA) 20% EGPhA nanogels. (N=3)

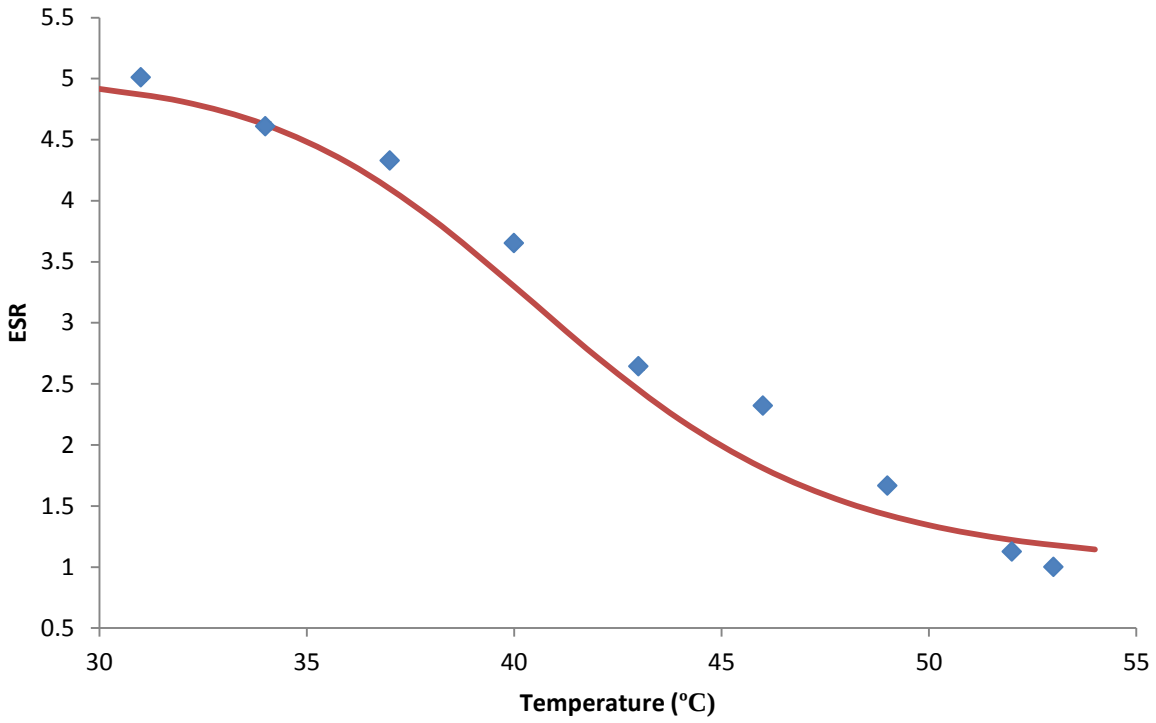

Figure 5.11: Equilibrium swelling ratio vs temperature of (NIPMAAm-co-AAm) 10% AAm nanogels. (N=3)

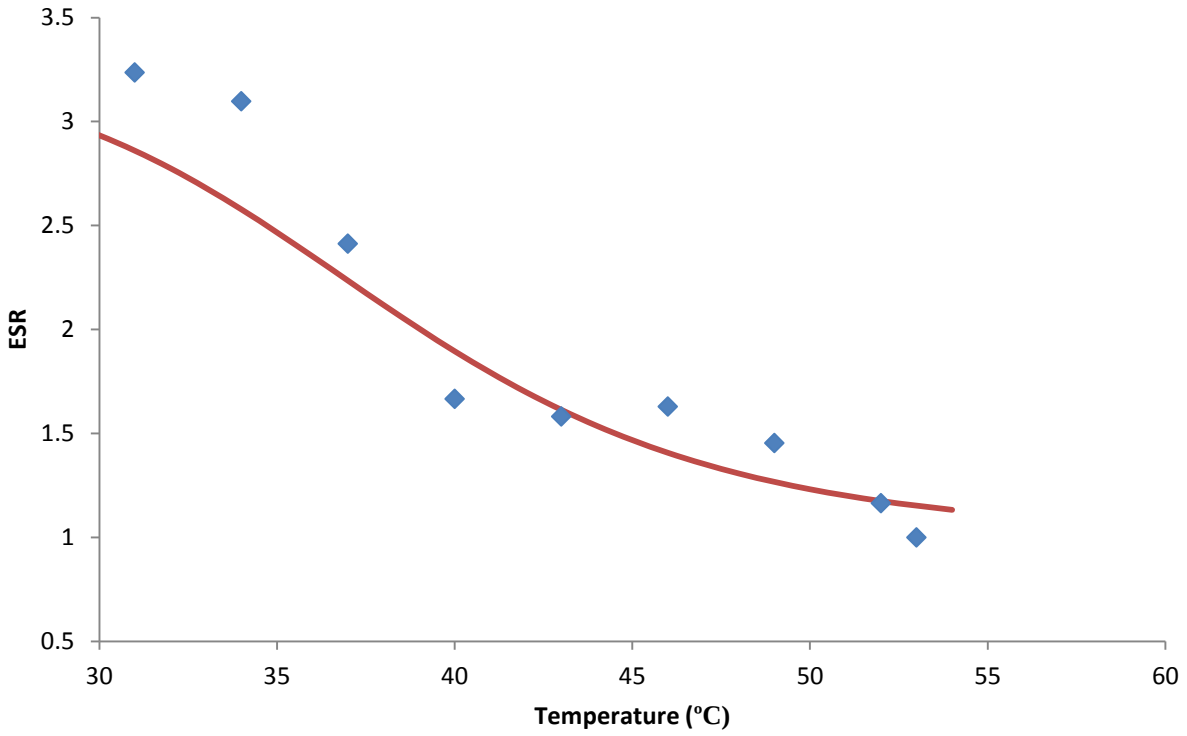

Figure 5.12: Equilibrium swelling ratio vs temperature of P(NIPMAAm-co-AAm) 20% AAm nanogels. (N=3)

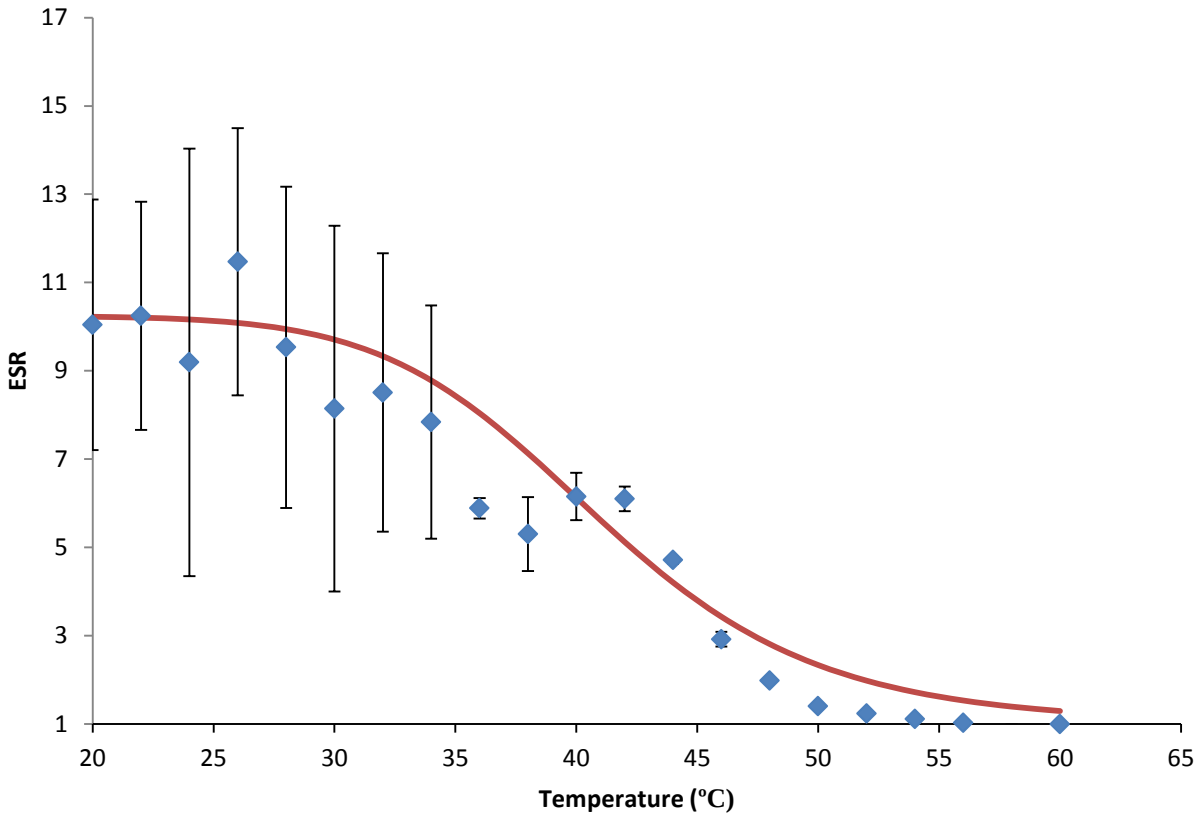

Figure 5.13: Equilibrium swelling ratio vs temperature of P(NIPMAAm-co-NVP) 20% NVP nanogels. (N=3)

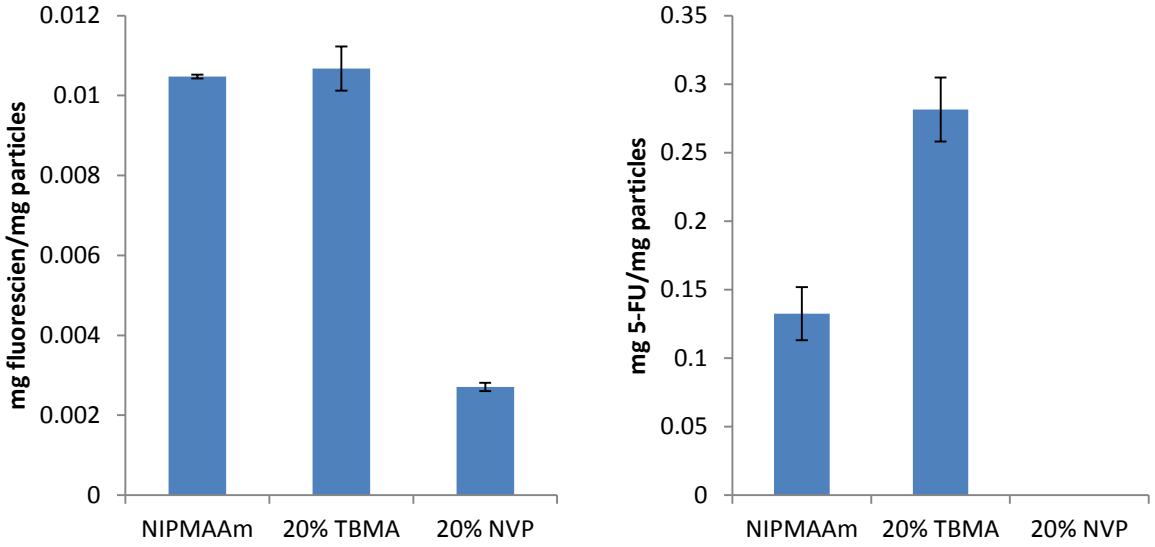

Figure 5.14: Loading of model chemotherapeutics into PNIPMAAm based copolymers. Percentages represent percent of total monomer in the feed solution. (N=3)

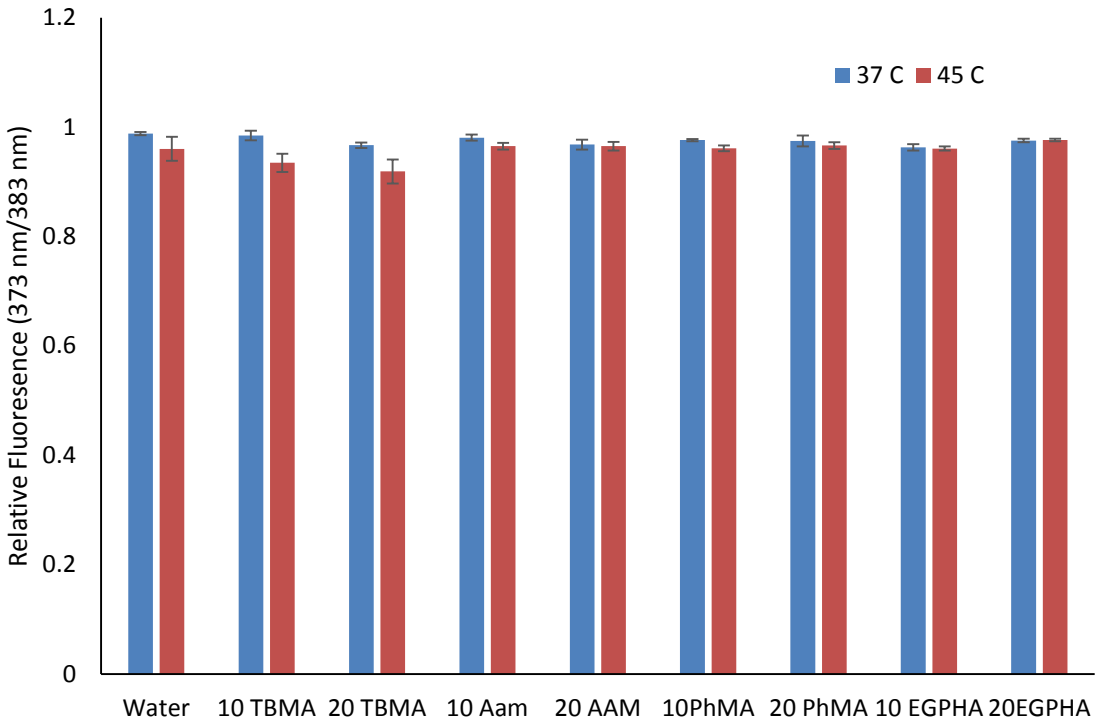

Figure 5.15: Pyrene fluorescence ratios of PNIPMAAm based copolymers at 37ºC. (N=3)

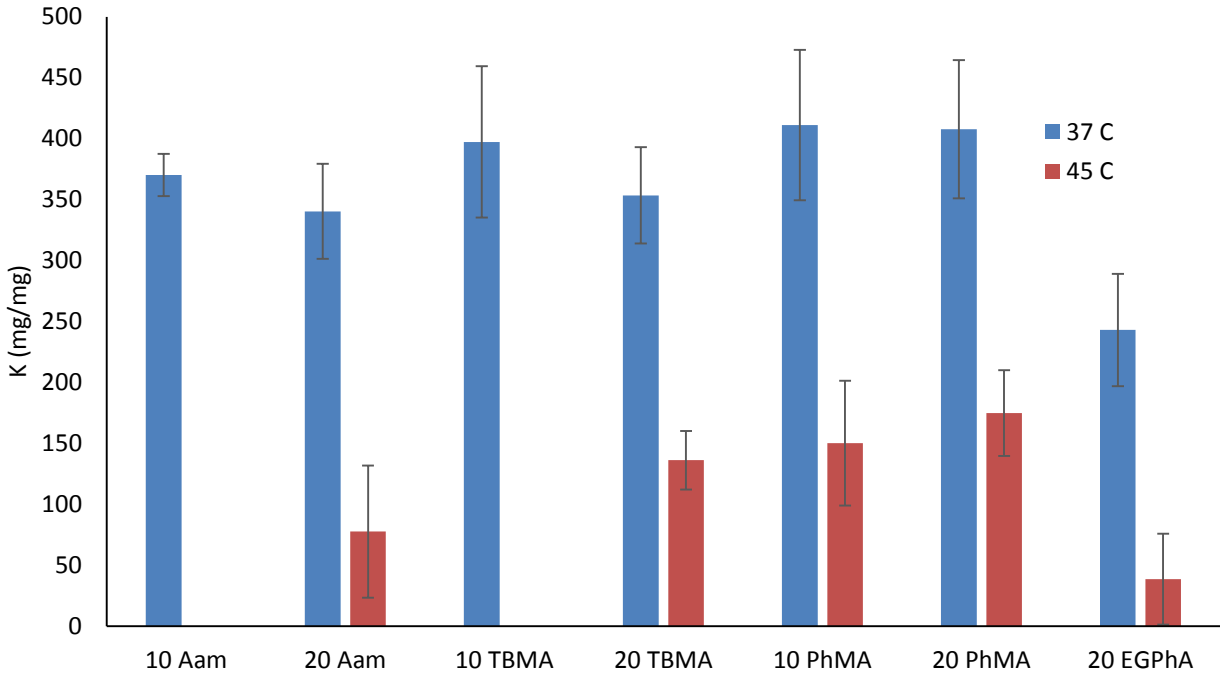

Figure 5.16: Dox nanoparticle partition coefficient studies at 37ºC and 45ºC. (N=3)

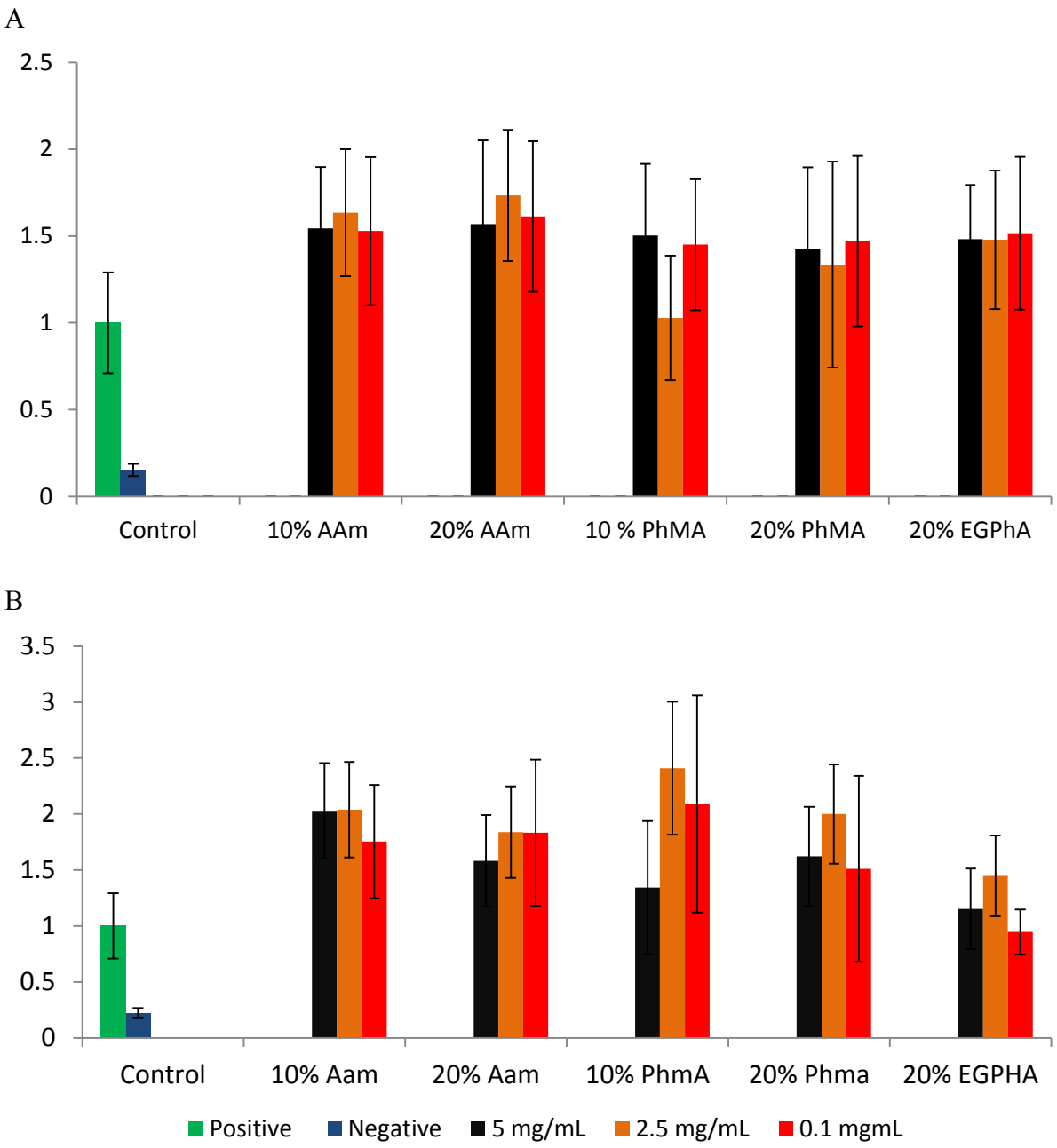

Figure 5.17: The effect of comonomer. MTS Assay of L929 fibroblasts at A. 6 hours. B. 24 hours. n=4. Positive control 2% FBS in DMEM. Negative control DI Water. Percentages are molar percentages of total monomer concentration in the feed. (N=4)

CHAPTER 6

Core/Shell Hydrogels for Improved Retention of Chemotherapeutics

6.1 Background

The development of temperature responsive systems has focused on the loading and release from the hydrated polymer mesh. This is abnormal, as hydrogel systems used for drug delivery depend on a collapsed mesh that restricts diffusion of the payload by decreasing the mesh size. Because of the small molecular weight of chemotherapeutics and the hydrated nanogels used to deliver them, the loading and release is based primarily on diffusive limitations and partitioning between the nanogel and the surrounding aqueous solution. Many of these LCST systems have a noticeable release, even at temperatures well below their critical point[56]. This release is observed in the work of Gran (Figure 6.1) with P(NIPAAm-co-AA) based copolymers [57].

Since the relative concentration of drug in the polymer is linked to the solubility of water, there can be a ceiling to the loading limit. However, these systems can still prove effective during the *in vitro* and *in vivo* test trials due to the slow mass transfer associated with diffusion and the relatively short time it takes particles to accumulate in tumors[5].

The slow diffusional release time scale allows for limited release as the particles accumulate, than the convective release that is experienced after triggering. However, results, as those depicted in Figure 6.1, are skewed due the schemes developed to test the loading and release of these particles. Because these systems are tested in closed environments, the seemingly asymptotic nature of the curve is an artifact of simple mass transfer limitations. So, *in vivo*, the only limitation to release is the long timescale associated with diffusion. As the relative equilibrium is achieved between the two volumes the rate of release decreases. However, unlike this closed environment, in the body the released drug is continuously metabolized, and taken up

by the cells and tissue in the body. This means that equilibrium is never achieved, and there is always a significant concentration gradient driving release.

There are two approaches to preventing the premature release of the drug payload. One method of addressing this problem is to conjugate the drug to the backbone of the polymer via using a physical linker, thus creating the so-called "pendant systems". However, drug release is now affected by the ability to hydrolytically free the incorporated drug, reproducibly and always at the same site so that what is released is the drug itself and not drug derivatives. There have been a number of systems that have pursued these covalently linked systems for preventing the release of their drug payloads[25].

Another method to limit this release while increasing loading capacity is to adjust the chemical potential of the drug in the polymer. This entails development of hydrogels that will allow high solubility of the drug in the matrix. This approach has two potential pitfalls. The first is implementation, since LCST hydrogels depend on a hydrated state at physiological conditions, including large amounts of a hydrophobic moiety could limit the temperature response. The second issue is that increasing the partition coefficient of the hydrogel would also limit the eventual release due to the high solubility in the hydrogel and limited solubility in physiological fluid. Core/Shell systems could provide a solution to both of these limitations, while still providing for increased drug retention. First, separating out the hydrophobic moiety into a shell material will limit the impact on the temperature response. In order to ensure a high release level, these systems will depend on a phenomenon observed when combining thermoresponsive nanogels with superparmagnetic iron oxide nanoparticles (SPIONS). Figure 6.2 shows release of BSA in response of a number of different stimuli. When this system is intensely heated in the presence of SPIONS it results in a burst release [59].

This mechanism could prove useful in emitting the entire drug payload of these core/shell systems, overcoming any limitations due to the increased partitioning of the drug payload.

6.2 Materials and Methods

6.2.1 Core Synthesis

NIPMAM, APS, and MBAM were obtained from Sigma (St. Louis, MO); and SDS from Fisher Scientific (Pittsburgh, PA) were all used as received. In a standard reaction, NIPMAM, MBAM, and SDS are mixed together in 18.2 MΩcm water in the amounts specified in the table below. This solution was purged for 30 minutes at 70ºC with Nitrogen under 200 rpm stirring with a football shaped stir bar in a round bottom flask. Then APS, dissolved in 18.2 MΩcm water was injected and the reaction was allowed to progress for 2 hours under constant stirring. The reaction was then terminated by exposure to air. Nanogels not intended to be used in shell development were then purified against 18.2 MΩcm water for two weeks with twice daily water changes and is then freeze dried.

Component	mol % of total solution	% of total monoer mol feed
NIPMAM	0.024%	95%
MBAM	5.0×10^{-5}%	5%
SDS	1.9×10^{-5}%	NA
Water	99.8%	NA

Table 6.1: Molar composition of core synthesis.

6.2.2 Shell Development

After 6 hours a solution of the comonomer MBAM, and APS was injected into the core synthesis reaction. The amount of shell comonomer added was 50% by mol of NIPMAAm used in the core synthesis.

Component	mol Percent	% monomer mol feed
TBMA, EGPhA, PhMA	0.024%	95%
MBAM	$5.0x10^{-5}$%	5%
Water	99.8%	NA

Table 6.2: Molar composition of shell synthesis.

6.2.3 Particle Sizing

The effect of temperature on particle size was measured using a Malvern Zetasizer ZS (Malvern, UK). The data were collected by dissolving freeze dried particles in 1 mL of DI water and adjusting the temperature by 3ºC increments and then allowed to equilibrate for 60 seconds. Temperature was ramped 20ºC to 59ºC and then down to 20ºC to examine the effect of hysteresis on the samples particle size.

6.2.4 DSC Studies

Modulated DSC studies were performed with a DSC (Q2000, TA instruments, New Castle, DE). Samples were loaded at a minimum weight of 5 mg into aluminum pans and sealed. Studies were run from 20-200ºC in a nitrogen environment.

6.2.5 NMR Studies

Nuclear magnetic resonance spectra were taken with a NMSR spectrophotometer (model 400 MHZ, Varian Palo Alto, CA) with a Direct Drive sample changer. Samples were dissolved in deuterated acetone at a concentration of 20 mg/mL.

6.2.6Pyrene Fluorescence

Pyrene was initially dissolved in acetone at a concentration of 0.2 mg/mL. A sample of 10 µL of this solution was then dropped into a 96 well plate and the acetone was allowed to evaporate in a fume hood. A sample of 200 µL of particles at a concentration of 0.1 mg/mL was then added to the wells and allowed to mix overnight. These samples were then read in a Biotek Cytation 3 plate reader (Bio Tek, Winooski, VT) at excitation wavelengths 333 nm and 338 nm and emission at 390 nm.

6.2.7 Fluorescein Loading Studies

Fluorescein loading was achieved by mixing particles and fluorescein at a concentration of 1 mg/mL, each; in a 9:1 water:DMSO solution. The particles were then separated from unloaded fluorescein by centrifugal filters. The loading levels were determined by measuring the concentration of fluorescein in the filtrate. This value was then subtracted from the initial concentration of fluorescein.

6.2.8 DOX Loading Studies

Loading studies were performed by dissolving particles and drug in a 50:50 DMSO:Water solution. The particles and drug were dissolved at concentrations of 5 mg/mL each. These solutions were then dialyzed against 18.2 MΩcm water until the dialysate was clear. These suspensions were then freeze dried for release studies.

6.2.9 Temperature Release Studies

Release studies were performed by preparing solutions of drug loaded particles suspended in a 37°C 1 X PBS solution at a concentration of 0.5 mg/mL. It was incubated for 6 hours taking intermittent time points. After 6 hours the temperature was then increased to 45°C and the incubation was allowed to proceed for another 2 hours taking more time points.

6.2.10 Magnetic Nanoparticle Incorporation

N-hydroxy succinimide ester coated magnetic nanoparticles (Sigma Aldrich, St Louis, MO) were purchased from Sigma Aldrich (St Louis, MO). These nanoparticles were then coated with vinyl groups by reacting with 2-amino ethyl methacrylate in borate buffer pH 8.4. These particles were then reacted in a standard core synthesis reaction described previously in section 6.1. The particles were first suspended in methanol and then this solution was mixed with a solution prepared from Table 6.1. These samples were then heated in a sonication bath at 70°C. After heating, an APS solution was then injected into the reaction to initiate the reaction, and the reaction was allowed to proceed for 2 hours.

6.2.11 TEM Images

Images were obtained on an Transmission Electron Microscope (FEI Tecnai, Hillsboro, OR) operating at 80 kV. Carbon coated copper grids (400 mesh) were plasma treated using an Emitech Glow Discharge instrument to render them hydrophilic prior to adding 5 µL of the nanoparticle suspension. After 30 seconds, the nanoparticle suspension was wicked off using Whatman 1 filter paper. The particles were negatively stained by placing a 5 µL drop of 2% phosophotungstic acid, pH 8.0, on the particle-coated grid for 30 seconds before being wicked off with Whatman 1 filter paper.

6.2.12 AMF Release Studies

Magnetic nanoparticle incorporated nanogels were loaded as described in the DOX Loading Studies section. These nanocomposites were then incubated at 37°C for 6 hours, and overall release was measured at the end of the 6 hours. The particles were then heated with an RDO.

6.3 Results and Discussion

6.3.1 DLS Swelling Responses

The results obtained here indicate that the swelling response of PNIPMAAm is relatively unaffected by the addition of the various shell comonomers. The graphs of the temperature response of PNIPMAAm/PTBMA, PNIPMAAm/EGPhA, and PNIPMAAm/PhMA core/shell systems are in Figure 6.4, 6.5, and 6.6 respectively. By fitting these swelling results to Equation 6A, we can quantify the sharpness of the responses of these systems by determination of the exponent p. These values can be found in Table 6.3, along with other characteristics of the system's swelling response.

$$ESR = \frac{ESR_{max} - 1}{1 + (\frac{T}{T_{LCST}})^P} + 1 \qquad \text{Equation 6A}$$

All core/shell systems altered the swelling response significantly. The large decrease in overall swelling response is due to the encapsulation of the PNIPMAAm core in a non-thermoresponsive shell. Because the shell does not collapse, its volume remains constant Even though the core still undergoes collapse, the overall volume does not change as drastically due to the constant shell thickness.

None of the systems have a large change in the LCST, with the largest shift in its critical temperature occurring with the PNIPMAAm/PTBMA core/shell system, down to 43ºC.

However, all of the systems remain swollen until 37ºC before syneresis begins and the full response is observed by 50ºC. This temperature response is essential for their application.

The PNIPMAAm/PTBMA core shell nanogels demonstrates a consistent volume swelling ratio up to 37ºC and a fairly sharp response with a sigmoidal exponent of 9.8. This is still half as sharp as the collapse of PNIPMAAm nanogels, though a large portion of its collapse is still achieved by 45ºC.

PNIPMAAm/PEGPhA core/shell nanogels exhibit the sharpest response of the core/shell materials. However, there is large variability of these systems in their swollen states. This is due to the hydrophilic polymers not being ideal for the emulsion based synthesis of these systems and the likelihood of a highly branched particle leading to large variation of hydrodynamic radii. However, the sharp collapse between 37ºC and 47ºC make it a viable option for drug delivery purposes.

The PNIPMAAm:PPhMA core/shell system demonstrates a response similar to that of the PNIPMAAm:PTBMA core/shell system due to the similarities of hydrophobicity. However, the PNIPMAAm/PPhMA nanogels experience a greater change in their overall swelling ratio.

6.3.2 Core/Shell Characterization

The NMR graphs for the different systems are seen in Figure 6.7-6.10. Figure 6.7 demonstrates the groups expected with a PNIPAAm nanogels. The chacteristic peak of the polymer backbone is seen at the 2.9 shift. The characteristic PNIMAAm shifts at the peaks of shifts 3.9 and 1.1. The shift at 1.1 corresponds to the isopropyl and vinyl methyl groups, while the shift at 3.9 corresponds to the tertiary carbon's lone proton. The shift at 3.9 is the important shift to identify, as it is unique to the structure of NIPMAAm. NMR measurements of crosslinked nanoparticles

are often not preferred due to the fact that fluid NMR only detects groups dissolved in water. This fact aids the confirmation of core/shell structure as solution NMR only detects the groups near the surface of a crosslinked nanoparticle.

Figure 6.8 shows the characteristic NMR of the PNIPMAAm/PTBMA core/shell system. This NMR structure shares many of the same shifts as the PNIPMAAm NMR spectra, such as the polymer backbone peak at 2.9 and the shift for methyl groups at 1.1. However, due to the lack of a peak at the 3.9 shift it can be concluded that the NMR of these samples did not detect the presence of NIPMAAm units.

Figure 6.9 shows the NMR of the EGPhA system, and again there is the lack of the characteristic NIPMAAm peak at the 3.9 shift. In its place are the shifts for EGPhA's ethyl groups. EGPhA's phenyl group shifts are seen at the 6.9 and 7.2 shifts and we see the characteristic backbone peak at the 2.9 shift.

The core/shell synthesis of PNIPMAAm/PhMA's NMR spectra is seen in figure 6.10. Unlike it's counterparts there are characteristic peaks of PPhMA and PNIPMAAAm. The phenyl group shifts at 7.2 and 7.4 as well as the isopropyl's tertiary carbon's hydrogen shift at 3.9. This result means that there is either not a strict separation between the core and shell domains or that PhMA was not able to fully coat the particle at these molar ratios.

DSC was also used to characterize the different domains of the core/shell systems, as seen in Figures 6.11-6.14. The uncoated PNIPMAAm based hydrogel's thermogram is seen in 6K and shows two glass transition temperatures (Tg), one at 75ºC and one at 110 ºC. The reported value for PNIPMAAm's Tg is 110ºC, meaning the Tg detected at 75ºC is due to the presence of a

plasticization agent, such as water or unpurified surfactant. Regardless, this result provides the baseline for characterization of the Core/Shell structures.

Figure 6.12 is the thermogram of the PNIPMAAm/PTBMA core/shell structures. This figure shows similar results to the thermogram PNIPMAAm nanogels, but this is largely due to the fact that PTBMA and PNIPMAAm have identical glass transition temperatures of 110ºC. The thermogram of the PNIPMAAm/PEGPhA nanogels demonstrates the separate Tgs indicative of multiple domains, with phase transitions at 90ºC, 127ºC and 190 ºC. There is a slight increase in the Tgs of the PNIPMAAm domains, likely due to domains of copolymers of P(NIPMAAm-co-EGPhA).

Figure 6.14 is the DSC thermogram of the PNIPMAAm:PPhMA core/shell system. This thermogram shows only one Tg at 127°C, again signifying potential copolymerization of PNIPMAAm with its shell comonomer.

6.3.4 Pyrene Fluorescence

The pyrene fluorescence in Figure 6.15 shows no significant impact on the hydrophobicity of this system. Meaning that the systems are still hydrated and have similar hydrophilic states to that of water, which is not surprising due to the hydrated nature of these nanogels.

6.3.5 Fluorescein Loading and Release

The loading of fluorescein into core/shell nanogels shows no significant improvement over their unmodified counterpart, as seen in Figure 6.16. The release in Figure 6.17 does show a significant impact on the release of the hydrophobic model. While the unmodified and PNIPMAAm/PEGPhA systems release their payload instantaneously and without stimulus, the PNIPMAAm/TBMA core/shell system demonstrates no release over the 6 hour period. At which point release is triggered and a significant release level is attained.

6.3.6 DOX-Nanogel Interactions

The partition coefficient studies in Figure 6.18 show a preference for the PNIPMAAm/PTBMA core/shell nanogels. The partition coefficient is almost double that of PNIPMAAm and PNIPMAAm/PPhMA core/shell systems. This is further visualized by the image of DOX loaded nanogels seen in Figure 6.19. In this image there is an increasing reddish color between PNIPMAAm and PNIPMAAm/PPhMA, and PNIPMAAm/PPhMA and PNIPMAAm/PTBMA systems. Although this is a qualitative method, this does help to identify that the PNIPMAAm/PTBMA system achieved a higher loading level than the other systems.

The DSC thermogram of DOX loaded PNIPMAAm/PTBMA core/shell nanogels is seen in Figure 6.20 shows the physical state of the materials. There is no characteristic crystalline melting curve that would indicate that the DOX is in a crystalline state. This shows that the DOX loaded in the particles are in an amorphous state, and altering the Tg of the system. The DSC thermogram of PNIPMAAm/PPhMA core/shell nanogels is seen in Figure 6.21. Again, the DOX does not impart a crystalline melting curve, however this system's Tg remains unaltered. This is likely due to the lower loading levels with PNIPMAAm/PPhMA core/shell nanogels.

The release profiles for PNIPMAAm/PTBMA and PNIPMAAm/PPhMA core/shell nanogels can be seen in Figures 6.22 and 6.23. Figure 6.22 shows a minimal release for the PNIPMAAm/PTBMA core/shell system at 37 ºC over a 6 hour period. The temperature response is then triggered in a water bath and an overall release of 8 µg DOX/mg of particles is achieved.

Similarly, the PNIPAAm/PPhMA system in Figure 6.23 shows zero release during the 6 hour period at 37ºC, and then the temperature trigger causes the release of the DOX payload, delivering 3.7 µg/mg. These results show that although the system incorporating TBMA had a

higher partitioning coefficient and could attain higher loading levels, it has little impact on the final delivery levels. The increased partition coefficient limits the release level due to the preference of the drug for the hydrogel system over the surrounding solution.

6.3.7 Iron Oxide Nanopartice Incorporation

Iron oxide nanoparticles coated in PNIPMAAm/PTBMA can be visualized with TEM, as seen in figure 6.24. These micrographs show that most nanocomposites contain 5 or more iron oxide nanoparticles. These particles have spherical morphology, and a thin shell of polymer, likely due to the dry state of the images taken. The temperature swelling response can be seen in Figure 6.25. The swelling responses of these materials are similar to the swelling response of the PNIPMAAm/PTBMA core/shell nanogels whose response is in Figure 6.4.

6.4 Conclusions

Core/Shell nanoparticles were synthesized and characterized by a number of techniques. The DLS swelling studies demonstrate a lower yet still discernible LCST response of the core/shell materials. The NMR and DSC results confirmed the core/shell structure of the PNIPMAAm/PTBMA and PNIPMAAm/PEGPhA core shell systems. However, the PNIPMAAm/PPhMA system does not demonstrate the same domain separation, exhibiting only one Tg and NMR peaks of both the core and shell material. This compounded with the partitioning results show that the PNIPMAAm/PPhMA synthesis route does not have the same effect as copolymerization with TBMA and EGPhA.

Core/Shell nanogels were characterized for their effectiveness as chemotherapeutic delivery vehicles. The inclusion of drug into nanogels is improved by the development of the core/shell materials, and the core/shell systems do prevent premature release of their drug payload. However, these systems demonstrate relatively low release levels in response to the gentle

heating from changes in environment temperature. Though these release levels are likely limited due closed system used to measure this.

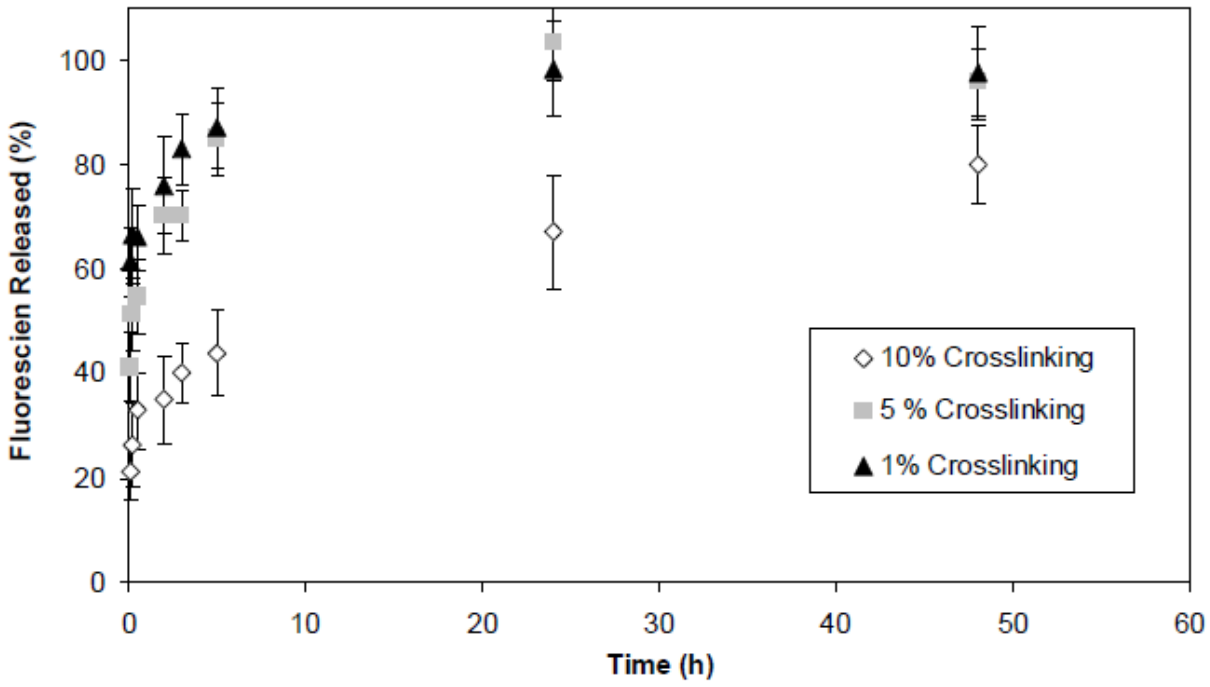

Figure 6.1: Measurement of release of a model therapeutic, fluorescein, from nanogels at 37 °C over a 48 h period. Release is quantified as a percentage of total amount of fluorescein loaded in the particles [58].

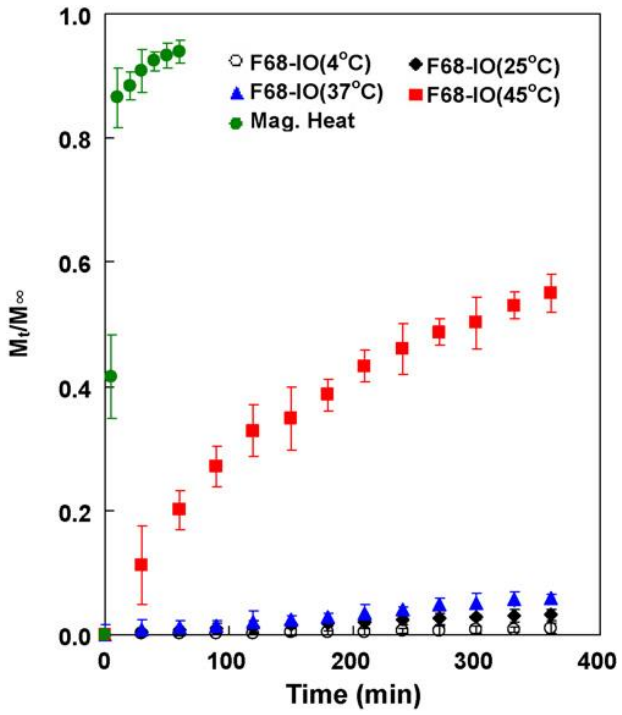

Figure 6.2: Release profiles from Pluronic F68-iron oxide nanocomposites as a function of time for various heating methods [59].

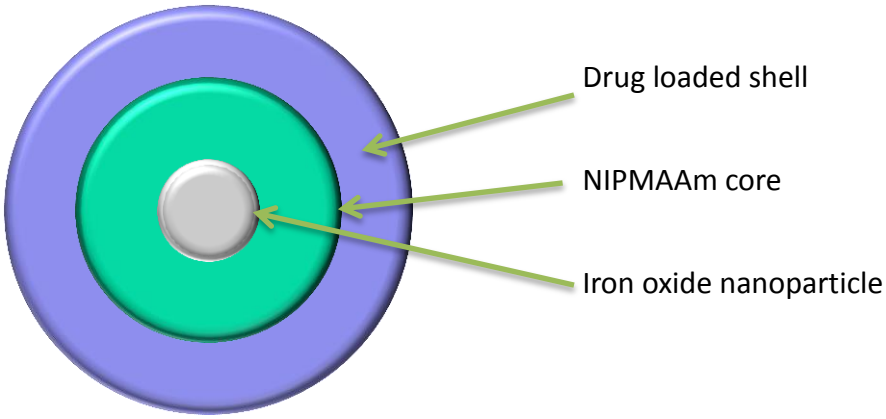

Illustration 6.1: Schematic for core shell systems.

Polymer	Z avg diameter 25ºC (nm)	PDI	LCST(ºC)	Overall Volume Swelling Response	Power Exponent	R^2 Value of Fit
PNIPMAAm	615.8	0.073	45	11.5	19.14	0.681
PNIPMAAm/PTBMA	351.9	0.231	43	0.82	9.8	0.821
PNIPMAAm/PEGPhA	222.5	0.36	44	1.4	10.0	0.465
PNIPMAAm/PPHMA	726.9	0.377	43	1.88	7.7	0.798

Table 6.3: Characteristics of the swelling responses of core/shell systems with 2:1 molar ratios of NIPMAAm:shell monomer in the feed ratio.

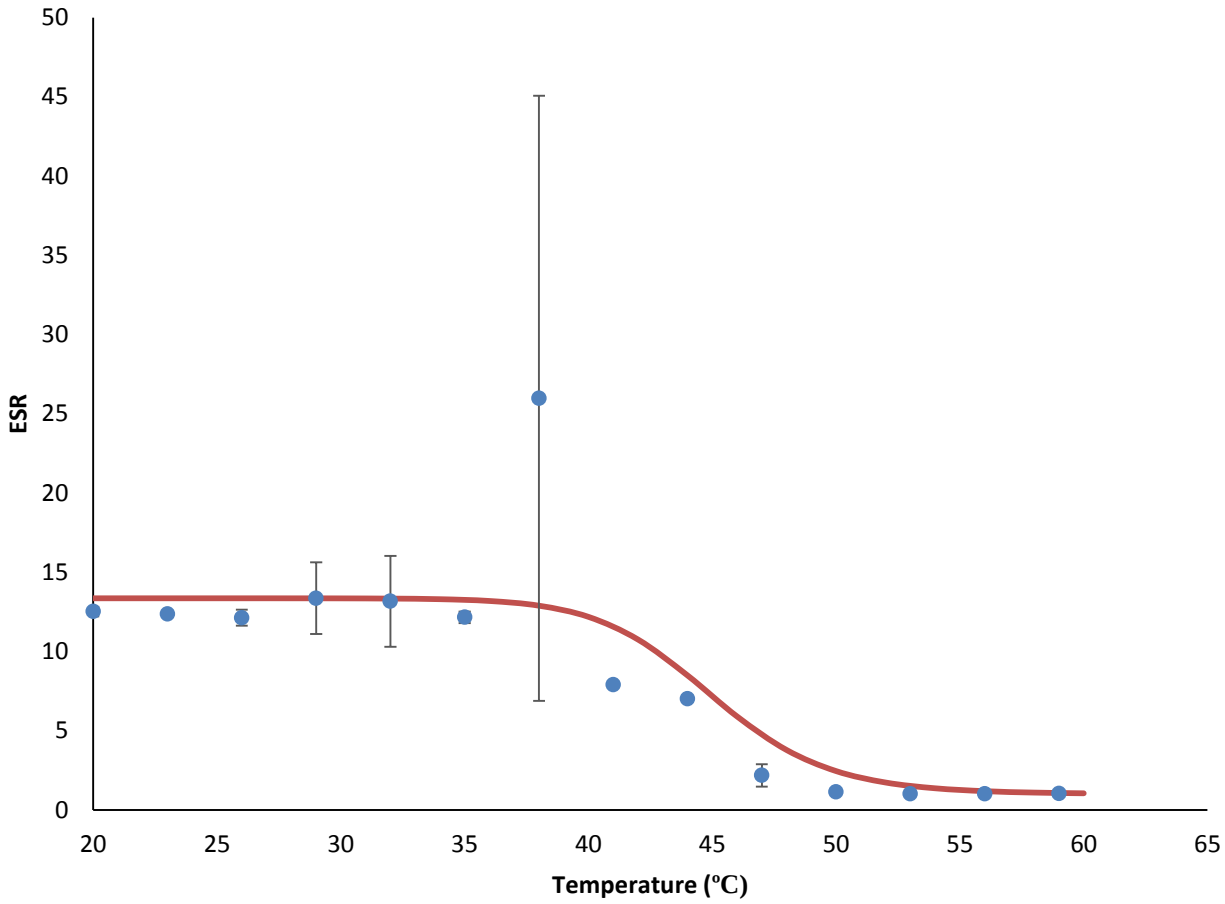

Figure 6.3: Equilibrium swelling ratio vs temperature of PNIPMAAm nanogels. 5% by mol MBAM in the feed. (N=3)

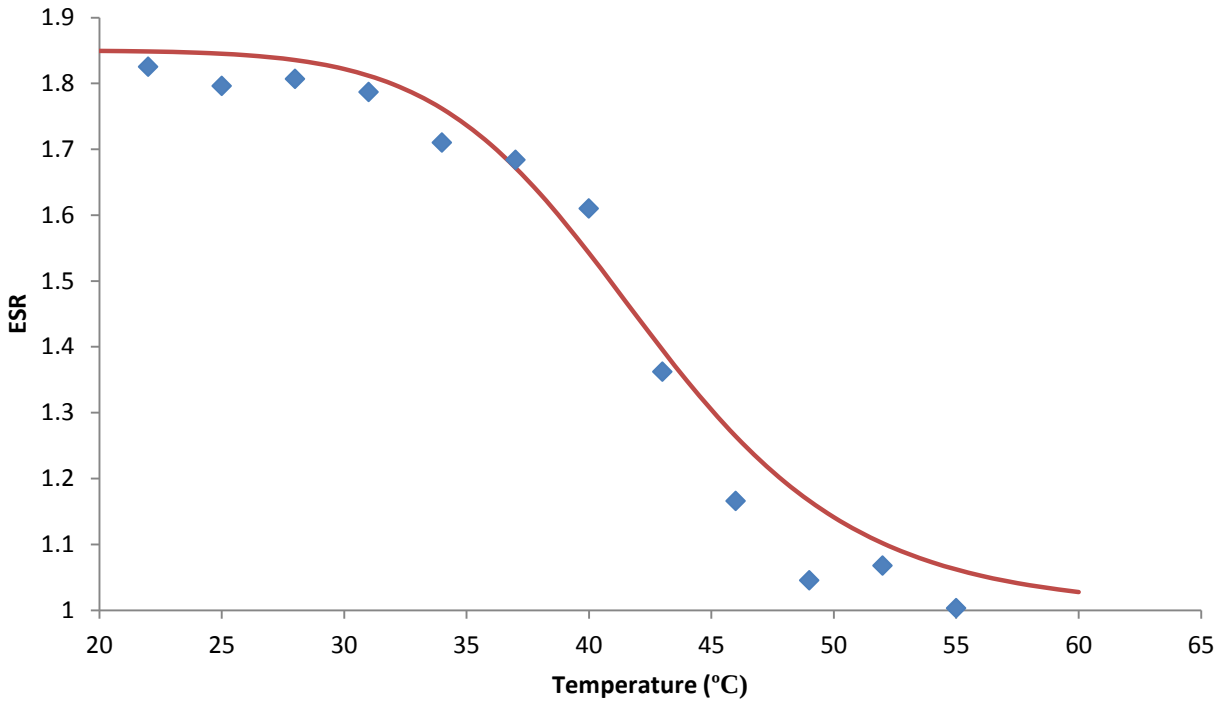

Figure 6.4: Equilibrium swelling ratio vs temperature of PNIPMAAm/PTBMA core/shell nanogels. 2:1 NIPMAAm:TBMA molar ratio. 5% by mol MBAM in the feed. (N=3)

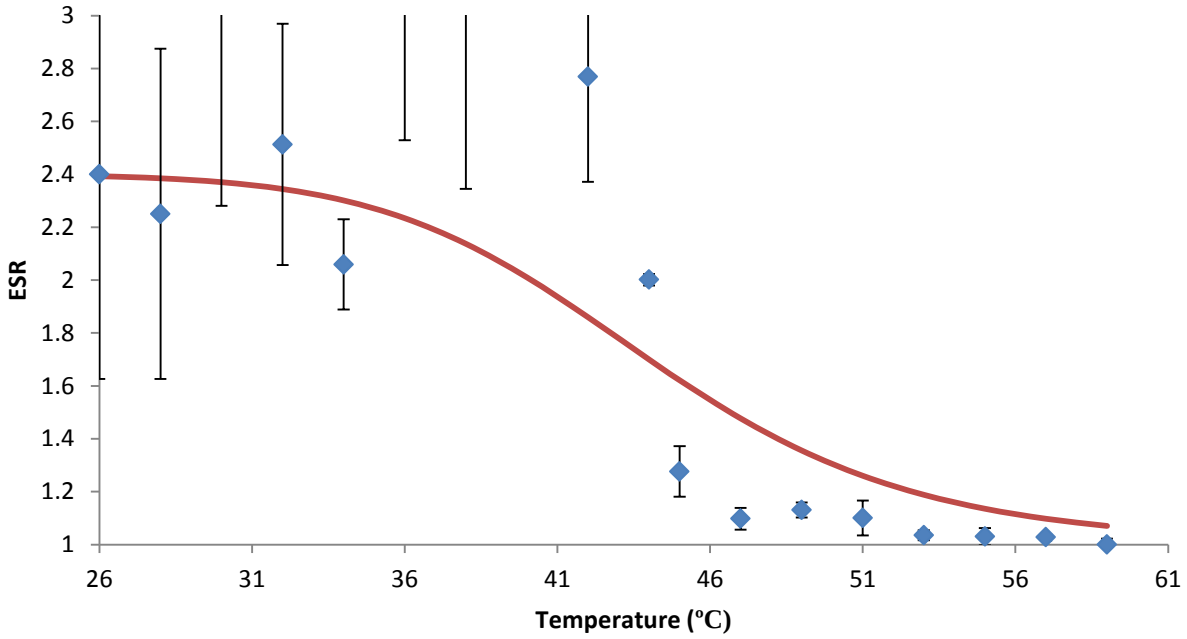

Figure 6.5: Equilibrium swelling ratio vs temperature of PNIPMAAm/EGPhA core/shell nanogels. 2:1 NIPMAAm:EGPhA molar ratio. 5% by mol MBAM. (N=3)

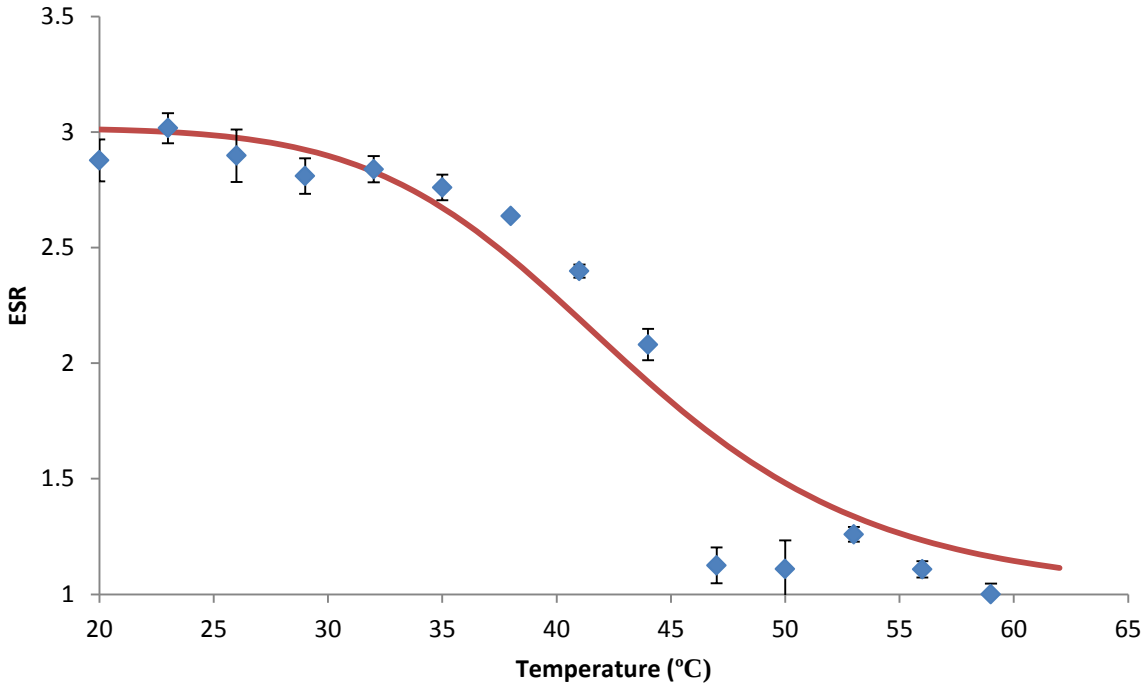

Figure 6.6: Equilibrium swelling ratio vs temperature of PNIPMAAm/PPhMA core/shell nanogels. 2:1 NIPMAAm:PhMA molar ratio. 5% by mol MBAM. (N=3)

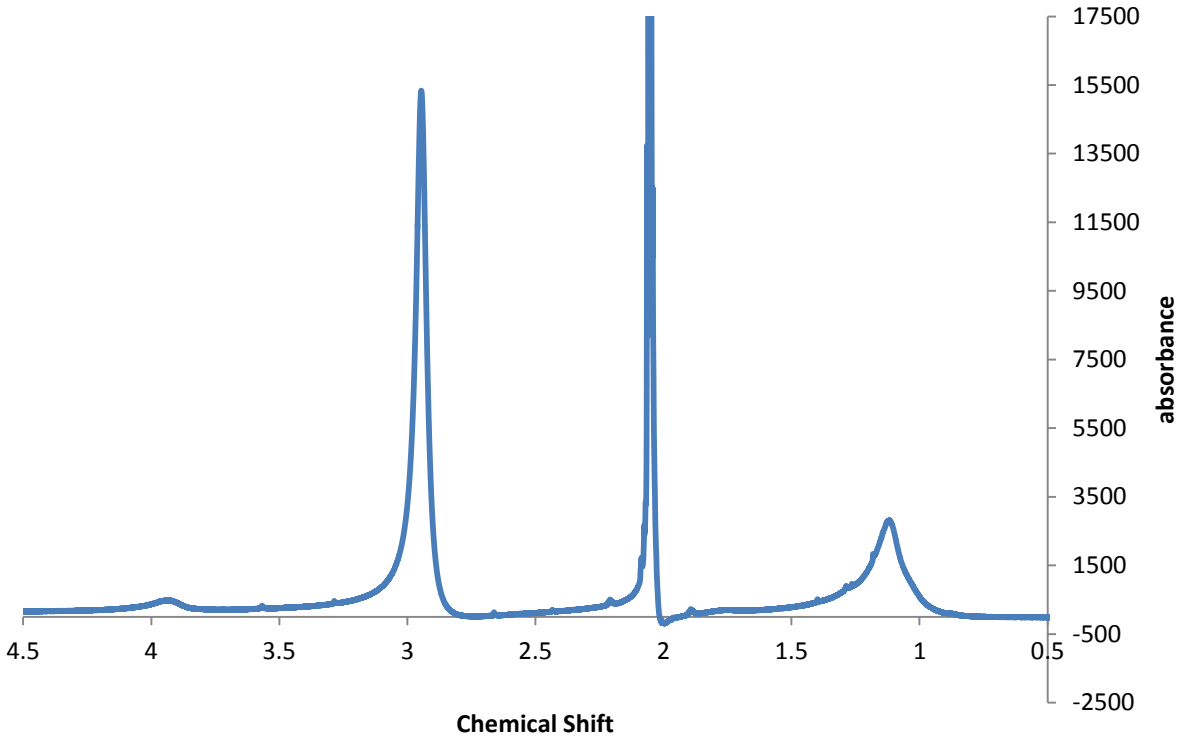

Figure 6.7: H^1 NMR of PNIPMAAm nanogels.

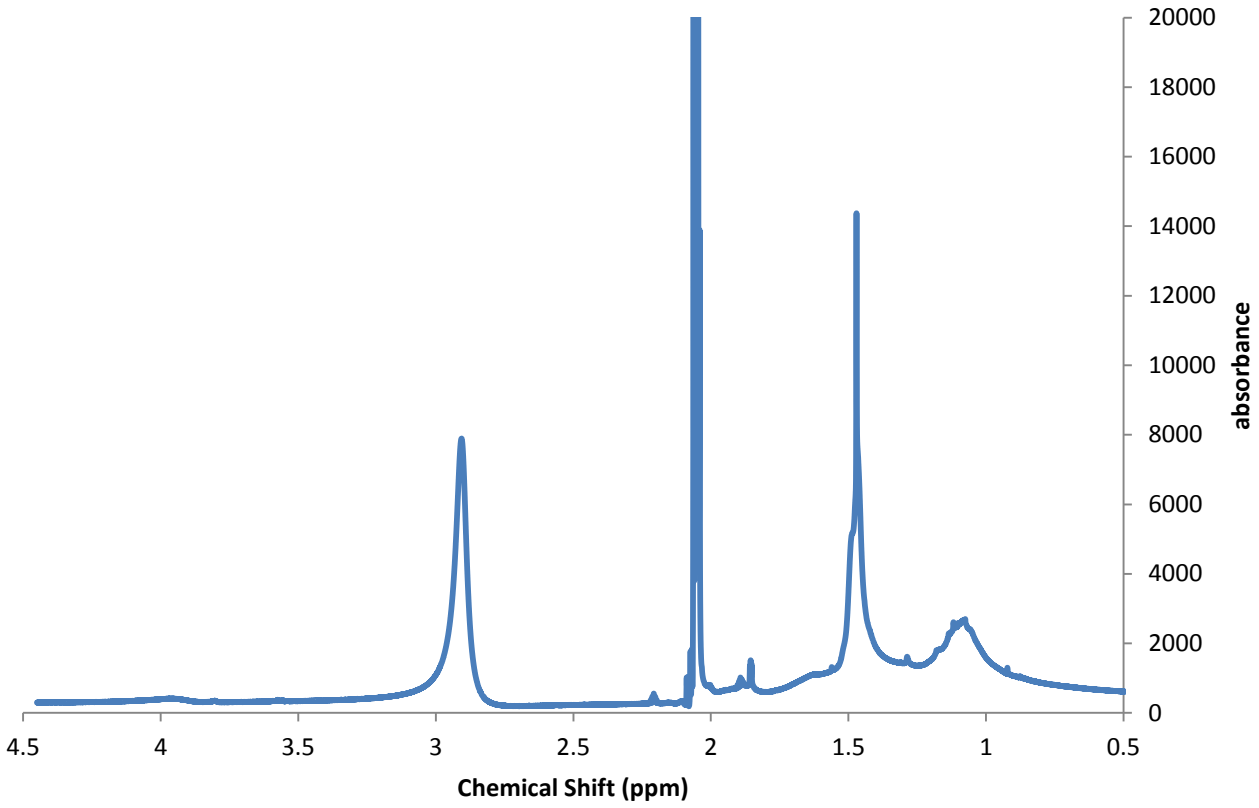

Figure 6.8: H^1 NMR of PNIPMAAm/PTBMA core/shell nanogels. 2:1 NIPMAAm:TBMA molar feed ratio. 5% MBAM.

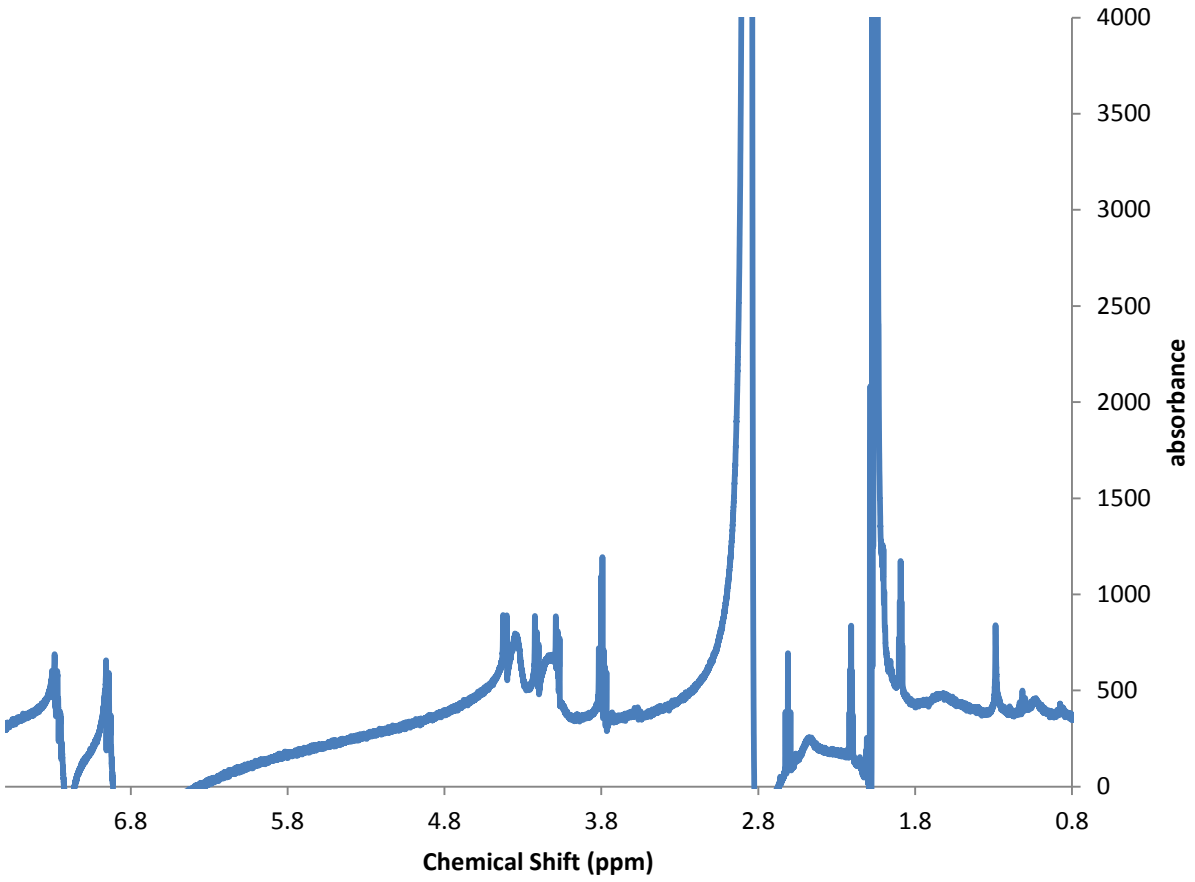

Figure 6.9: H^1 NMR of PNIPMAAm/PEGPhA core/shell nanogels. 2:1 NIPMAAm:EGPhA molar feed ratio. 5% MBAM.

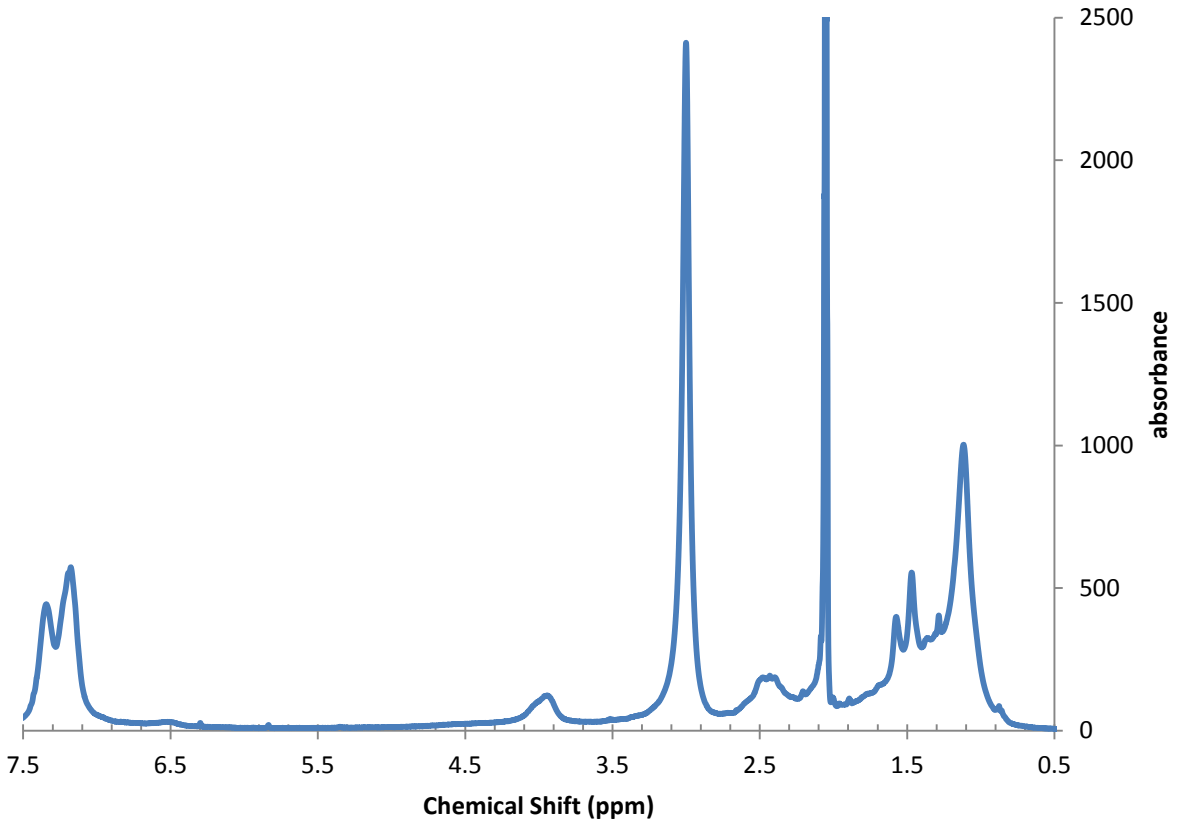

Figure 6.10: H^1 NMR of PNIPMAAm/PhMA core/shell nanogels. 2:1 NIPMAAm:PhA molar feed ratio. 5% MBAM.

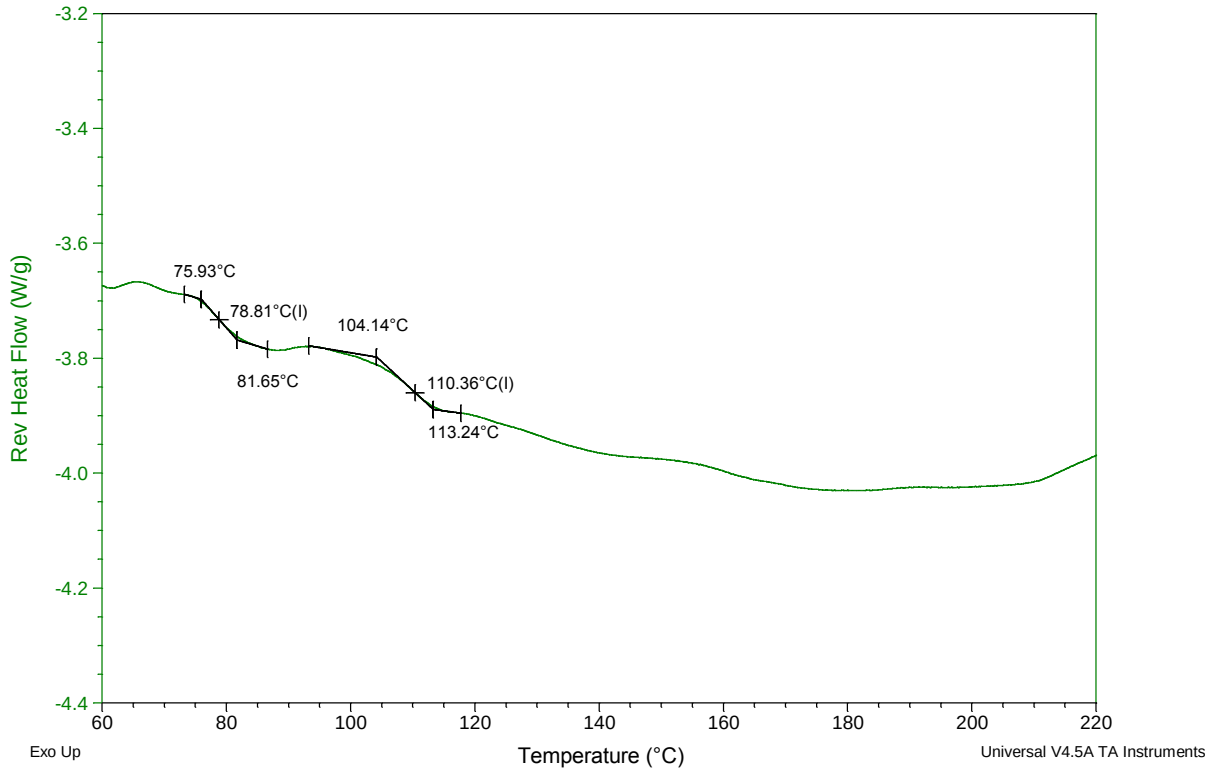

Figure 6.11: DSC thermogram of PNIPMAAm nanogels.5% MBAM.

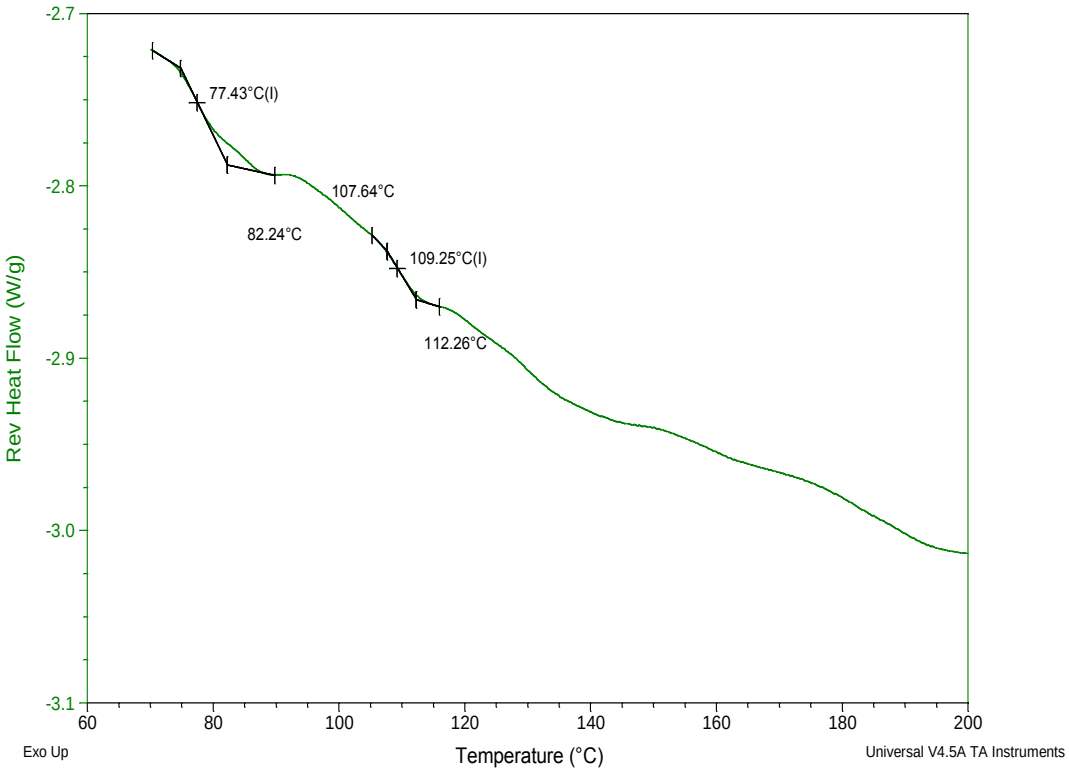

Figure 6.12: DSC Thermogram of PNIPMAAm/PTBMA core/shell nanogels. 2:1 NIPMAAm:TBMA molar feed ratio. 5% MBAM.

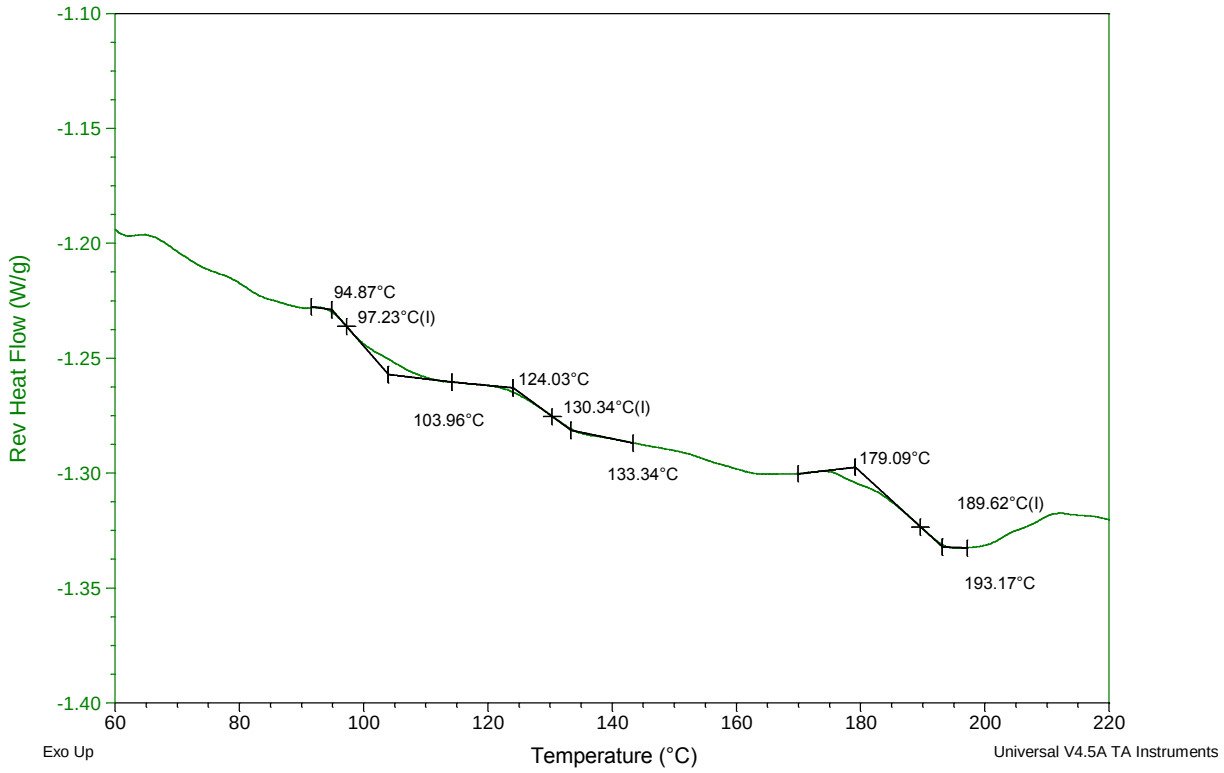

Figure 6.13: DSC Thermogram of PNIPMAAm/PEGPhA core/shell nanogels. 2:1 NIPMAAm:EGPhA molar feed ratio. 5% MBAM.

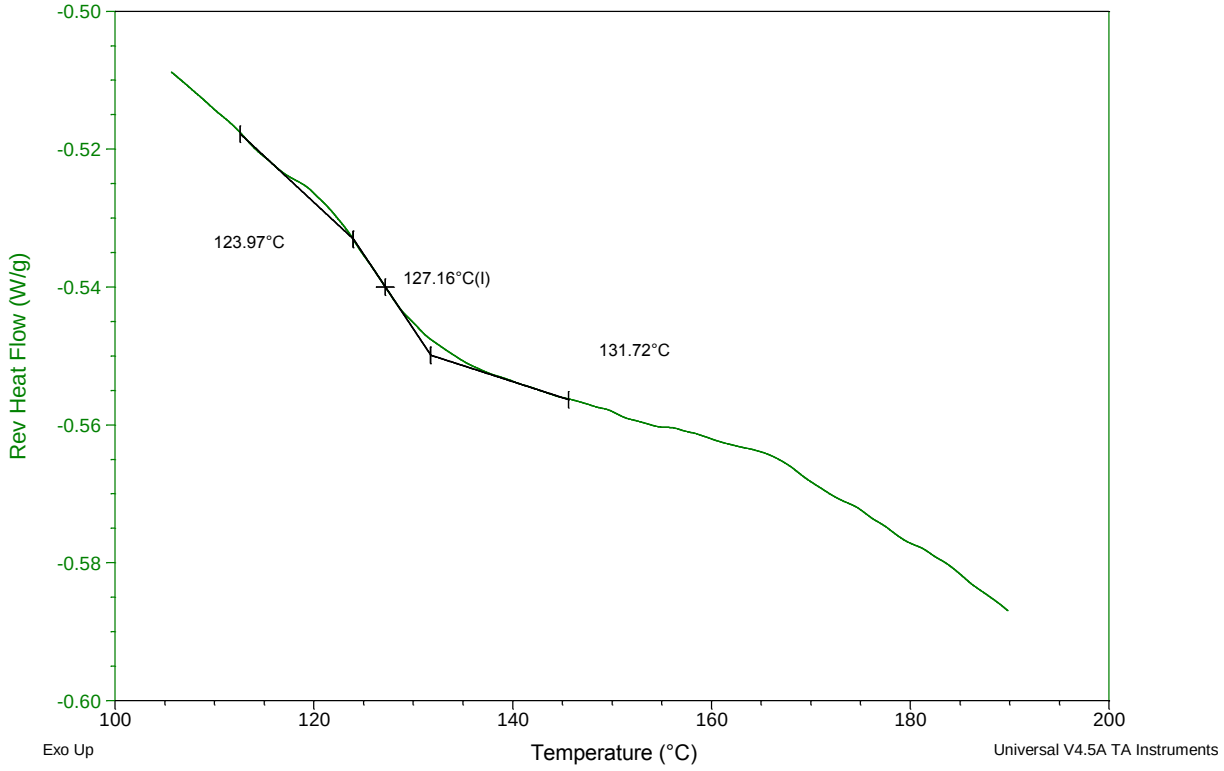

Figure 6.14: DSC Thermogram of PNIPMAAm/PPhMA core/shell nanogels. 2:1 NIPMAAm:PhMA molar feed ratio. 5% MBAM.

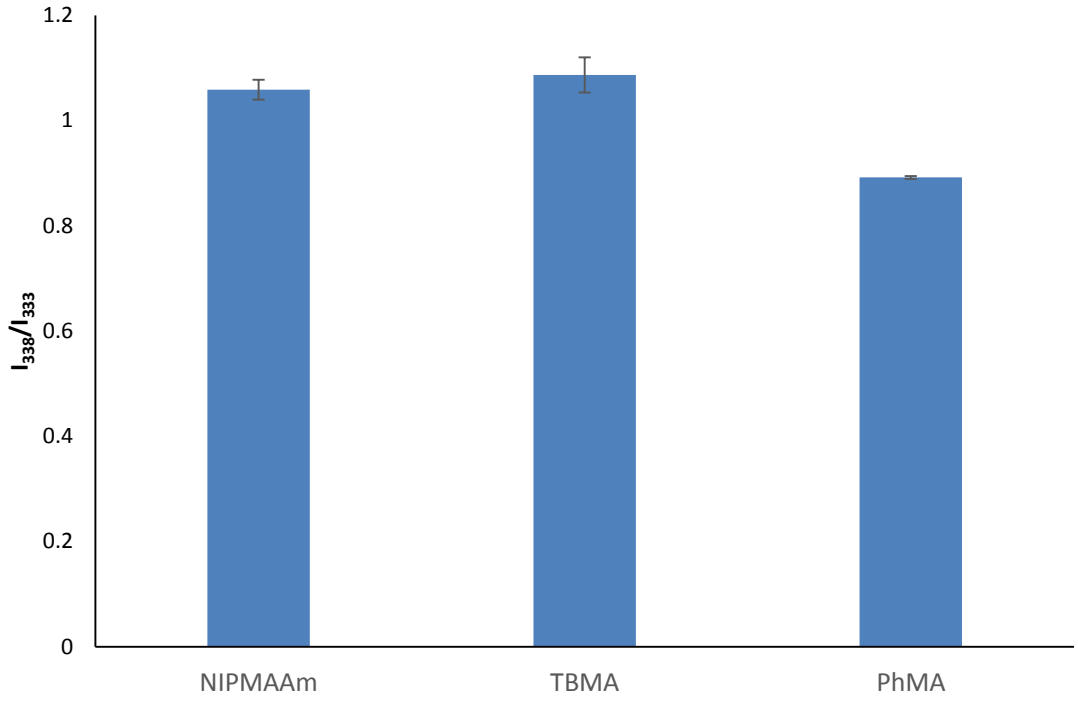

Figure 6.15: Pyrene fluorescence studies of PNIPMAAm core/shell nanogels. 2:1 molar ratios of PNIPMAAm: shell comonomer. 5% MBAM. (N=3)

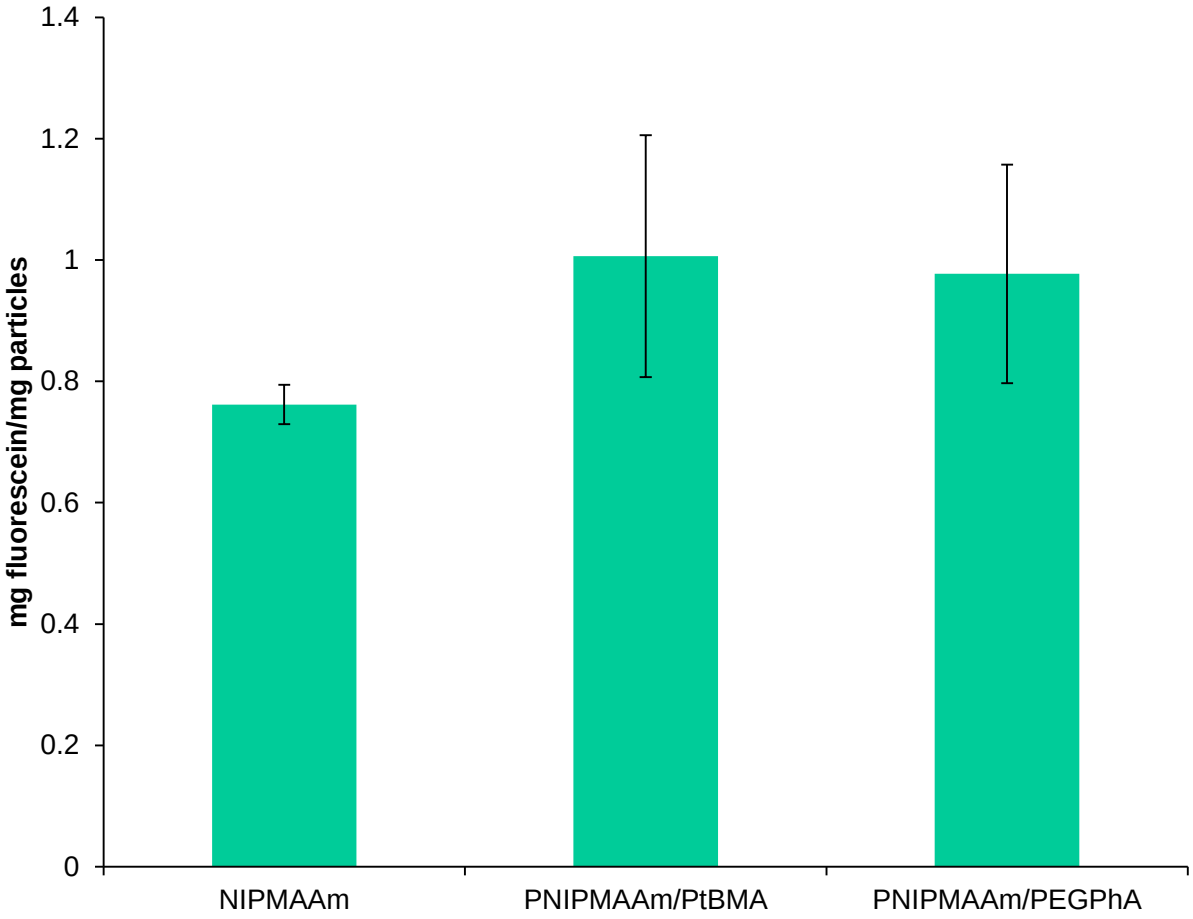

Figure 6.16: Fluorescein loading of PNIPMAAm core/shell nanogels. 2:1 molar ratios of PNIPMAAm: shell comonomer. 5% MBAM. (n=3)

A.

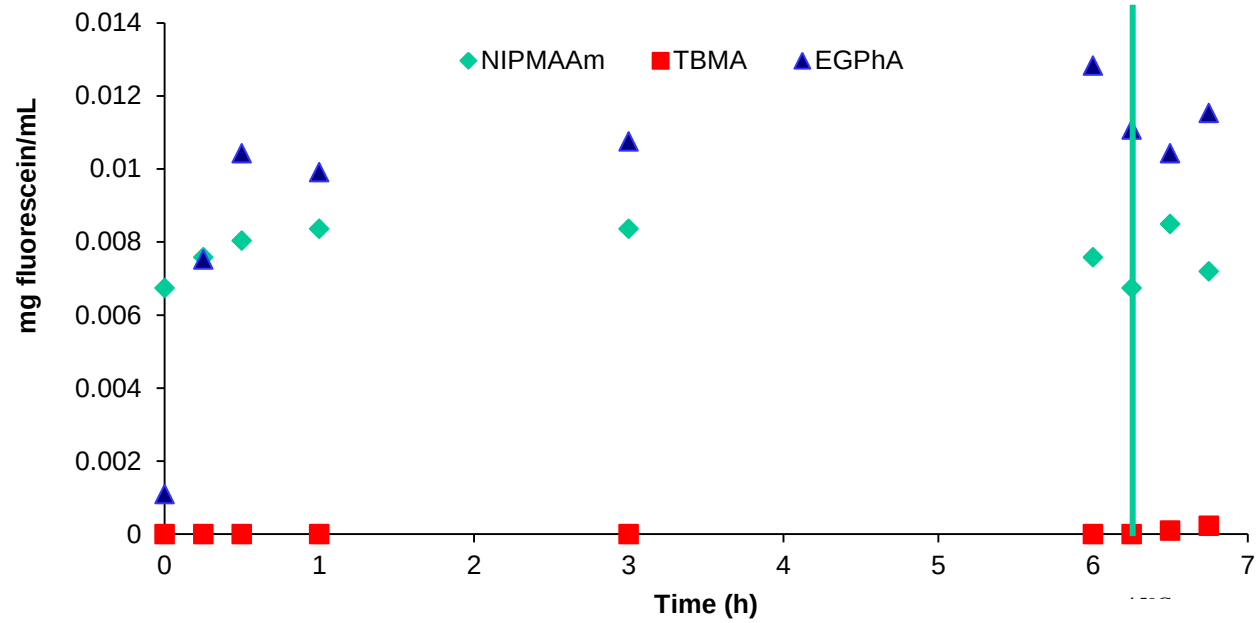

B.

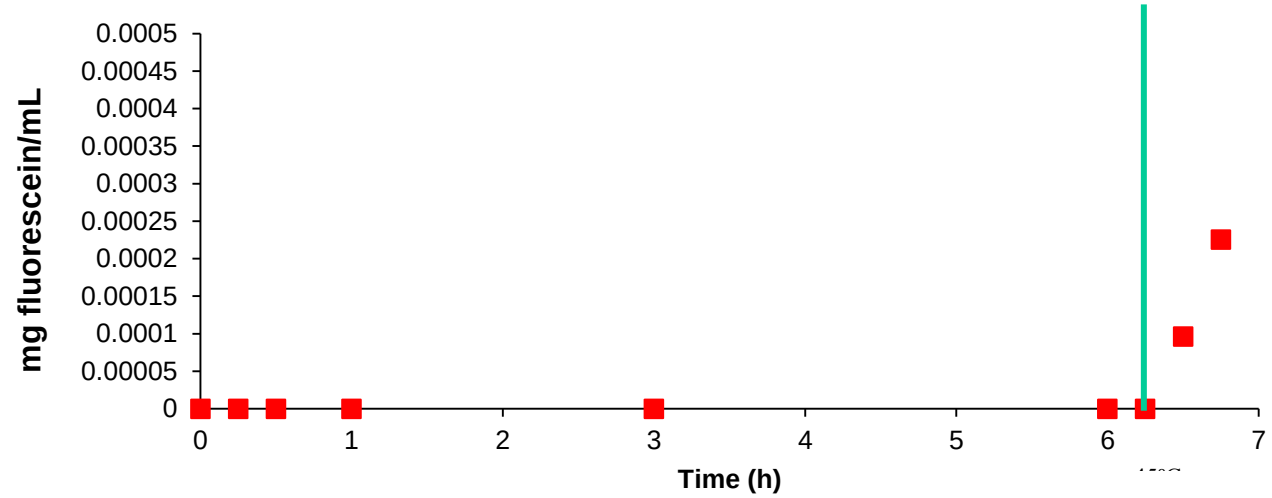

Figure 6.17: Fluorescein release from PNIPMAAm core/shell nanogels. 2:1 molar ratios of PNIPMAAm: shell comonomer. 5% MBAM. (1 mg/mL particles in DI water) This caption id not clear.

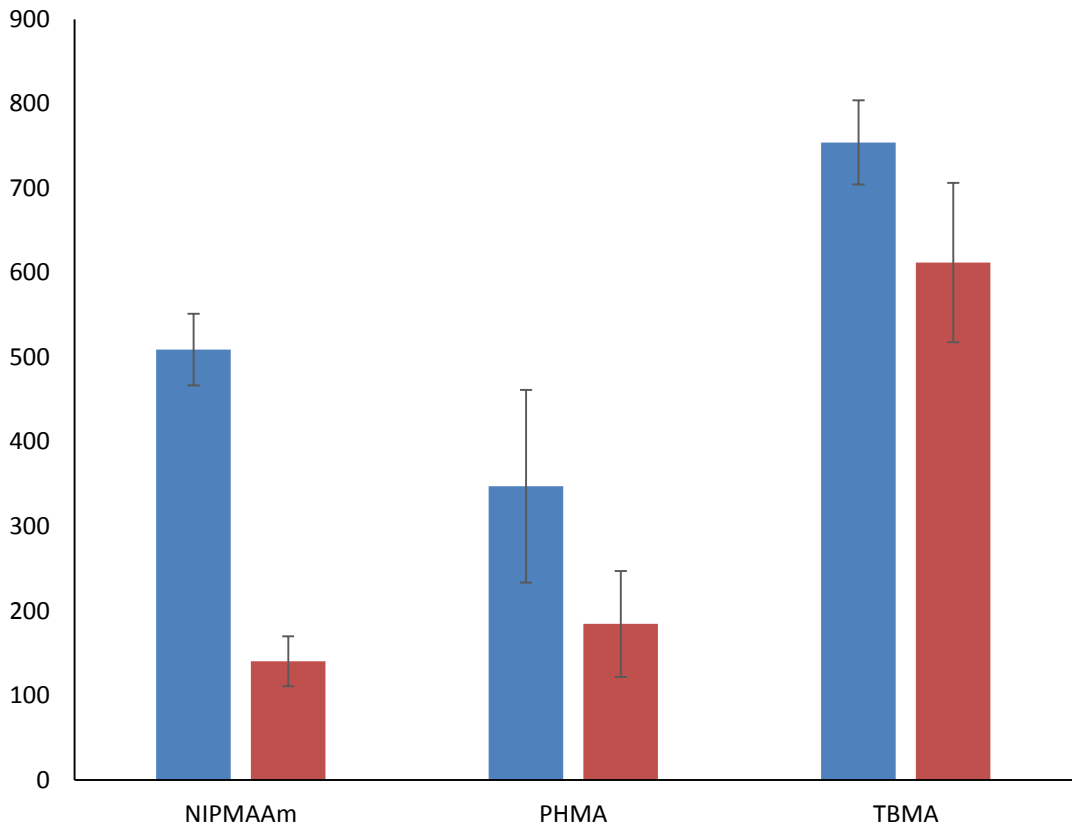

Figure 6.18: DOX partition coefficient of PNIPMAAm core/shell nanogels. 2:1 molar ratios of PNIPMAAm: shell comonomer. 5% MBAM. (N=3)

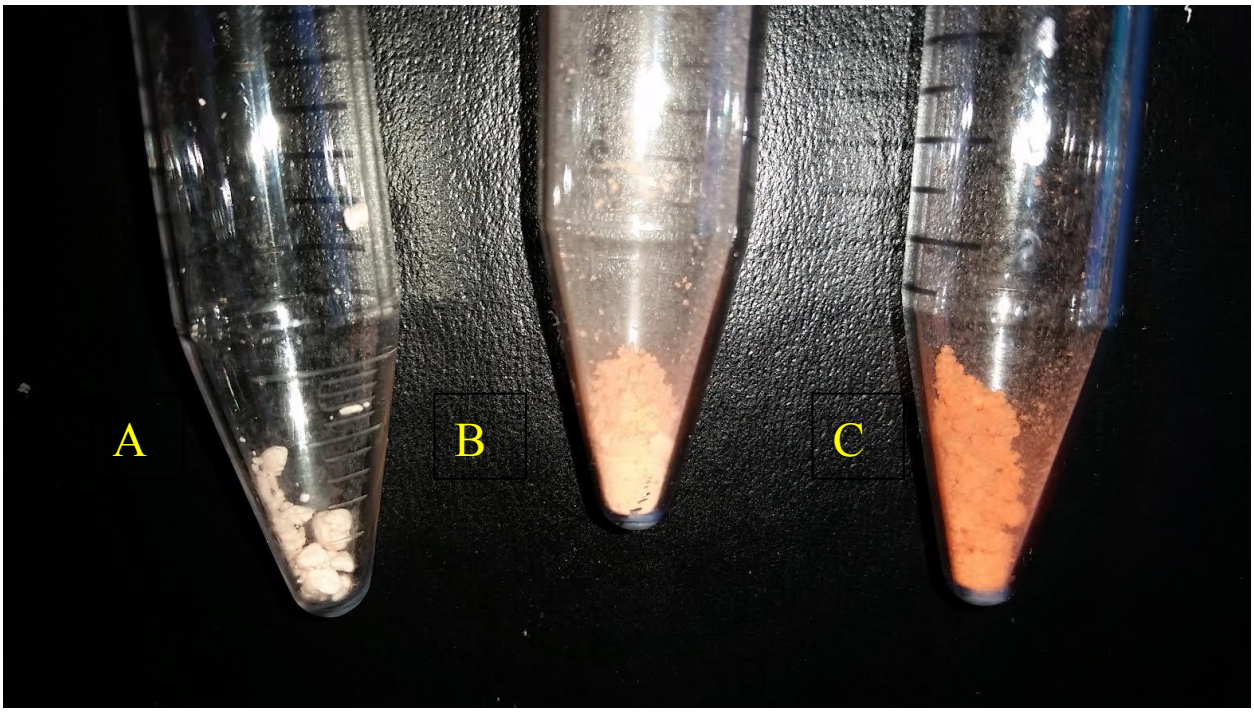

Figure 6.19: Images of freeze dried DOX loaded PNIPMAAm core shell nanogels. 2:1 molar ratios of PNIPMAAm: shell comonomer. 5% MBAM. A. PNIPMAAm. B. PNIPMAAm:PPhMA core:shell. C:PNIPMAAm:PTBMA core:shell nanogels.

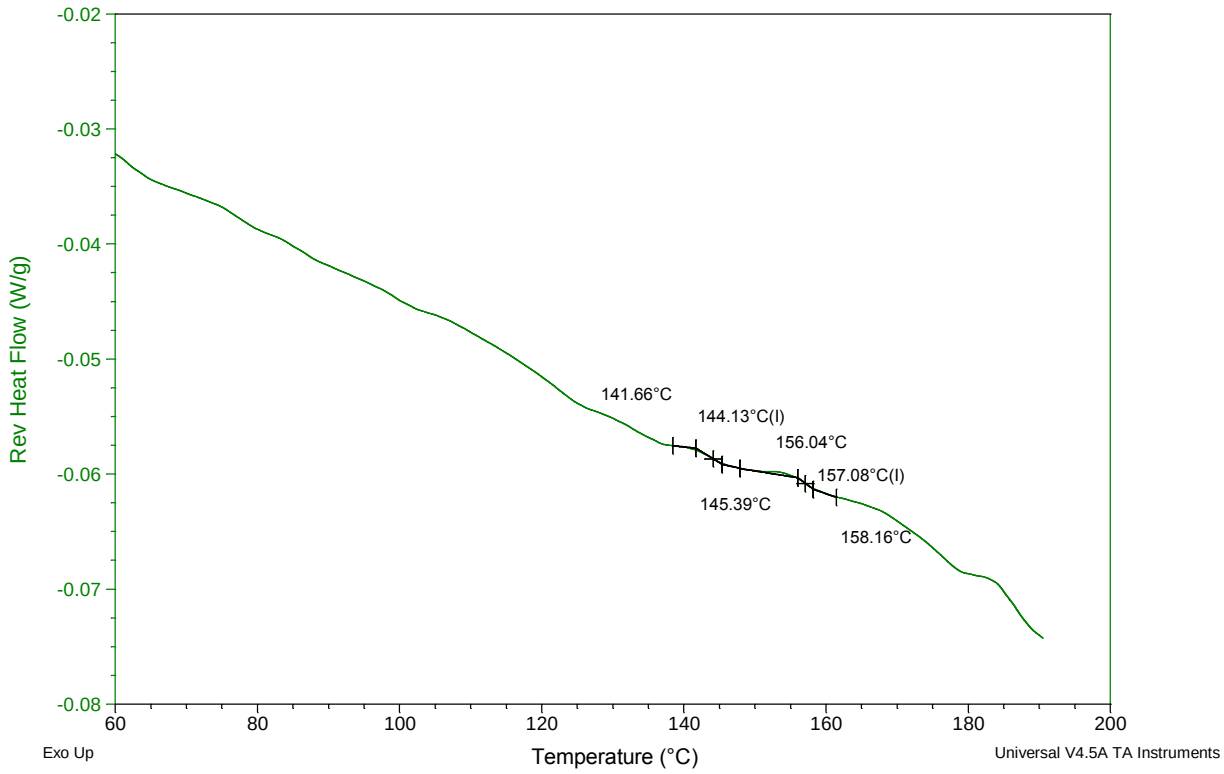

Figure 6.20: DSC Thermogram of PNIPMAAm:PTBMA core/shell nanogels loaded with DOX. 2:1 NIPAAm:TBMA monomer molar ratio.

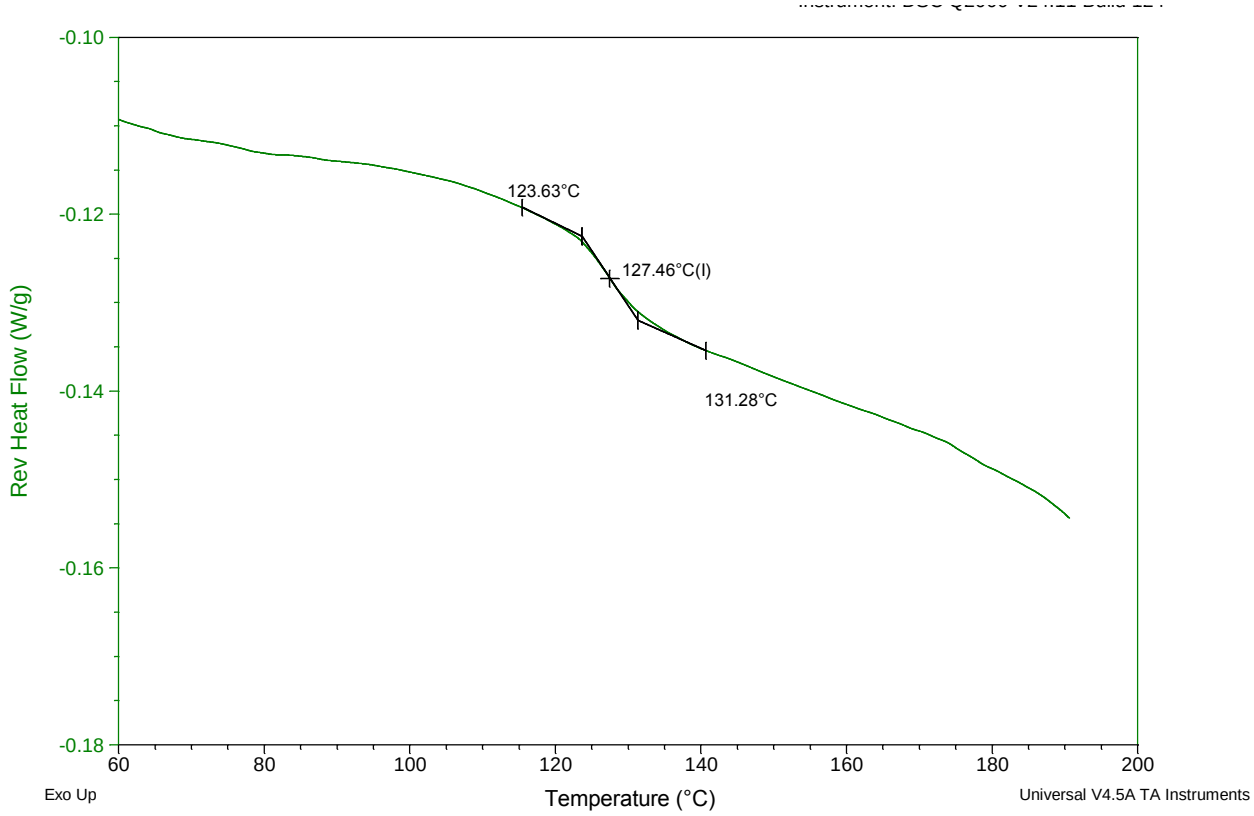

Figure 6.21: DSC Thermogram of PNIPMAAm:PPhMA core/shell nanogels loaded with DOX. 2:1 NIPAAm:TBMA monomer molar ratio.

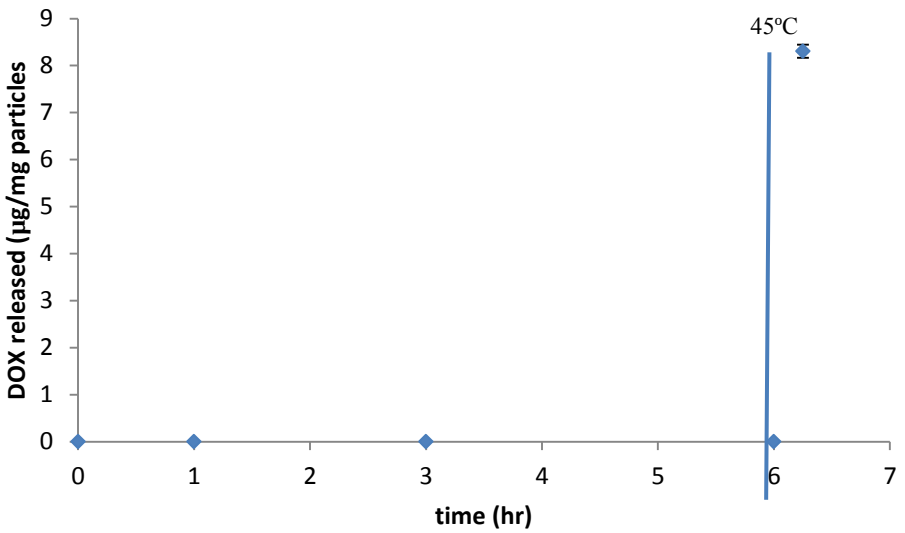

Figure 6.22: DOX release from PNIPMAAm/PTBMA core/shell nanogels. 2:1 molar ratio of PNIPMAAm:TBMA. 37ºC for 6 hours, then release triggered in a water bath at 45ºC. (N=3)

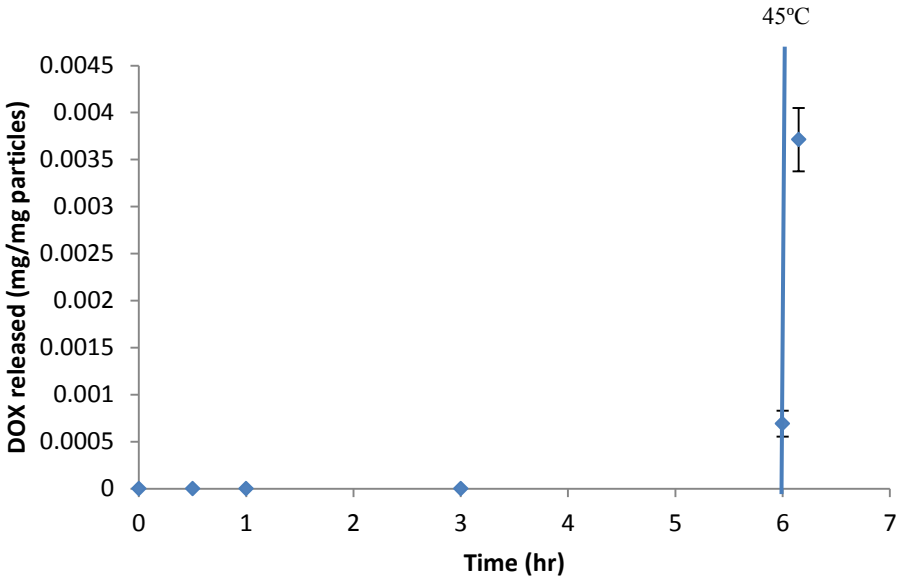

Figure 6.23: DOX release from PNIPMAAm/PPhMA core/shell nanogels. 2:1 molar ratio of PNIPMAAm:TPhMA. 37ºC for 6 hours, then release triggered in a water bath at 45ºC. (N=3)

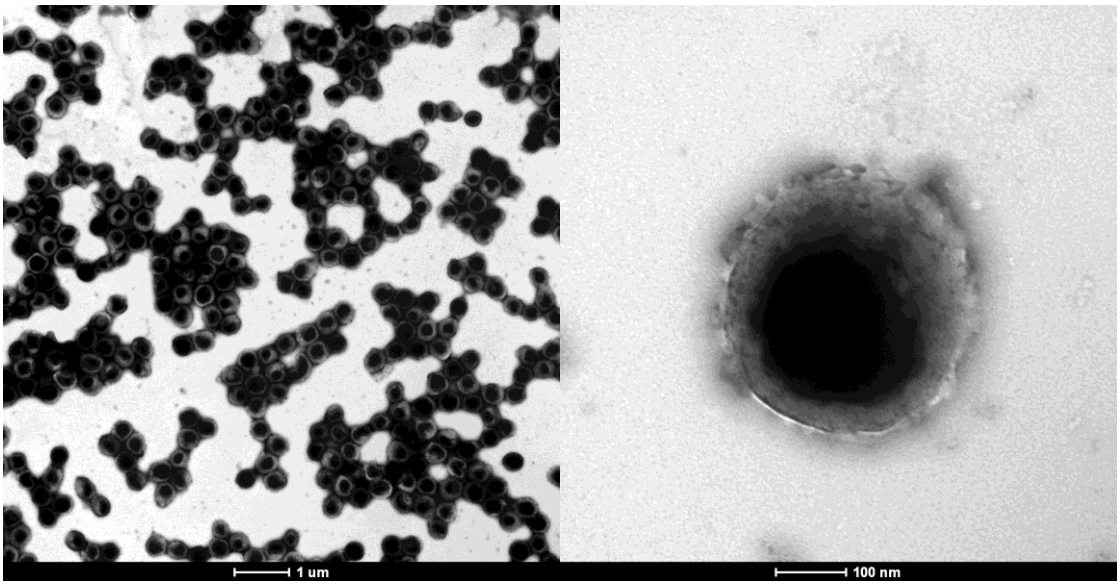

Figure 6.24: TEM micrograph of 30 nm iron oxide nanoparticles PNIPMAAm/PTBMA core/shell 2:1 molar ratio.

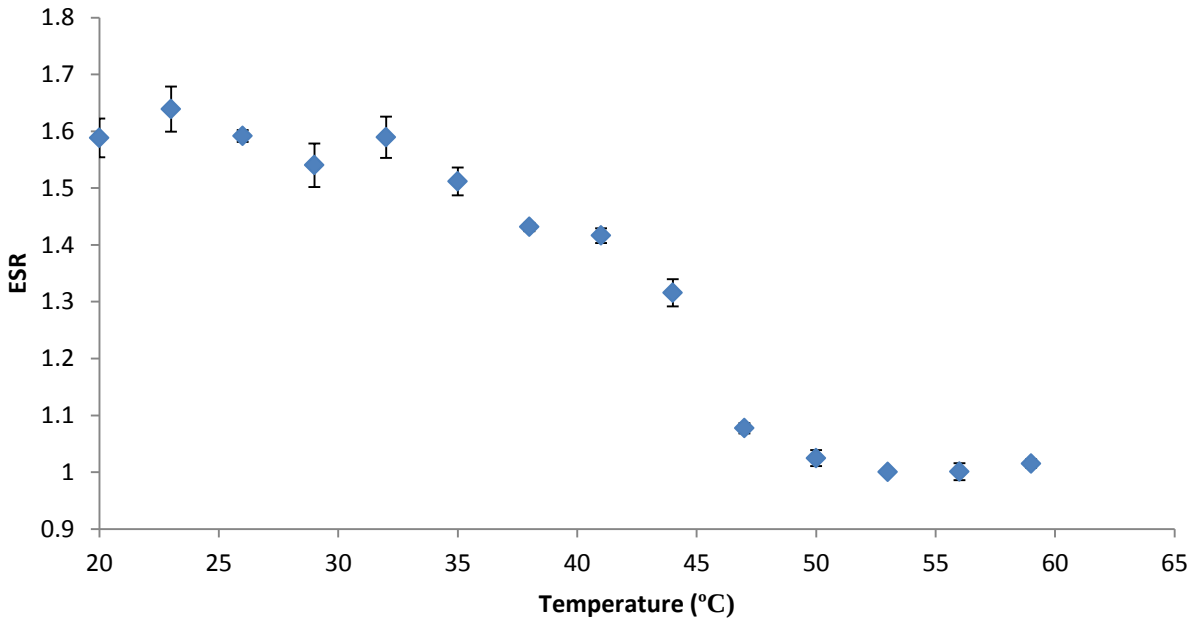

Figure 6.25: Equilibrium swelling ratio versus temperature for 30 nm Iron Oxide nanoparticles encapsulated in PNIPMAAm/PTBMA 2:1 core/shell systems.

CHAPTER 7

Schizophrenic Block Copolymers for the Synthesis of Complex Core/Shell Theranostic Composites

7.1 Background

As discussed previously in chapter 6, a new style of drug delivery systems is necessary in order to utilize deswelling nanogels. The development of these complex systems requires new applications of recently discovered chemistries. There has been a big push in recent years to use the self-assembly and post-synthesis crosslinking of amphiphilic particles to form these core/shell hydrogel systems [40, 58, 59]. These systems are desirable due to the increased control over size and polymerization, limiting large discrepancies in polymer molecular weight and particle size. The incorporation of cross-links, however, is still a statistical problem, as the cross-linking comonomers are still included randomly throughout the blocks.

The standard reaction schemes for the development of these block copolymers include reversible addition-fragmentation chain-transfer (RAFT) and atom-transfer radical-polymerization (ATRP). These are two types of controlled polymerizations that limit the concentration of growing polymer by including an intermediate ligand that reversibly reacts with free radicals[60]. However, these are polymerization mechanisms that depend on low oxygen concentrations and high levels of other dangerous chemicals. New forms of ATRP polymerizations offer avenues around these issues. Initiators for continuous activator regeneration (ICAR) and activators regenerated by electron transfer (ARGET) ATRP systems include mechanisms to regenerate the copper catalysts that are necessary for ATRP reactions, allowing for higher oxygen content and less pure monomers [61].

ARGET ATRP has been shown to work with a number of monomers including NIPAAm, making it a promising candidate for a synthesis mechanism of these particles. ARGET ATRP works as shown in illustration 7.1. Essentially, the reaction is initiated when the reduced copper/ligand complex reduces the initiator to start the reaction. This reaction is in equilibrium, favoring the deactivated state. Normally, in ATRP reactions, oxygen acts as a free radical scavenger terminating the reaction and oxidizing the copper. ARGET overcomes this by charging the solution with a reducing agent to regenerate the reduced copper catalyst[60].

This methodology has been shown to work with NIPAAm and functionalized methacrylate based systems, and provides an easy mechanism for the attachment of PEG via a macroinitiator[62]. There has also been great success including monomers that provide a variety of cross linking strategies. These strategies are outlined in Table 7.1. With these mechanisms and the relatively robust nature of ARGET ATRP reactions, compared to other controlled polymerizations, amphiphilic block copolymers can be easily synthesized for self-assembled covalently cross linked micelles, imparting all of the factors necessary for an effective delivery method.

Much as in chapter 6, these methods will be used to develop hydrophobic shell/temperature responsive core system. The system is visualized in illustration 7.2, where, by using a PEG corona and the hydrophobic collapse of PNIPMAm gels, systems can be synthesized like those in image 7B with a hydrophobic middle section. Cross-linking comonomers can be incorporated into both the core and shell systems, and the micelles can be cross-linked to form nanogels.

7.2 Materials and Methods

7.2.1Block co-polymer synthesis

Block copolymers were synthesized using an ARGET ATRP reaction scheme. The first step involved dissolving a PEG macroinitiator (PEG ethyl isobutyrate) with ligand (tris pyridyl methyl amine (TPMA), Copper (II) Bromide, TBMA, and glycidyl methacrylate (GMA) in 35 mL ofwater in the values seen in Table 7.2. This reaction was then purged with nitrogen and a solution of the reducing agent, ascorbic acid (ASC), in water was injected. This solution was then allowed to react for 2 hours, at which point a solution of 0.008 mol of NIPMAAm and 0.4 mol of GMA in 20 mL of water was nitrogen purged and transferred into the reaction to form the final block. These solutions were then dialyzed against 18.2MΩ cm water for 1 week with twice daily water changes.

Component	Mol
Glycidyl methacrylate	0.00039
TBMA	0.0039
Copper (II) Bromide	2.67×10^{-5}
PEG-bromoisobutyrate	1.3×10^{-4}
Tris pyridyl methyl amine	2.61×10^{-5}

Table 7.2: Molar quantities of triblock copolymer synthesis initial solution.

7.2.2 Post-Micellarization Crosslinking

The nanogels were then formed by heating a solution of 1 mg/mL of the block copolymers to 80ºC. After attaining temperature a solution of 1 mg/mL NH_2-PEG-NH_2 was injected to crosslink the GMA units to form spherical nanogels.

7.2.3 Measurement of Micelle formation: DLS

The effect of temperature on the formation of micelles was measured using a Malvern Zetasizer ZS (Malvern, UK). The data were collected by dissolving freeze dried particles in 1 mL of DI water and adjusting the temperature by 3ºC increments and then allowed to equilibrate for 60 seconds. Temperature was ramped 20ºC to 59ºC and then down to 20ºC

7.2.4 NMR Spectroscopy

Nuclear magnetic resonance spectra were taken with a NMSR spectrophotometer (model 400 MHZ, Varian Palo Alto, CA) with a Direct Drive sample changer. Samples were dissolved in deuterated acetone at a concentration of 20 mg/mL.

7.2.5 DSC

Modulated DSC studies were performed with a DSC (Q2000, TA instruments, New Castle, DE). Samples were loaded at a minimum weight of 5 mg into aluminum pans and sealed. Studies were run from 20-200ºC in a nitrogen environment.

7.2.6 TEM Imaging

Images were obtained on an Transmission Electron Microscope (FEI Tecnai, Hillsboro, OR) operating at 80 kV. Carbon coated copper grids (400 mesh) were plasma treated using an Emitech Glow Discharge instrument to render them hydrophilic prior to adding 5 µL of the nanoparticle suspension. After 30 seconds, the nanoparticle suspension was wicked off using Whatman 1 filter paper. The particles were negatively stained by placing a 5 µL drop of the staining solution (2% uranyl acetate for the crosslinked micelles, 2% phosophotungstic acid, pH 8.0 for the polymer-magnetic particle composites) on the particle-coated grid for 30 seconds before being wicked off with Whatman 1 filter paper.

7.3 Results and Discussion

7.3.1 Uncrosslinked Micelle Formation

Figure 7.1 shows the DLS temperature trend of a 1 mg/mL suspension of linear P(EG-b-TBMA-b-NIMAAm). At temperatures below the LCST of about 44ºC, the system demonstrates no repeatable size. This point is also where the counts detected by the DLS drop below a potentially critical value of 20,000 kilo counts per second (kcps) as seen in Figure 7.2.

Investigation of characteristic intensity peaks and correlation functions from above and below the LCST also show a significant change in the quality of data, as seen in Figure 7.3 and 7.4. The intensity peak below the LCST is jagged and the correlation function does not demonstrate the sigmoidal shape necessary for the DLS to produce accurate measurements of hydrodynamic radius. These results are indicative of polymers that are solubilized in the solution rather than spherical nanoparticles. The characteristic results from above the LCST are seen in Figure 7.4. Here, there is a smooth intensity curve and sigmoidal correlation function, signifying low polydispersity and spherical morphology.

The NMR results in Figure 7.5 show the presence of PEG, PNIPMAAm, and PTBMA characteristic shifts. The characteristic PNIPMAAm tertiary isopropyl carbon shift and PEG ethylene shifts at 3.9 and 4.0, respectively, are present in about equal quantiles signifying a ratio of 4:1 NIPMAAm to ethylene glycol units, which is to be expected with the molar quantities of these components in the feed. The exact TBMA incorporation is muddled by the similar shifts it shares with PNIPMAAm. Although its presence can be confirmed from the size of the methyl proton peak comparted to the peak of the PNIPMAAm. Normally this ratio for PNIPMAAm alone is 9:1, in this instance this ratio is 10.5:1.

7.3.2 Post-Micellerization Crosslinking for Nanogel Formation

The TEM nicrographs of these nanoparticles are seen in Figure 7.6. These images show spherical polymeric nanogels. Since the micelles only form at temperatures well above room temperature, the TEM images prove that the micelles were crosslinked during the crosslinking step. If they were not, the TEM images would show no spherical structures.

7.4 Conclusions

Tri-block copolymers have been synthesized and their self-assembling nature characterized with DLS. These systems have demonstrated ability to self-assemble in response to increase in temperature above the LCST. They also can be crosslinked after self-assembly to form permanent nanogels.

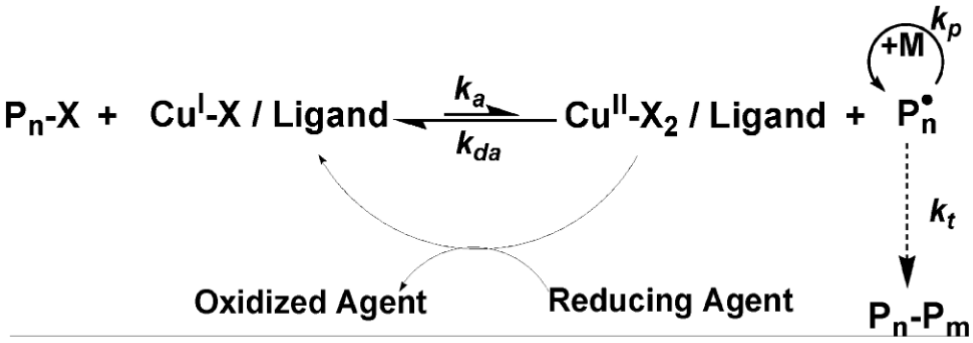

Illustration 7.1: Schematic for a general ARGET-ATRP reaction[63].

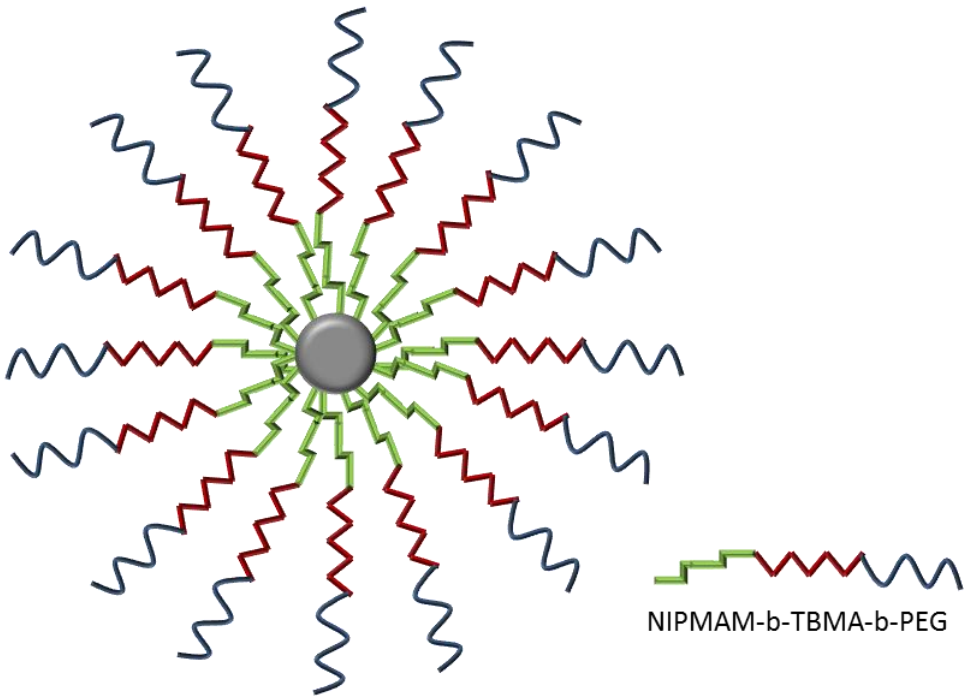

Illustration 7.2: Micelle formation of tri-block copolymers around a magnetic core.

Entry	–X	R–
1	$–NH_2$	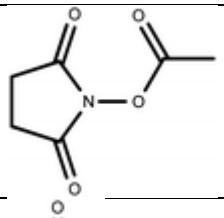
		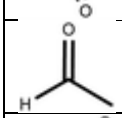
		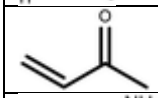
		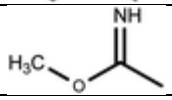
2	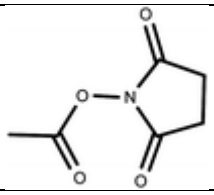	$NH_2–$
3	–N=C=O	$NH_2–$
4	–C≡C–H	$N_3–$
5	$–N_3$	H–C≡C–
6	–OH	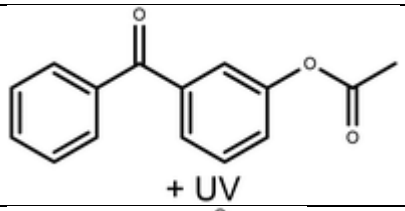 + UV
		R-R = 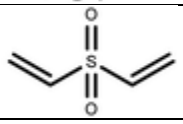
7	–COOH	$NH_2–$
8	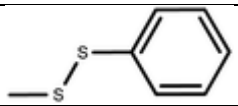	HS–
9		$NH_2–$
10	$–NR_2$	I–

Table 7.1: Functional groups of micelle cross-linkers used to date. Functional group X-on back bone of polymer. Functional group R- disubstituted on cross linker[64].

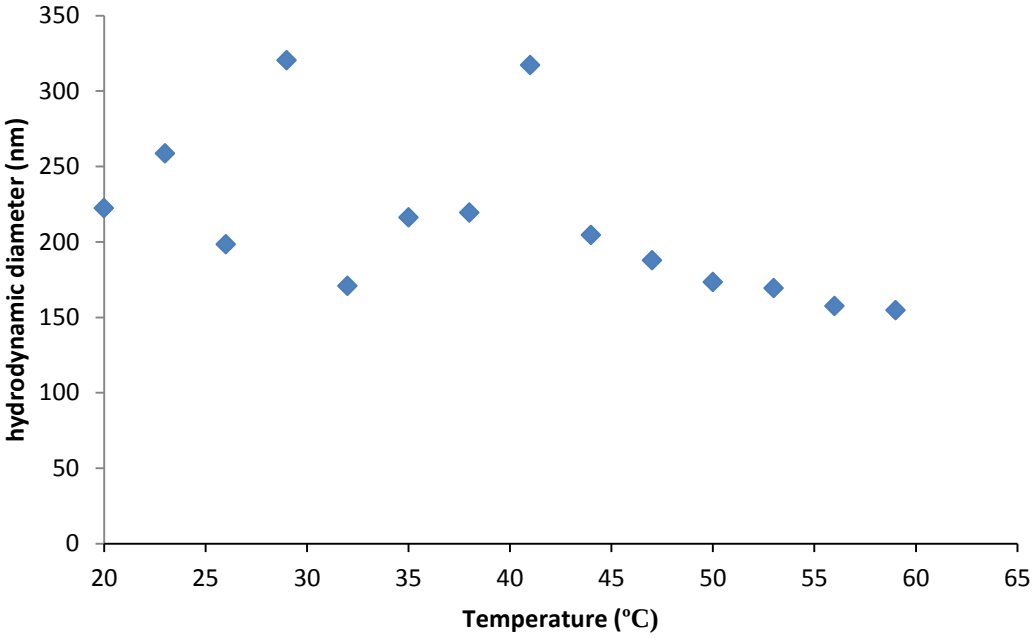

Figure 7.1: Hydrodynamic diameter versus temperature of triblock copolymers. PEG-b-PTBMA-b-PNIPMAAm. (N=1)

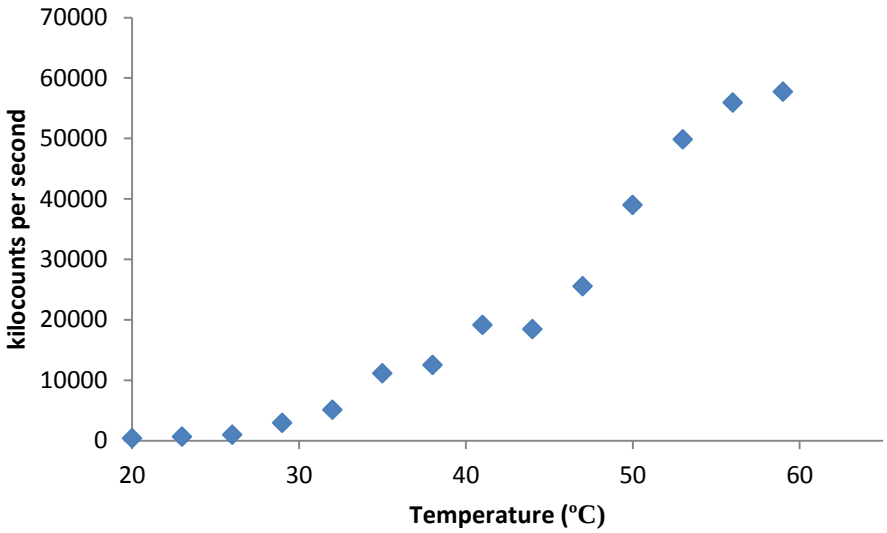

Figure 7.2: DLS kcps versus temperature of PEG-b-PTBMA-b-PNIPMAAm.

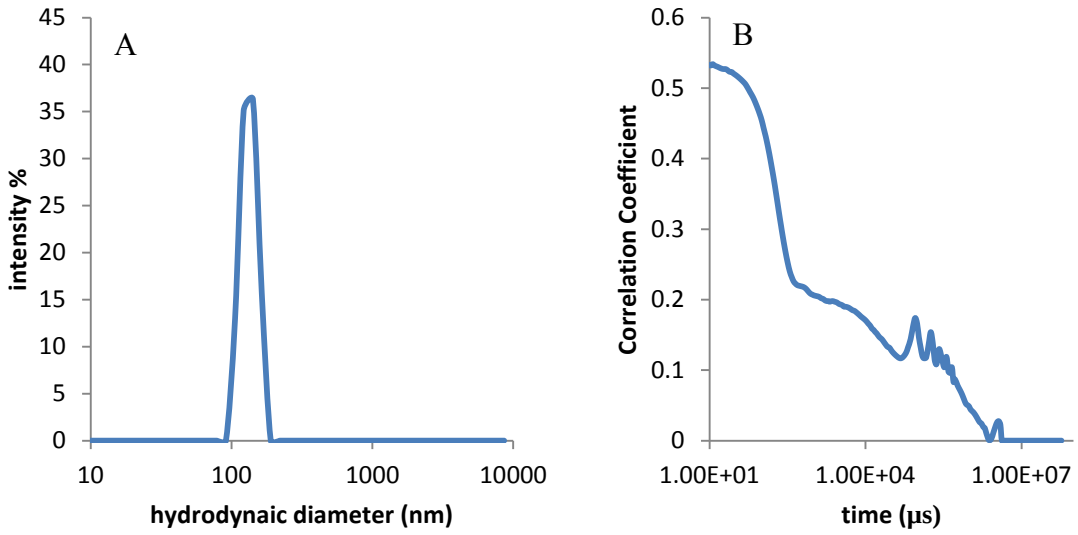

Figure 7.3: DLS supplemental graphs at 40ºC for PEG-b-PTBMA-b-PNIPMAAm. A. Intensity percent vs. hydrodynamic diameter. B. Correlation coefficient vs. relaxation time.

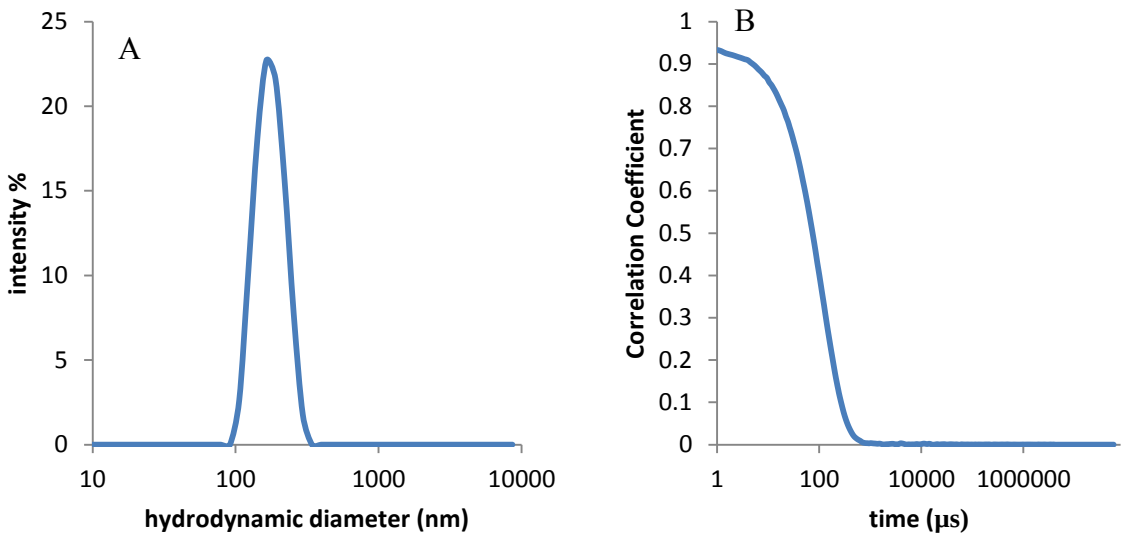

Figure 7.4: DLS supplemental graphs at 45ºC for PEG-b-PTBMA-b-PNIPMAAm. A. Intensity percent vs. hydrodynamic diameter. B. Correlation coefficient vs. relaxation time.

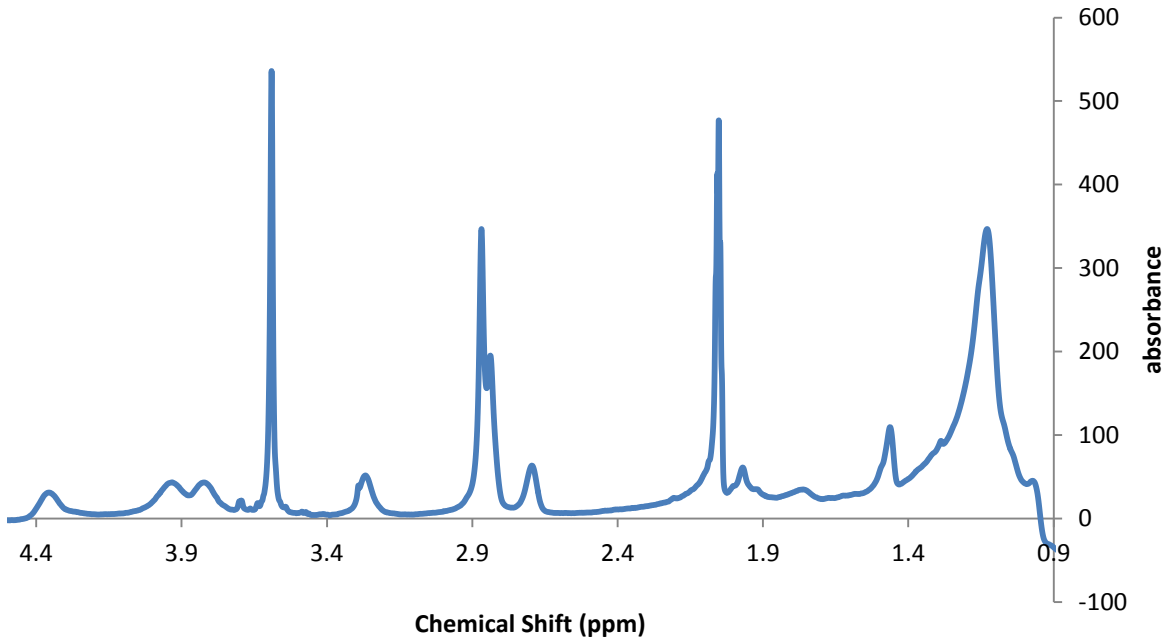

Figure 7.5: H^1 NMR Spectra of P(EG-b-TBMA-b-NIPMAAm) in Acetone.

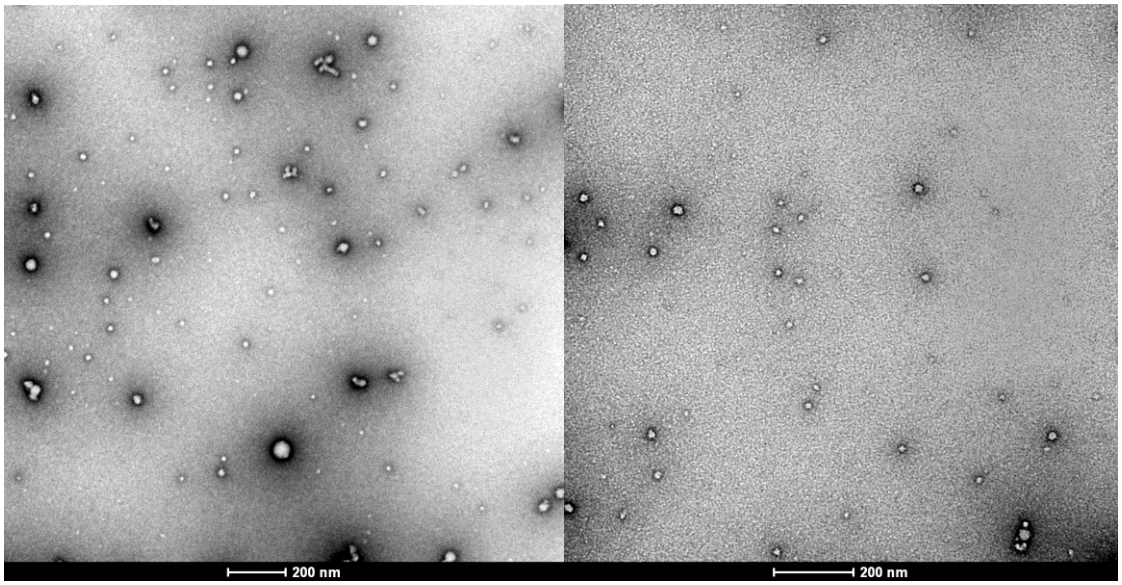

Figure 7.6: TEM micrographs of PEG-b-PTBMA-b-PNIPMAAm micelles crosslinked with GMA and NH_2-PEG- NH_2.

CHAPTER 8

Conclusions

The development of new systems to improve the localization and increase the toxic threshold of chemotherapeutics is necessary to provide oncologists anther tool to help combat the wide array of cancerous diseases in the world. To this end, this thesis has focused on developing and improving thermoresponsive polymer nanogels for use in externally triggered nanocomposites.

Passivation was the first hurdle that was addressed in order to develop systems for drug delivery *in vivo*. The lack of effective strategies for PEG attachment to PNIPAAm nanogels called for development of new surface modification processes to surface-localize the PEG tethers. In order to do this, surface hydrolysis was explored as a method to surface modify higher percentages of AAm. Surface hydrolyzed nanogels were examined for incorporation of carboxylic acid comonomers to quantify the extent of hydrolysis and the surface localization of the functional groups. The 15% AAm system demonstrated an extent of hydrolysis consistent with surface hydrolysis, while 20% AAm exhibited a functional group concentration indicative of hydrolysis of the bulk, however results eventually showed that the system still localized most of these groups near the surface of the nanogels.

After this, these systems were analyzed by DLS for the effect of surface hydrolysis on the swelling response of the P(NIPAAm-co-AAm) nanogels. Although these systems had varying responses to the surface hydrolysis process, neither had their overall swelling response negatively affected. Furthermore, the PEG attachment via an EDC/NHS reaction demonstrated significant stealthing in terms of change of zeta potential while still allowing the nanogels to maintain their critical temperature response.

These systems were further analyzed for their *in vitro* effectiveness as stealthing agents. First these systems were tested for cytotoxicity against RAW 264.7 macrophages, to ensure that their uptake would not result in significant cell death. These studies proved that at fairly high concentrations of up to 1 mg/mL, PNIPAAm nanogels exhibit no cytotoxic effects, and the surface hydrolysis process does not impart any toxicity. This thesis has also proven surface hydrolysis PEGylation prevents significant adsorption of BSA, as a model protein for the indication of opsonization. The surface hydrolysis PEGylation has proven an effective means of surface modification while also providing a sufficient coating to stealth these systems.

Beyond the passivation, PNIPMAAm based hydrogels were synthesized and their effectiveness as externally triggerable delivery vehicles was analyzed. Copolymers with NIPMAAm were analyzed for the impact of the various types of copolymers on the swelling response and shift of the LCST. No general trends were observed based on hydrophilicity or hydrophobicity. Each copolymer limited the rate of temperature response. Most copolymers also caused a decrease in the onset of the response. This decrease in onset lead to a decrease in the LCST, as they all achieved complete syneresis at 50ºC. Copolymerization with EGPhA, AAm, NVP, and PhMA all demonstrated this phenomenon. The only system to positively affect the LCST is TBMA. P(NIPMAAm-co-TBMA) nanogels exhibited an LCST of 46ºC with the sharpest change of any of the PNIPMAAm copolymer nanogels.

The P(NIPMAAm-co-TBMA) systems also proved to be more compatible with DOX. The higher partition coefficient and the larger change in the partition coefficient between 37°C and 45°C signifies the driving force for release from these systems. Because of a number of factors, including volume decrease, . Due to the impact on both the swelling response and partition

coefficients, copolymers with the hydrophobic copolymers demonstrate more favorable characteristics than those copolymerized with hydrophilic comonomers.

Novel core/shell systems were synthesized with a few different copolymers. These systems were characterized, and their structure confirmed with DSC and NMR spectroscopy. The addition of the copolymer shells were shown to have little impact on the LCST of the core, while significantly decreasing the overall swelling response. These Core/shell structures were shown to improve drug partitioning, while limiting the release of both DOX and fluorescein. These studies showed the importance of hydrophobicity for drug loading and retention. In terms of loading, PTBMA proved to improve drug-polymer compatibility, however in terms of overall drug delivery TBMA has no improvement over PhMA.

In order to address other means for synthesis of these nanocomposites ARGET ATRP was used to synthesize schizophrenic triblock copolymers based around PNIPMAAm. These copolymers were then proven to form micelles in response to increases in temperature. These micelles were then crosslinked to form PEGylated nanogels. This is a promising method to form core/shell nanogels with a PEG corona.

This thesis has developed a number of nanogel systems that could be used for externally triggered drug delivery vehicles. It has gone towards addressing two key issues, the biocompatibility and factors that affect the polymer/drug interactions. It has gone further, to develop novel systems to create more efficient drug carriers that can be loaded at higher levels while limiting the diffusional release that accompanies these systems. One constant for all systems were the beneficial effects of the inclusion of more hydrophobic comonomers. TBMA has proven an effective means to both impart drug compatibility with DOX while also limiting its release *in vitro*.

The next step in this work is to combine the successful results in this thesis to produce a full drug carrier for *in vivo* studies. The surface hydrolyzed nanogels should be examined for their circulation half-life *in vivo* to confirm effectiveness of the surface modification scheme. Then they can be synthesized with iron oxide nanoparticles and characterized for their drug delivery efficacy.

The nanogels synthesized with NIPMAAm have yielded two promising candidates for further testing, PNIPMAAm/TBMA and PNIPMAAm/PPhMA at 2:1 molar ratios. In order for these systems to be viable for clinical use, they must first be synthesized with a PEG corona. The post-micelle crosslinking scheme provides a robust way to achieve this. However it must be accomplished with a variety of the comonomers and used to incorporate a stimuli responsive nanoparticle. Another cross-linking scheme could be selected to incorporate a biodegradable scheme to the particles. If these next steps are successful, these particles could prove viable drug delivery vehicles.

APPENDIX

List of Acronyms

5-FU – 5-Flurouracil

AA – Acrylic acid

AAm - Acrylamide

AMF – Alternating magnetic field

AMPS - 2-acrylamido-2-methyl-1-propanesufonic acid

APS – Ammonium Persulfate

ARGET – activators regenerated by electron transfer

ATRP – Atom transfer radical polymerization

DMEM – Dulbecco's modified eagle's medium.

DOPE – Dioleoylphosphatidylethanolamine

DOX – Doxorubicin

DSPE – istearoylphosphatidylethanolamine

EDC - 1-Ethyl-3-(3-dimethylamiopropyl)carbodiimide

EGPhA – Ethylene glycol phenyl ether acrylate

ESR – Equilibrium swelling ratio

$$ESR = \left(\frac{d}{d_{50^{o}C}}\right)^{3}$$

EPR – Enhanced permeability and retention effect

FBS – Fetal bovine serum

IPN- Inter penetrating network

ICAR – initiators for continuous activator regeneration

LCST – lower critical solution temperature

MBAM – N'N'- Methylenebisacrylamide

MNP – Magnetic nanoparticles

NHS –N-Hydroxysuccinimide

NIPAAm – N- Isopropyl Acrylamide

NIPMAm – N-Isopropylmethacrylamide

NIR – Near infrared laser

NVP – N-Vinyl pyrrolidone

PBS – Phosphate buffered saline

PEG – Polyethylene glycol

PhMA- Phenyl methacrylate

RAFT – reversible addition-fragmentation chain-transfer

RES – Reticuloendotheial system

SDS – Sodium Dodecyl sulfate

SEM – Scanning electron microscope

SPION – Super paramagnetic iron oxide nanoparticles

TBMA – tert-Butyl methacrylate

TEM – Transmission electron microscope

UCST – Upper critical solution temperature

Bibliography

1. Gautier, J., et al., *Recent advances in theranostic nanocarriers of doxorubicin based on iron oxide and gold nanoparticles.* Journal of Controlled Release. **169**(1–2): p. 48-61.

2. Maeda, H., *The enhanced permeability and retention (EPR) effect in tumor vasculature: the key role of tumor-selective macromolecular drug targeting.* Advances in enzyme regulation, 2001. **41**(1): p. 189-207.

3. *Treatment Types*. 2011 08/25/2011 [cited 2013 8/12/2013]; Available from: http://www.cancer.org/treatment/treatmentsandsideeffects/treatmenttypes/index.

4. Cohen, M.S., et al., *Prevention of HIV-1 Infection with Early Antiretroviral Therapy.* New England Journal of Medicine, 2011. **365**(6): p. 493-505.

5. Gabizon, A., H. Shmeeda, and Y. Barenholz, *Pharmacokinetics of Pegylated Liposomal Doxorubicin.* Clinical Pharmacokinetics, 2003. **42**(5): p. 419-436.

6. Brannon-Peppas, L. and J.O. Blanchette, *Nanoparticle and targeted systems for cancer therapy.* Advanced Drug Delivery Reviews, 2012. **64, Supplement**: p. 206-212.

7. Park, J.-H., et al., *Biodegradable luminescent porous silicon nanoparticles for in vivo applications.* Nature Materials, 2009. **8**(4): p. 331-336.

8. Nagayasu, A., K. Uchiyama, and H. Kiwada, *The size of liposomes: a factor which affects their targeting efficiency to tumors and therapeutic activity of liposomal antitumor drugs.* Advanced Drug Delivery Reviews, 1999. **40**(1–2): p. 75-87.

9. De Jong, W.H., et al., *Particle size-dependent organ distribution of gold nanoparticles after intravenous administration.* Biomaterials, 2008. **29**(12): p. 1912-1919.

10. Owens Iii, D.E. and N.A. Peppas, *Opsonization, biodistribution, and pharmacokinetics of polymeric nanoparticles.* International Journal of Pharmaceutics, 2006. **307**(1): p. 93-102.

11. Sokolov, K., et al., *Real-Time Vital Optical Imaging of Precancer Using Anti-Epidermal Growth Factor Receptor Antibodies Conjugated to Gold Nanoparticles.* Cancer Research, 2003. **63**(9): p. 1999-2004.

12. de Smet, M., et al., *Magnetic resonance imaging of high intensity focused ultrasound mediated drug delivery from temperature-sensitive liposomes: An in vivo proof-of-concept study.* Journal of Controlled Release, 2011. **150**(1): p. 102-110.

13. Needham, D., et al., *A New Temperature-sensitive Liposome for Use with Mild Hyperthermia: Characterization and Testing in a Human Tumor Xenograft Model.* Cancer Research, 2000. **60**(5): p. 1197-1201.

14. Sawant, R.M., et al., *"SMART" Drug Delivery Systems: Double-Targeted pH-Responsive Pharmaceutical Nanocarriers.* Bioconjugate Chemistry, 2006. **17**(4): p. 943-949.

15. Ishida, T., et al., *Targeted delivery and triggered release of liposomal doxorubicin enhances cytotoxicity against human B lymphoma cells.* Biochimica et Biophysica Acta (BBA) - Biomembranes, 2001. **1515**(2): p. 144-158.

16. Kwon, G., et al., *Block copolymer micelles for drug delivery: loading and release of doxorubicin.* Journal of Controlled Release, 1997. **48**(2–3): p. 195-201.

17. Ma, Y., T. Cao, and S.E. Webber, *Polymer Micelles from Poly(acrylic acid)-graft-polystyrene.* Macromolecules, 1998. **31**(6): p. 1773-1778.

18. Cha, E.-J., J.E. Kim, and C.-H. Ahn, *Stabilized polymeric micelles by electrostatic interactions for drug delivery system.* European Journal of Pharmaceutical Sciences, 2009. **38**(4): p. 341-346.

19. Lee, I.-H., et al., *A duplex oligodeoxynucleotide–dendrimer bioconjugate as a novel delivery vehicle for doxorubicin in in vivo cancer therapy.* Journal of Controlled Release, 2011. **155**(1): p. 88-95.

20. Kim, J.O., et al., *Polymeric Micelles with Ionic Cores Containing Biodegradable Cross-Links for Delivery of Chemotherapeutic Agents.* Biomacromolecules, 2010. **11**(4): p. 919-926.

21. Gao, Z.-G., H.D. Fain, and N. Rapoport, *Controlled and targeted tumor chemotherapy by micellar-encapsulated drug and ultrasound.* Journal of Controlled Release, 2005. **102**(1): p. 203-222.

22. Xiong, X.-B. and A. Lavasanifar, *Traceable Multifunctional Micellar Nanocarriers for Cancer-Targeted Co-delivery of MDR-1 siRNA and Doxorubicin.* ACS Nano, 2011. **5**(6): p. 5202-5213.

23. Fox, M.E., et al., *Synthesis and In Vivo Antitumor Efficacy of PEGylated Poly(l-lysine) Dendrimer−Camptothecin Conjugates.* Molecular Pharmaceutics, 2009. **6**(5): p. 1562-1572.

24. Lai, P.-S., et al., *Doxorubicin delivery by polyamidoamine dendrimer conjugation and photochemical internalization for cancer therapy.* Journal of Controlled Release, 2007. **122**(1): p. 39-46.

25. Wijagkanalan, W., S. Kawakami, and M. Hashida, *Designing Dendrimers for Drug Delivery and Imaging: Pharmacokinetic Considerations.* Pharmaceutical Research, 2011. **28**(7): p. 1500-1519.

26. Acton, A.L., et al., *Janus PEG-Based Dendrimers for Use in Combination Therapy: Controlled Multi-Drug Loading and Sequential Release.* Biomacromolecules, 2013. **14**(2): p. 564-574.

27. Gref, R., et al., *'Stealth' corona-core nanoparticles surface modified by polyethylene glycol (PEG): influences of the corona (PEG chain length and surface density) and of the core composition on phagocytic uptake and plasma protein adsorption.* Colloids and Surfaces B: Biointerfaces, 2000. **18**(3–4): p. 301-313.

28. Peppas, N.A., et al., *Hydrogels in biology and medicine: From molecular principles to bionanotechnology.* Advanced Materials, 2006. **18**(11): p. 1345-1360.

29. Kennedy, L.C., et al., *A New Era for Cancer Treatment: Gold-Nanoparticle-Mediated Thermal Therapies.* Small, 2011. **7**(2): p. 169-183.

30. Hergt, R., et al., *Magnetic particle hyperthermia: nanoparticle magnetism and materials development for cancer therapy.* Journal of Physics: Condensed Matter, 2006. **18**(38).

31. Owens, D.E., et al., *Thermally Responsive Swelling Properties of Polyacrylamide/Poly(acrylic acid) Interpenetrating Polymer Network Nanoparticles.* Macromolecules, 2007. **40**(20): p. 7306-7310.

32. Katono, H., et al., *Thermo-responsive swelling and drug release switching of interpenetrating polymer networks composed of poly(acrylamide-co-butyl methacrylate) and poly (acrylic acid).* Journal of Controlled Release, 1991. **16**(1–2): p. 215-227.

33. Abulateefeh, S.R., et al., *Thermoresponsive Polymer Colloids for Drug Delivery and Cancer Therapy.* Macromolecular Bioscience, 2011. **11**(12): p. 1722-1734.

34. Varaprasad, K., et al., *Design and development of temperature sensitive porous poly(NIPAAm-AMPS) hydrogels for drug release of doxorubicin-a cancer chemotherapy drug.* Journal of Applied Polymer Science, 2010. **116**(6): p. 3593-3602.

35. Yıldız, B., B. Işık, and M. Kış, *Synthesis and characterization of thermoresponsive isopropylacrylamide–acrylamide hydrogels.* European Polymer Journal, 2002. **38**(7): p. 1343-1347.

36. Bae, Y.H., T. Okano, and S.W. Kim, *Temperature dependence of swelling of crosslinked poly(N,N'-alkyl substituted acrylamides) in water.* Journal of Polymer Science Part B: Polymer Physics, 1990. **28**(6): p. 923-936.

37. Xie, R., Y. Li, and L.-Y. Chu, *Preparation of thermo-responsive gating membranes with controllable response temperature.* Journal of Membrane Science, 2007. **289**(1–2): p. 76-85.

38. Gan, D. and L.A. Lyon, *Synthesis and Protein Adsorption Resistance of PEG-Modified Poly(N-isopropylacrylamide) Core/Shell Microgels.* Macromolecules, 2002. **35**(26): p. 9634-9639.

39. Jiang, X., et al., *Fabrication of Multiresponsive Shell Cross-Linked Micelles Possessing pH-Controllable Core Swellability and Thermo-Tunable Corona Permeability.* Biomacromolecules, 2007. **8**(10): p. 3184-3192.

40. You, Y.-Z., et al., *Dually Responsive Multiblock Copolymers via Reversible Addition−Fragmentation Chain Transfer Polymerization: Synthesis of Temperature- and Redox-Responsive Copolymers of Poly(N-isopropylacrylamide) and Poly(2-(dimethylamino)ethyl methacrylate).* Macromolecules, 2007. **40**(24): p. 8617-8624.

41. Kawaguchi, H., K. Fujimoto, and Y. Mizuhara, *Hydrogel microspheres III. Temperature-dependent adsorption of proteins on poly-N-isopropylacrylamide hydrogel microspheres.* Colloid and Polymer Science, 1992. **270**(1): p. 53-57.

42. Pankhurst, Q.A., et al., *Applications of magnetic nanoparticles in biomedicine.* Journal of Physics D: Applied Physics, 2003. **36**(13).

43. Hyeon, T., *Chemical synthesis of magnetic nanoparticles.* Chemical Communications, 2003(8): p. 927-934.

44. Sun, C., J.S.H. Lee, and M. Zhang, *Magnetic nanoparticles in MR imaging and drug delivery.* Advanced Drug Delivery Reviews, 2008. **60**(11): p. 1252-1265.

45. Huang, X., et al., *Cancer Cell Imaging and Photothermal Therapy in the Near-Infrared Region by Using Gold Nanorods.* Journal of the American Chemical Society, 2006. **128**(6): p. 2115-2120.

46. Leonov, A.P., et al., *Detoxification of Gold Nanorods by Treatment with Polystyrenesulfonate.* ACS Nano, 2008. **2**(12): p. 2481-2488.

47. Kokufuta, E., et al., *Effects of surfactants on the phase transition of poly(N-isopropylacrylamide) gel.* Macromolecules, 1993. **26**(5): p. 1053-1059.

48. Zhang, Y., et al., *Specific Ion Effects on the Water Solubility of Macromolecules: PNIPAM and the Hofmeister Series.* Journal of the American Chemical Society, 2005. **127**(41): p. 14505-14510.

49. Hoare, T. and R. Pelton, *Functional Group Distributions in Carboxylic Acid Containing Poly(N-isopropylacrylamide) Microgels.* Langmuir, 2004. **20**(6): p. 2123-2133.

50. Rasmusson, M., A. Routh, and B. Vincent, *Flocculation of Microgel Particles with Sodium Chloride and Sodium Polystyrene Sulfonate as a Function of Temperature.* Langmuir, 2004. **20**(9): p. 3536-3542.

51. Kong, G., R.D. Braun, and M.W. Dewhirst, *Characterization of the Effect of Hyperthermia on Nanoparticle Extravasation from Tumor Vasculature.* Cancer Research, 2001. **61**(7): p. 3027-3032.

52. Feil, H., et al., *Effect of comonomer hydrophilicity and ionization on the lower critical solution temperature of N-isopropylacrylamide copolymers.* Macromolecules, 1993. **26**(10): p. 2496-2500.

53. Geever, L.M. and C.L. Higginbotham, *Temperature-triggered gelation and controlled drug release via NIPAAm/NVP-based hydrogels.* Journal of Materials Science, 2011. **46**(9): p. 3233-3240.

54. *5-Fluorouracil 51-21-8*. 2014 [cited 2014 1/21/2014]; Available from: http://www.chemicalbook.com/ChemicalProductProperty_EN_CB8162744.htm.

55. *Fluorescien 2321-07-5*. 2014 [cited 2014 1/21/2014]; Available from: http://www.chemicalbook.com/ChemicalProductProperty_EN_CB7753558.htm.

56. Liu, T.-Y., et al., *Biomedical nanoparticle carriers with combined thermal and magnetic responses.* Nano Today, 2009. **4**(1): p. 52-65.

57. Gran, M., *Metal-Polymer Nanoparticulate Systems for Externally-Controlled Delivery*, in *Chemical Engineering*2010, The University of Texas at Austin: Austin, TX. p. 189.

58. Lokitz, B.S., et al., *Aqueous RAFT Synthesis of Micelle-Forming Amphiphilic Block Copolymers Containing N-Acryloylvaline. Dual Mode, Temperature/pH Responsiveness, and "Locking" of Micelle Structure through Interpolyelectrolyte Complexation†.* Macromolecules, 2007. **40**(18): p. 6473-6480.

59. Wei, H., et al., *Self-assembled thermoresponsive micelles of poly(N-isopropylacrylamide-b-methyl methacrylate).* Biomaterials, 2006. **27**(9): p. 2028-2034.

60. Webster, O.W., *Group Transfer Polymerization: A Critical Review of Its Mechanism and Comparison with Other Methods for Controlled Polymerization of Acrylic Monomers*, in *New Synthetic Methods*2004, Springer Berlin Heidelberg. p. 1-34.

61. Mueller, L., et al., *Successful Chain Extension of Polyacrylate and Polystyrene Macroinitiators with Methacrylates in an ARGET and ICAR ATRP.* Macromolecules, 2007. **40**(18): p. 6464-6472.

62. Cao, L., et al., *Poly(N-isopropylacrylamide) and poly(2-(dimethylamino)ethyl methacrylate) grafted on an ordered mesoporous silica surface using atom transfer radical polymerization with activators regenerated by electron transfer.* Journal of Materials Chemistry, 2012. **22**(14): p. 6939-6946.

63. Min, K., H. Gao, and K. Matyjaszewski, *Use of ascorbic acid as reducing agent for synthesis of well-defined polymers by ARGET ATRP.* Macromolecules, 2007. **40**(6): p. 1789-1791.

64. van Nostrum, C.F., *Covalently cross-linked amphiphilic block copolymer micelles.* Soft Matter, 2011. **7**(7).